REVIEWS OF MODERN PHYSICS, VOLUME 77, JULY 2005

Microscopic dynamics in liquid metals: The experimental point of view

Tullio Scopigno* and Giancarlo Ruocco

SOFT-INFM-CNR and Dipartimento di Fisica, Universitá di Roma "La Sapienza," I-00185, Roma, Italy

Francesco Sette

European Synchrotron Radiation Facility, B.P. 220, F-38043 Grenoble, Cedex, France

(Published 7 September 2005)

The experimental results relevant for the understanding of the microscopic dynamics in liquid metals are reviewed, with special regard to the ones achieved in the last two decades. Inelastic neutron scattering played a major role since the development of neutron facilities in the 1960s. The last ten years, however, saw the development of third generation radiation sources, which opened the possibility of performing inelastic scattering with x rays, thus disclosing previously unaccessible energy-momentum regions. The purely coherent response of x rays, moreover, combined with the mixed coherent or incoherent response typical of neutron scattering, provides enormous potentialities to disentangle aspects related to the collectivity of motion from the single-particle dynamics. If the last 20 years saw major experimental developments, on the theoretical side fresh ideas came up to the side of the most traditional and established theories. Beside the raw experimental results therefore models and theoretical approaches are reviewed for the description of microscopic dynamics over different length scales, from the hydrodynamic region down to the single-particle regime, walking the perilous and sometimes uncharted path of the generalized hydrodynamics extension. Approaches peculiar of conductive systems, based on the ionic plasma theory, are also considered, as well as kinetic and mode coupling theory applied to hard-sphere systems, which turn out to mimic with remarkable detail the atomic dynamics of liquid metals. Finally, cutting edge issues and open problems, such as the ultimate origin of the anomalous acoustic dispersion or the relevance of transport properties of a conductive system in ruling the ionic dynamic structure factor, are discussed.

CONTENTS

*Electronic address: tullio.scopigno@phys.uniroma1.it; URL: http://glass.phys.uniroma1.it

I. INTRODUCTION

Liquid metals are an outstanding example of systems combining great relevance in both industrial applications and basic science. On the one hand, they find broad technological application ranging from the production of industrial coatings (walls of refinery coker, drill pipe for oil search) to medical equipments (reconstructive devices, surgical blades) or high performance sporting goods. Most metallic materials, indeed, need to be refined in the molten state before being manufactured.

On the other hand, liquid metals, in particular the monatomic ones, have been recognized since long ago to be the prototype of simple liquids, in the sense that they encompass most of the physical properties of real fluids without the complications which may be present in a particular system (Balucani and Zoppi, 1983).

In addition to that, metallic fluids such as molten sodium, having similar density and viscosity to water, find application as coolant in nuclear reactors.

The thermodynamic description of liquid metals can be simplified by assuming a few parameters. Usually, if compound formation is weak physical theory alone can be used while, if there is strong compound formation, chemical theory alone is used. The lowest-melting liquid metals are those that contain heavier elements, and this may be due to an increase in ease of creating a free-electron solution. Alkali metals are characterized by low melting points, and they tend to follow trends. Binary associating liquids show a sharp melting point, with the most noticeable example being mercury (T_m=234 K). Melting points can be lowered by introducing impurities into the metal. Often, to this purpose, another metal with a low melting point is used. Mixing different metals may often result in a solution that is eutectic. In other words, from Henry's law it is understood that a melting point depression occurs, and the system becomes more disordered as a result of the perturbation to the lattice. This is the case, for instance, of the well-known eutectic Pb-Tin alloy, widely used in soldering applications (T_m =453 K).

Until the 1960s the understanding of the physical properties of metals proceeded rather slowly. It was Ziman, indeed, who made the theory of liquid metals respectable for the first time (Ziman, 1960), and the Faber-Ziman theory, developed in 1961–1963 and dealing with electronic and transport properties, is attractively introduced in Faber's book, which is an excellent treatise of the physical properties of liquid metals (Faber, 1972).

The other text which can be considered a classic is March's book (March, 1968), along with the more recent one (March, 1990), which provides a comprehensive overview over liquid metals. It is from these texts that a first clear definition of liquid metal can be outlined. At first glance, indeed, the words "liquid metal" are self-explanatory: by definition any metal heated to its melting point can be cast in this category. Liquid metals, however, are implicitly understood to be less general than the above definition, and no literature clearly states an exact definition. Although no precise agreement has been made, there are certain characteristics shared by liquid metals, descending from a close interplay between ionic structure, electronic states, and transport properties.

The book of Shimoji (1977) deals with the fundamentals of liquid metals in an elementary way, covering the developments achieved after the first book by March. It does not address, however, the dynamical properties in great detail.

Addison's book (1986) is much like March's general book, but is more focused on applications of alkali metals, especially on their use in organic chemistry. In addition, Addison discusses many methods for purifying and working with liquid alkali metals. March is more theoretical whereas Addison is practical, but both authors focus on a thermodynamic explanation of liquid metals.

For an appealing general introduction to the physics and chemistry of the liquid-vapor phase transition (beyond the scope of this review) the reader should certainly make reference to Hensel and Warren's work (1999), which also provides a bird's-eye view of the practical applications of fluid metals, such as high-temperature working fluid or key ingredients for semiconductor manufacturing.

There are, then, a number of books which are more general and more specific at the same time, in the sense that they deal with with the wider class of simple liquids (including noble fluids, hard-sphere fluids, etc.), but they are mainly concerned with structural and dynamical properties only (Egelstaff, 1967; Boon and Yip, 1980; Balucani and Zoppi, 1983; Hansen and McDonald, 1986; March and Tosi, 1991). They are practically ineludible for those aiming at a rigorous approach to the statistical mechanics description of the liquid state.

It can be difficult to find an exhaustive updated database of the physical properties of liquid metals, especially as far as dynamics is concerned. But the handbooks of Iida and Guthrie (1993) and Ohse (1985) are remarkable exceptions, with the second one specifically addressing liquid alkali metals.

A. Historical background

Early phenomenological approaches to the study of relaxation dynamic in fluids can be dated back to the end of the 19th century (Maxwell, 1867; Kelvin, 1875).

Only in the mid-20th century, however, was it realized that a deeper understanding of the physical properties of liquids could have been reached only through a microscopic description of the atomic dynamics. This became possible through the achievements of statistical mechanics which provided the necessary tools, such as correlation functions, integral equations, etc. The mathematical difficulties related to the treatment of real liquids brought to the general attention the importance of simple liquids, as systems endowed with the rich basic phenomenology of liquids but without the complications arising, for instance, by orientational and vibrational degrees of freedom.

As a consequence, the end of the 1950s saw major experimental efforts related to the development of inelastic neutron scattering (INS) facilities which, as we shall see, constitutes a privileged probe to access the microscopic dynamics in condensed matter and, in particular, in the liquid state (Egelstaff, 1959). A sizable library of experimental data on liquid metals has been constituted since then, realizing the prototypical structural and dynamical properties of these systems, representative of the whole class of liquids.

In the 1960s, the advent and the broad diffusion of computational facilities brought a new era for two main reasons: on the one side, realistic computer simulation experiments become possible (Schiff, 1969), on the other side the new computation capabilities greatly facilitated the interpretation of INS experiments. For instance, new protocols for accurate estimates of the multiple-scattering contribution affecting neutron scattering were proposed (Copley, 1975). The theoretical framework of inelastic neutron scattering and the guidelines to interpret the results have been reviewed in the classical textbooks (Marshall, 1971; Lovesey, 1987).

The dynamics of liquid metals has been extensively investigated by INS and computer simulations with the main purpose of ascertaining the role of the mechanisms underlying both collective and single-particle motions at the microscopic level. In the special case of collective density fluctuations, after the seminal inelastic neutron-scattering study by Copley and Rowe (1974) and the famous molecular-dynamics simulation of Rahman (1974) in liquid rubidium, the interest in performing more and more accurate experiments is continuously renewed: it was soon realized, indeed, that well-defined oscillatory modes could be supported even outside the strict hydrodynamic region. In molten alkali metals, moreover, this feature is found to persist down to wavelengths of one or two interparticle distances, making these systems excellent candidates to test the various theoretical approaches developed so far for the microdynamics of the liquid state.

Up to ten years ago the only experimental probe appropriate to access the atomic dynamics over the interparticle distance region were thermal neutrons, and using this probe fundamental results have been gained. There are, however, certain limitations of this technique which can restrict its applicability: first, the presence of an incoherent contribution to the total neutron-scattering cross section. If, on one hand, this allows one to gather richer information, being simultaneously sensitive to collective and single-particle dynamics, on the other hand, poses the problem of decoupling the two contributions, when aiming at the determination of collective properties only [i.e., of the coherent dynamic structure factor $S(Q,\omega)$]. In liquid sodium, for instance, the incoherent cross section dominates; even in more favorable cases (Li, K) at small Q the intensity of the collective contribution is low, and its extraction requires a detailed knowledge of the single-particle dynamics.

The second reason is dictated by the need of satisfying both the energy and momentum conservation laws which define the $(Q\text{-}E)$ region accessible to the probe (Balucani and Zoppi, 1983). Roughly speaking, when the sound speed of the system exceeds the velocity of the probing neutrons ($\sim$1500 m/s for thermal neutrons) collective excitations can hardly be detected for Q values below, say, Q_m, the position of the main diffraction peak of the sample, which is the region where collective properties show the richer phenomenology. As we shall see in Sec. III.A.5, given a certain kinematic region accessible to neutrons (basically ruled by their thermal energy), by virtue of the $m^{-1/2}$ dependence of the sound velocity of an atomic system, the higher its atomic number, the wider is the accessible energy-momentum region of the excitations which can be studied. Taking as an example alkali metals, indeed, accurate INS data are available for heavier elements such as rubidium ($v \sim 1260$ m/s; Copley and Rowe, 1974; Chieux *et al.*, 1996; Pasqualini *et al.*, 1999) and cesium ($v \sim 970$ m/s; Bodensteiner *et al.*, 1992), while more difficulties are met in the case of lighter atoms. In particular, lithium represents the most critical case due to its high sound speed ($v \sim 4500$ m/s) and to the weak scattering cross section which, moreover, results from comparable values of the coherent and incoherent contributions: for this reason INS aiming to the study of collective properties of Li represented a very hard challenge (De Jong, 1993; De Jong *et al.*, 1993). From a general point of view the main outcome of most of these early INS experiments, as far as collective properties are concerned, is the evidence of inelastic excitations in $S(Q,\omega)$ which have been necessarily analyzed within simple models such as the damped harmonic oscillator (DHO) (Fåk and Dorner, 1997), suitable to extract reliable and resolution-corrected information on the peak positions but not about the detail of the whole line shape. Some additional information has been achieved, for instance, in the case of cesium (Bodensteiner *et al.*, 1992), where information about an average relaxation time has been extracted utilizing Lovesey's viscoelastic model (Lovesey, 1971) or, more recently, in molten potassium, where a generalized hydrodynamic treatment as the one described in Sec. II.F

is undertaken (Cabrillo *et al.*, 2002) and electronic screening effects have been explicitly taken into account (Bove *et al.*, 2003).

Paralleling the development of INS facilities, new ideas arose on both theoretical and numerical fields from 1975 and in intervening decades, driven by kinetic theory applied to Enskog's fluid (de Schepper and Cohen, 1980; Alley and Alder, 1983; Alley *et al.*, 1983; de Schepper *et al.*, 1983; Kamgar-Parsi *et al.*, 1987), allowing one to describe the hydrodynamic region in terms of the three-pole approximation, or to reproduce the dynamic structure factor at wavelengths comparable to the inverse mean particle distance in terms of extended heat mode (Cohen *et al.*, 1987). Kinetic approaches were eventually complemented by memory function formalism and by mode coupling theory (Götze and Zippelius, 1976; Sjögren and Sjölander, 1978, 1979; de Schepper and Ernst, 1979; Sjögren, 1979, 1980; Wahnström and Sjögren, 1982; Bengtzelius *et al.*, 1984).

Turning attention to numerical advances in the liquid metals field, the major achievements are probably related to the introduction of the pseudopotential concept (Austin *et al.*, 1962; Harrison, 1966; Heine, 1970; Ashcroft and Stroud, 1978) which, besides offering a deeper comprehension of physical properties such as electrical resistivity, provided a clue for realistic numerical simulations. In molecular dynamics, indeed, the choice of a realistic interatomic potential—i.e., a potential model able to reproduce structural properties—is crucial to allow the determination of the dynamics of the system via the integration of the classical Newton equations. Exploiting the pseudopotential theory, it has been possible to express the atomic interaction as a sum of pairwise interactions, ruled by an effective density-dependent interaction. In this respect, one of the most successful expressions is the effective potential proposed for alkali metals (Price *et al.*, 1970).

The numerical simulation framework is particularly useful since the single-particle and the collective dynamics can easily be investigated within technical restrictions due to the finite box size (defining the minimum accessible wave vector) and computation time (related to the statistical quality and to the energy resolution of the calculated spectra). Broadly speaking, the features of the atomic collective motion, i.e., the details of the $S(Q,\omega)$ line shape, as an outcome of the molecular-dynamics run, turns out to be less noisy and more straightforward than the corresponding INS results: no absolute normalization is required, no mixing between coherent and incoherent dynamics occurs, and, above all, basically no resolution corrections are needed.

The major experimental breakthrough, however, happened in the last ten years when x rays came up by the side of neutrons to study the collective dynamics in a similar frequency and wavelength region. The intriguing theoretical possibility of performing inelastic x-ray scattering (Burkel, 1991) became real due to the advent of the third generation sources (Masciovecchio *et al.*, 1996), disclosing previously unaccessible tasks in the physics of disordered systems (Ruocco *et al.*, 1996; Sette *et al.*, 1998; Scopigno *et al.*, 2003; Sinn *et al.*, 2003). In this case, the cross section is mainly coherent, and the combination of the two techniques can in principle serve to disentangle the two contributions. Unfortunately, such complementarity has not yet been exploited in full.

B. Dynamical aspects

There are mainly two routes to approach the dynamics of a viscous melt. The first one stems from a quasicrystalline picture, and relies on the observation that, often, the diffusion coefficient D linearly depends on $1/T$. The same dependence, in fact, is induced in crystalline solids by vacancies and defects. This analogy suggests that diffusion in liquids is an activated process, and many attempts have been made to relate the activation energy in the liquid to the thermodynamics of its solid.

The other point of view is the kinetic theory, a gaslike picture where the correlation functions are different in view of the density which is typically much higher than in the gas state. Within this framework an expression for the behavior of diffusion coefficient and viscosity can be gained in terms of the friction coefficient ξ. When a particle of the melt is moving with constant velocity v a net retarding force results from the different rate between front and back collisions of the form $F=-\xi v$. For a hard-sphere gas it turns out from Fick's law of diffusion that $\xi=[8ng(\sigma)\sigma^2/3]\sqrt{\pi m k_B T}$, where ρ is the atomic density, m the atom mass, and $4\pi\sigma^2 g(\sigma)$ the density probability of finding two units at distance σ. The diffusion coefficient is therefore $D=k_B T/\xi$, while the viscosity $\eta=\xi/3\pi\sigma$ (Longuet-Higgins and Pople, 1956). These simple expressions turn out to describe remarkably well the dynamics of liquid metals as long as the one of other simple fluids. However, better quantitative agreement can be obtained introducing the velocity autocorrelation function $\psi(\Delta t)=\langle \mathbf{v}(t+\Delta t)\cdot\mathbf{v}(t)\rangle/\langle v^2\rangle$, whose time integral determines the diffusion coefficient. $\psi(t)$ plays a central role in liquid dynamics, not only for providing a rigorous way to calculate D, but also because through its Fourier transform one can grasp an insight into the detail of the interatomic interactions. It can be accessed either by molecular simulations (the calculation trivially follows from its definition) or experimentally, mainly by inelastic neutron scattering (INS) with the methods detailed in Sec. III.

Broadly speaking, $\psi(\Delta t)$ is related to the knowledge of $G_s(r,t)$, i.e., the probability that a given particle travels a distance r in the time interval t. INS is always sensitive to a combination of $G_s(r,t)$ and $G_d(r,t)$, this latter quantity being the probability of finding two distinct particles at a space distance r and time distance t. The way to separate these two contributions mixed in the instrumental response is one of the major conundrums of the neutron-scattering technique. The direct knowledge of the coherent response, gained by means of inelastic x-ray scattering, opens the possibility to the understanding of the high-frequency modes that have been seen to survive since the famous INS experiments on the highly

coherent scatterer liquid rubidium (Copley and Rowe, 1974). In particular, from a solid point of view, the main issue is to ascertain the relation between these modes and the phonon excitations in the corresponding polycrystal just below the melting. In a perfect crystal (i.e., a periodic assembly of atoms or ions), indeed, atomic dynamics is mainly vibrational, characterized by normal modes which are plane waves, due to the harmonic nature of the interatomic forces. Consequently, a well defined ratio (the sound velocity) exists between the frequency and the wave vector of the density fluctuations, named in this case *phonon*. In real crystals therefore the energy spectrum of a scattered probe results in sharp peaks, whose linewidth is related to the presence of anharmonicities or lattice defects. In a liquid things are more involved: other effects arise besides anharmonicity, both structural (the average atomic positions are randomly distributed) and dynamical (mass diffusion and activated processes join the purely vibrational motion). But even in this complex scenario distinct peaks survive and one can extract dispersion relations.

Interestingly, the relation between crystals and liquids involves more than the mere similarity between the sound velocity of the crystalline acoustic branches and of the mode observed in the liquid (i.e., the low Q limit of the dispersion relation). Despite the lack of periodicity intrinsic to the inherent liquid structure, indeed, the presence of some residual correlation (testified by the oscillation in static structure factor) seems to warrant a support for the existence of umklapp modes similar to the one existing in crystals. Such processes, i.e., the presence of inelastic modes characterized by wave vectors which differ by multiples of the reciprocal-lattice spacing, have been early reported by means of INS in liquid lead (Cocking and Egelstaff, 1965a; Dorner *et al.*, 1965; Randolph and Singwi, 1966) and more recently in liquid lithium by means of inelastic x-ray scattering (Scopigno, D'Astuto, *et al.*, 2001). As correctly pointed out by Faber, the presence of these excitations does not imply the existence of genuine high Q modes, it rather indicates that umklapp processes may occur in liquid as much as in solid (Faber, 1972).

From the liquid point of view the interest in this phenomenology lies in the challenging extension of the simple hydrodynamics, describing the density fluctuations in the long-wavelength limit, down to the length scale of the mean interparticle distances. As it will be shown in the following, such an extension relies on serious and sometimes not fully justified assumptions necessary to walk in the uncharted and perilous territory between hydrodynamics and single-particle regimes.

C. Peculiarities of liquid metals

Apparently at odds with the previously mentioned classification of liquid metals as a prototype of simple liquids, even in the simplest monatomic case, metallic fluids are actually two-component systems. The interplay between electron and ions, indeed, is an intrinsic aspect of liquid metals, and a rigorous approach should therefore mimic the formalism utilized for binary mixtures. For many aspects, however, one might be interested in ionic properties only, and as far as atomic dynamics is concerned, this seems to be the case. In such circumstance, one can look at a liquid metal as an ionic assembly whose interaction is mediated by the conduction electron gas. The treatment is in such way reduced to a one-component system, as for noble fluids one can introduce a pairwise interaction, but this latter will be ruled by a density-dependent pseudopotential.

Although within the pseudopotential approach many results for liquid metals are qualitatively similar to those for ordinary nonconductive fluids, some remarkable differences exist. One of the most relevant of these differences concerns peculiar structural properties involving short-range order: in several liquid metals the static structure factor exhibits an asymmetry or even a shoulder just above the main peak. The origin of this anomaly has been highly debated, and ascribed to the peculiar shape of the interaction potential in those metals in which the hard-sphere description fails (Tsay and Wang, 1994). More specifically, it can be interpreted in terms of a repulsive interaction composed by a hard-sphere part plus an adjacent ledge induced by electronic effects, by a curvature change occurring at the nearest-neighbor distance, or by the interplay with Friedl oscillations.

The reported peculiarities extend also to the dynamics: while in the long-wavelength limit they are expected to behave similarly to nonconductive fluids, at finite wave vectors their departure from ordinary hydrodynamics can in principle be influenced by the high values of the thermal conductivity (Faber, 1972; Singh and Tankeshwar, 2003, 2004; Scopigno and Ruocco, 2004). One of the most striking quantitative differences with ordinary fluids concerns the "visibility" of the inelastic features, i.e., the inelastic to elastic ratio, which seems to be related to the softness of the interaction potential (Balucani *et al.*, 1992; Canales and Padró, 1999). This latter is responsible, for example, for the very favorable inelastic to elastic ratio which makes alkali metals ideal systems to study collective properties.

Though the whole dynamics of liquid metals seems to be conveniently rationalized treating them as ordinary fluids interacting via an effective, density-dependent, pairwise interaction potential, there is an alternative route which explicitly takes into account electronic screening effect on the ionic dynamics, relying on the introduction of a suitable model for the wavelength-dependent dielectric function. In this way one is able to test different approximations comparing the predictions for the mechanical compressibility (or, equivalently, for the sound velocity) with the experimental values (Bove *et al.*, 2003; Said *et al.*, 2003).

D. Why this review

As previously pointed out, some books offer a broad coverage of the physics and chemistry of liquid metals, but none of them is focused on the dynamical aspects. On the other side, books dealing with liquid dynamics

do not focus on liquid metals in great detail. Egelstaff's review (1966) offers an exhaustive coverage of transport phenomena in liquids but dynamical properties of liquid metals are marginally addressed. The Copley and Lovesey review (1975) provides an invaluable sight on the dynamics of simple liquids, and it presents many results obtained for liquid metals, but again does not emphasize the peculiarity of these systems. Moreover, it also addresses in detail numerical results and last, but not least, it is necessarily not up to date given the large amount of experiments recently performed. The last decade, indeed, has seen important advances in the dynamics of liquid metals, especially on the experimental side, driven by the advent of new x-ray facilities and by the upgrades of the neutron ones. On the theoretical side, in the 1980s, impressive results have been achieved working on hard-sphere models and/or mode coupling approaches which, again, remain uncovered in the Copley and Lovesey review. To conclude, it is certainly worth mentioning the more recent review article by Verkerk (2001), which offers a clear overview of the theoretical models developed so far for liquid dynamics, presenting a selection of experimental results for liquified rare gases, molten metals, and binary mixtures.

Given this background, it seemed to us helpful to focus on the experiments on liquid metals, and to discuss and summarize the results and their interpretations in terms of the existing theories, trying to emphasizes advantages and weakness of each approach. This turned out to be a difficult task, given the broadness of the matter, and we necessarily had to make some choices. We left out, for instance, mixtures and alloys, and we tried to focus on the most recent experimental achievements, say of the last ten years: in most cases we quickly reference older results, unless they are particularly relevant in view of the most recent ones.

The review is organized as follows. In Sec. II we present different theoretical approaches to the dynamics of liquid metals. We develop in parallel subsections the treatment of the self- and collective properties which are, in turn, organized according to the different wavelength domains: hydrodynamic, nonhydrodynamic, and single particle. We also include a subsection dealing with hard-sphere treatment and one presenting the ionic plasma approach, which is peculiar of conductive systems. In Sec. III we describe the experimental approach to the investigation of microscopic dynamics in liquids, outlining the basics of the inelastic scattering problem. Since the case of x rays is relatively newer, we decided to treat it in detail, but continuous reference is made to neutron scattering in an effort to emphasize merit, drawbacks, and complementarities of the two methods. Section IV is the bulk part of this paper, in which the experimental results are reviewed and ordered element by element. Here we make constant reference to Sec. II to recall the different approaches utilized by different authors to describe the experimental result. In Sec. V, finally, we try to summarize the arising scenario, pointing out the issues which, in our opinion, deserve further investigations and trying to draw, when possible, some conclusive pictures.

II. THEORETICAL BACKGROUND

A. General overview

1. Some basic definitions

The investigation of microscopic dynamics of an ensemble of N identical atomic or molecular units usually proceeds through the study of correlation functions of dynamical variables, i.e., of functions of the phase-space variables, defined as the $6N$ positions $\mathbf{r}_i(t)$ and momenta $\mathbf{p}_i(t)=m\mathbf{v}_i(t)$ of the particles. Relevant dynamical variables are those stemming from the microscopic density $\rho(\mathbf{r},t)$ [whose average is related to the number density $\rho=\langle\rho(\mathbf{r},t)\rangle$], momentum density $\mathbf{J}(\mathbf{r},t)$, and kinetic energy density $E(\mathbf{r},t)$:

$$\rho(\mathbf{r},t) \doteq \frac{1}{\sqrt{N}}\sum_i \delta[\mathbf{r}-\mathbf{r}_i(t)],$$

$$\mathbf{J}(\mathbf{r},t) \doteq \frac{1}{\sqrt{N}}\sum_i \mathbf{v}_i(t)\,\delta[\mathbf{r}-\mathbf{r}_i(t)],$$

$$E(\mathbf{r},t) \doteq \frac{1}{\sqrt{N}}\sum_i \frac{1}{2}mv_i^2(t)\,\delta[\mathbf{r}-\mathbf{r}_i(t)]. \tag{1}$$

In many cases, the study of the dynamics of a tagged particle i can be of interest, and it relies on similar definitions for the single-particle dynamical variables:

$$\rho_s(\mathbf{r},t) \doteq \delta[\mathbf{r}-\mathbf{r}_i(t)],$$

$$\mathbf{J}_s(\mathbf{r},t) \doteq \mathbf{v}_i(t)\,\delta[\mathbf{r}-\mathbf{r}_i(t)],$$

$$E_s(\mathbf{r},t) \doteq \frac{1}{2}mv_i^2(t)\,\delta[\mathbf{r}-\mathbf{r}_i(t)].$$

The well-known van Hove distribution functions $G_d(r,t)$ and $G_s(r,t)$ are related in the classic (not quantum) case to the microscopic self- and collective densities through

$$G(\mathbf{r},t) = G_s(\mathbf{r},t) + G_d(\mathbf{r},t),$$

with

$$G_s(\mathbf{r},t) = \frac{1}{N}\left\langle \sum_i \delta[\mathbf{r}+\mathbf{r}_i(0)-\mathbf{r}_i(t)]\right\rangle,$$

$$G_d(\mathbf{r},t) = \frac{1}{N}\left\langle \sum_i \sum_{j\neq i} \delta[\mathbf{r}+\mathbf{r}_j(0)-\mathbf{r}_i(t)]\right\rangle.$$

As we shall see, experiments usually give information on the correlation functions in the reciprocal Q space. Therefore it can be useful to define the space Fourier transform of the microscopic quantities previously introduced:

$$\rho(\mathbf{Q},t)=\frac{1}{\sqrt{N}}\sum_i e^{-i\mathbf{Q}\cdot\mathbf{r}_i(t)},$$

$$\mathbf{J}(\mathbf{Q},t)=\frac{1}{\sqrt{N}}\sum_i \mathbf{v}_i(t)e^{-i\mathbf{Q}\cdot\mathbf{r}_i(t)},$$

$$E(\mathbf{Q},t)=\frac{1}{\sqrt{N}}\sum_i \frac{1}{2}mv_i^2(t)e^{-i\mathbf{Q}\cdot\mathbf{r}_i(t)},$$

and similarly for the single-particle variables.

The time evolution of these microscopic variables is cross linked and can be studied by replacing them with their average over small but statistically significant volumes. A closed set of equations, basically conservation laws and constitutive relations, can easily be written for these averages.[1] Once the expression for $a(\mathbf{Q},t)$ is known ($a=\rho,\mathbf{J},E$) one can calculate

$$\Phi_{\alpha\beta}(Q,t)=\langle a_\alpha^*(\mathbf{Q})e^{\mathcal{L}t}\alpha_\beta(\mathbf{Q})\rangle_N, \tag{2}$$

in which $a_\alpha(\mathbf{Q})$ are the appropriate dynamical variables, and $\mathcal{L}$ is the Liouville operator ruling the time evolution in the configurational space. The $\langle\cdots\rangle_N$ indicates thermal averages evaluated over the N-particle ensemble (from now on we will omit the subscript N).

In particular, the autocorrelation functions of the microscopic density (both self and collective) play a privileged role, and we define, therefore,

$$F(Q,t)=\langle\rho(Q,t)\rho(-Q,0)\rangle,$$

$$S(Q)=\langle|\rho(Q,t)|^2\rangle,$$

$$\Phi(Q,t)=\Phi_{11}(Q,t)=\frac{F(Q,t)}{S(Q)},$$

$$F_s(Q,t)=\langle\rho(Q,t)\rho_s(-Q,0)\rangle,$$

$$\Phi_s(Q,t)=F_s(Q,t). \tag{3}$$

Consequently,

$$\Phi(Q,t)=\frac{1}{NS(Q)}\sum_{i,j}\langle e^{-i\mathbf{Q}\cdot\mathbf{r}_i(0)}e^{-i\mathbf{Q}\cdot\mathbf{r}_j(t)}\rangle$$

$$=\frac{1}{NS(Q)}\sum_{i,j}\langle e^{-i\mathbf{Q}\cdot\mathbf{r}_i(0)}e^{\mathcal{L}t}e^{-i\mathbf{Q}\cdot\mathbf{r}_j(0)}\rangle, \tag{4}$$

$$\Phi_s(Q,t)=\frac{1}{N}\sum_i\langle e^{-i\mathbf{Q}\cdot\mathbf{r}_i(0)}e^{-i\mathbf{Q}\cdot\mathbf{r}_i(t)}\rangle. \tag{5}$$

The above autocorrelation functions $F(Q,t)$ and $F_s(Q,t)$ are, in fact, connected through their time Fourier transform to the self- and collective dynamic structure factor $S_s(Q,\omega)$ and $S(Q,\omega)$, respectively. These latter, in turn, are the experimentally accessible quantities in neutrons and x-ray inelastic scattering experiments and therefore, in the following, we will mainly refer to the density-density correlation functions.

2. Spectral moments

Before illustrating some models for the evolution of the density autocorrelation function, it is worthwhile to recall here some basic relations involving the frequency moments of the dynamic structure factor. These can be very useful to the experimentalist, as a way to normalize the data [an example is given in Sec. III.B, as well as to any theoretical approach, as a direct test of sum rules—for example, we shall see how the hydrodynamic expression for the density-density time correlation function is valid up to the second frequency moment, because in hydrodynamics the liquid is treated as continuum without atomic structure, and such an information on structure and interatomic potentials appears only within the fourth and higher frequency moments of $S(Q,\omega)$]. By expanding the density autocorrelation function in a Taylor series, one can easily find a connection with the frequency moments of the dynamic structure factor as

$$\left.\frac{d^nF(Q,t)}{dt^n}\right|_{t=0}=(-1)^n\int_{-\infty}^{+\infty}\omega^nS(Q,\omega)d\omega=(-i)^n\langle\omega^n\rangle. \tag{6}$$

Equation (6) holds for the frequency moments of both the collective ($\langle\omega^n\rangle_S$) and the self- ($\langle\omega^n\rangle_{S_s}$) dynamic structure factor. From the previous definitions, it easily follows that $\langle\omega^0\rangle_S=S(Q)$ and $\langle\omega^0\rangle_{S_s}=1$. The first frequency momentum are, on the other side, $\langle\omega^1\rangle_S=\langle\omega^1\rangle_{S_s}=\hbar Q^2/2m$ and therefore are zero for any classical theory, characterized by symmetric spectral functions. The second frequency moments are $\langle\omega^2\rangle_S=\langle\omega^2\rangle_{S_s}=k_BTQ^2/m+O(\hbar^2)$. Higher-order spectral moments depend on the details of the microscopic interactions, and can be analytically derived for additive pairwise interatomic potential (de Gennes, 1959). Some examples will be given in Secs. II.E.5 and II.F.2, while practical usage of sum rules for normalization purposes will be outlined in Sec. III.B.

3. Quantum aspects

The models that we will illustrate in the next sections have been developed for a classical system. The main effect of quantum-mechanical corrections stems from the well-known inequality of the positive- and negative-frequency parts of the spectra, connected by the detailed balance factor $e^{\hbar\omega/k_BT}$. Additional sources of nonclassical behavior, such as those associated with a finite value of the de Broglie wavelength $\Lambda=(2\pi\hbar^2/mk_BT)^{1/2}$, are small (for lithium at melting Λ is only 0.11 times the average interparticle distance, and this ratio decreases for heavier metals) and can safely be neglected. Since the effects of the detailed balance are clearly visible in the experimentally measured dynamic structure factors, we briefly discuss a possible procedure to account for this quantum feature in a consistent way, while preserving the inherent advantages of the classical description. In

[1]From here on we will implicitly assume that we are not dealing with microscopic quantities but rather with the hydrodynamic quantities resulting from their averages

doing this, for the sake of clarity we shall denote all the previous classical quantities with the subscript cl, while the notation q will refer to the quantum case.

The natural theoretical counterpart of the classical density correlation function is the so-called Kubo canonical relaxation function (Kubo and Tomita, 1954),

$$K_q(Q,t) = \frac{1}{\beta N}\sum_{i,j}\int_0^\beta d\lambda \langle e^{-i\mathbf{Q}\cdot\hat{\mathbf{r}}_i(0)} e^{-\lambda\hat{H}} e^{-i\mathbf{Q}\cdot\hat{\mathbf{r}}_j(t)} e^{\lambda\hat{H}}\rangle, \quad (7)$$

where $\beta = 1/k_B T$ and the angular brackets denote now a quantum statistical average. In the classical limit ($\beta \to 0, \hbar \to 0$) the quantum operators become classical commuting dynamical variables and $K_q(Q,t) \to F_{\rm cl}(Q,t)$. It has been shown (Lovesey, 1971) that $K_q(Q,t)$ is a real even function of time, so that its spectrum $K_q(Q,\omega)$ is an even function of frequency. On the other hand, the experimental scattering cross section involves the Fourier transform $S_q(Q,\omega)$ of the quantum density correlator $F_q(Q,t) = (1/N)\Sigma_{i,j}\langle e^{-i\mathbf{Q}\cdot\hat{\mathbf{r}}_i(0)} e^{i\mathbf{Q}\cdot\hat{\mathbf{r}}_j(t)}\rangle$. The relation between $S_q(Q,\omega)$ and $K_q(Q,\omega)$ reads (Lovesey, 1987)

$$S_q(Q,\omega) = \frac{\beta\hbar\omega}{1 - e^{-\beta\hbar\omega}} K_q(Q,\omega),$$

and, as can be easily checked, satisfies the detailed balance condition. Moreover, it can be seen that the relation

$$\langle \omega^{2n}\rangle_K = \frac{2}{\beta\hbar}\langle \omega^{2n-1}\rangle_S \quad (8)$$

connects the even frequency moments of K_q with the odd ones of S_q. In addition, the same memory function framework which will be outlined in Secs. II.E.5 and II.F.1 can be phrased for the Kubo relaxation function and for its Laplace transform $\tilde{K}_q(Q,s)$.

By virtue of all these properties, in a situation where the quantum aspects not associated with detailed balance are marginal, it is reasonable (although not strictly rigorous) to identify the spectrum $K_q(Q,\omega)$ with the classical quantity $S_{\rm cl}(Q,\omega)$ so that

$$S_q(Q,\omega) \simeq \frac{\beta\hbar\omega}{1 - e^{-\beta\hbar\omega}} S_{\rm cl}(Q,\omega). \quad (9)$$

Having assumed such a correspondence, from now on we will drop the subscript cl and refer to the classical quantities as in fact done at the beginning of this section.

The transformation (9) allows one to test classical models against experimental data. It is worthwhile to point out, however, that it alters the frequency moments: as shown in the previous section, for instance, it introduces a $\hbar^2$ correction to the second frequency moment, though this effect has been shown to be hardly noticeable in liquid metals (Scopigno *et al.*, 2000a).

B. Single-particle dynamics in the hydrodynamic regime

The time evolution of the single-particle density can be easily obtained through the continuity equation and the constitutive relation (Fick's law) relating density and current variables:

$$\dot{\rho}_s(\mathbf{r},t) + \Delta\cdot\mathbf{J}_s(\mathbf{r},t) = 0,$$

$$\mathbf{J}_s(\mathbf{r},t) = -D\Delta\rho_s(\mathbf{r},t).$$

It is worthwhile to stress that while the first equation is exact, the second is a phenomenological "closure." Combining the two equations, one gets the diffusion equation straightforward:

$$\dot{\rho}_s(\mathbf{r},t) = D\nabla^2\rho_s(\mathbf{r},t), \quad (10)$$

which, in the reciprocal space, has the solution

$$\rho_s(Q,t) = \rho_s(Q)e^{-DQ^2 t}. \quad (11)$$

The normalized autocorrelation function of the single-particle density is

$$\Phi_s(Q,t) = \langle \rho_s(Q,t)\rho_s(-Q)\rangle = e^{-DQ^2 t}, \quad (12)$$

while its Fourier transform, the self-dynamic structure factor, reads

$$S_s(Q,\omega) = \frac{1}{\pi}\frac{DQ^2}{\omega^2 + (DQ^2)^2}, \quad (13)$$

i.e., a Lorentzian function centered at $\omega = 0$ with full width at half maximum (FWHM) equal to $2DQ^2$. It is worthwhile to point out how, in the hydrodynamic limit, the diffusion coefficient is related to the dynamic structure factor as $D = \lim_{Q\to 0}(\omega^2/Q^2)\pi S_s(Q,\omega)$.

Finally, for completeness, the corresponding van Hove self-correlation function is

$$G_s(r,t) = \frac{1}{(4\pi Dt)^{3/2}} e^{-r^2/4Dt}. \quad (14)$$

C. Collective dynamics in the hydrodynamic regime

In a similar manner as in the previous section, one can build again a set of closed equations but, in this case, Fick's law does not apply, and the situation is more involved. The constitutive relations, indeed, couple together the three conservation laws for the microscopic variables density, momentum, and energy, which in terms of the correspondent fluxes reads

$$\dot{\rho}(\mathbf{r},t) + \boldsymbol{\nabla}\cdot\mathbf{J}(\mathbf{r},t) = 0,$$

$$\dot{\mathbf{J}}(\mathbf{r},t) + \boldsymbol{\nabla}\cdot\sigma(\mathbf{r},t) = 0,$$

$$\dot{E}(\mathbf{r},t) + \boldsymbol{\nabla}\cdot\mathbf{H}(\mathbf{r},t) = 0, \quad (15)$$

where we have defined the momentum flux $\sigma(\mathbf{r},t)$ and the energy flux $\mathbf{H}(\mathbf{r},t)$:

$$\sigma_{\alpha,\beta}(\mathbf{r},t) = \delta_{\alpha,\beta}P(\mathbf{r},t) - \eta\left(\frac{\partial u_\alpha(\mathbf{r},t)}{\partial\tau_\beta} + \frac{\partial u_\beta(\mathbf{r},t)}{\partial\tau_\alpha}\right) + \delta_{\alpha,\beta}\left(\frac{2}{3}\eta - \xi\right)\boldsymbol{\nabla}\cdot\mathbf{u}(\mathbf{r},t),$$

$$\mathbf{H}(\mathbf{r},t) = h\mathbf{u}(\mathbf{r},t) - \kappa \nabla T(\mathbf{r},t),$$

where η and ξ are the shear and bulk viscosities, P and T are the local pressure and temperature fields, h is the enthalpy density, and κ is the thermal conductivity.

Two additional constitutive relations (the Navier-Stokes equation and the Fourier law) call into play the two additional thermodynamic variables pressure P and temperature T. Invoking the thermal equilibrium and the equations of state one obtains a closed set of equations which can be solved to get the density-density correlation function. The detailed derivation of $\rho(Q,t)$ is beyond the purpose of the present review, and can be easily retrieved in classical textbooks (Berne and Pecora, 1976; Hansen and McDonald, 1986). Here we will only recall the final *approximate* results[2] which are

$$\frac{\rho(Q,t)}{\rho(Q)} = \left[\left(\frac{\gamma-1}{\gamma}\right)e^{-D_T Q^2 t} + \frac{1}{\gamma}e^{-\Gamma Q^2 t}\cos c_s Q t\right]$$

$$\frac{S(Q,\omega)}{S(Q)} = \frac{1}{2\pi}\left[\left(\frac{\gamma-1}{\gamma}\right)\frac{2D_T Q^2}{\omega^2 + (D_T Q^2)^2}\right],$$

$$+\frac{1}{\gamma}\left[\frac{\Gamma Q^2}{(\omega + c_s Q)^2 + (\Gamma Q^2)^2} + \frac{\Gamma Q^2}{(\omega - c_s Q)^2 + (\Gamma Q^2)^2}\right], \tag{16}$$

having defined

$$\gamma = \frac{c_P}{c_V},$$

$$D_T = \frac{\kappa}{\rho m C_P},$$

$$\Gamma = \frac{1}{2\rho m}\left[\frac{4}{3}\eta_s + \eta_B + \frac{(\gamma-1)\kappa}{c_P}\right]. \tag{17}$$

In the above expressions c_P and c_V are the specific heat ratios at constant pressure and volume, η_s and η_B are the shear and bulk viscosities, κ is the thermal conductivity, and $c_s = \sqrt{(\gamma/m)(\partial P/\partial \rho)_T}$ is the adiabatic sound velocity.

Classical hydrodynamics therefore predicts in the long-wavelength limit ($Q \to 0$) a frequency spectrum for the density fluctuations constituted by two main features. The central part of the spectrum is dominated by a quasielastic, nonpropagating mode related to entropy fluctuations (Rayleigh component) of linewidth $\Gamma_{qe} = 2D_T Q^2$, which reflects the fact that thermal fluctuations decay over a finite lifetime $\tau = 2/\Gamma_{qe}$. Beside, two symmetrically shifted inelastic components peaked at frequency $\omega_s = \pm c_s Q$ are the signature of propagating pressure waves (Brillouin doublet), which are damped by a combination of viscous and thermal effects. The ratio between the Rayleigh and the Brillouin component is given by the Landau-Placzeck ratio

$$\frac{I_R}{2I_B} = \gamma - 1. \tag{18}$$

Usually, the hydrodynamic regime is investigated by visible light-scattering spectroscopy (Brillouin light scattering). In the case of liquid metals, the light-scattering study of density fluctuations is prevented by the nontransparent nature of these systems.[3]

Inelastic scattering experiment can, in fact, only be performed by means of higher energy photons (x rays) or by neutrons, but in both cases the probed wave vectors are fairly outside the strict hydrodynamic region.

The way the Brillouin triplet evolves at finite Q is far from being fully understood, though some simplified phenomenological models have been proposed in the past (McGreevy and Mitchell, 1985). Primarily, one should account for the frequency dependence of the transport coefficients which, as we shall see, corresponds to abandon the hypothesis of Markovian dynamics. Second, once the wave vector approaches the inverse interparticle distances, structural effects are expected in the form of a Q dependence of all the thermodynamic quantities. Last, but not least, it is highly questionable whether the role of the thermal and viscous processes remains well separated at high Q. In particular, specifically in the case of liquid metals, due to the high thermal conductivity one expects $D_T Q^2$ to become soon of the order of the Brillouin frequency, so that entropy and density fluctuations become closely interwoven. Strangely enough, this aspect, with a few exceptions (Faber, 1972) did not receive much attention in the past, although lately it has been the matter of some debate (Singh and Tankeshwar, 2003, 2004; Scopigno and Ruocco, 2004).

Before coming in the discussion of the evolution of $S(Q,\omega)$ at increasing Q values, above the hydrodynamic limit, it is worthwhile to discuss another analytically solvable case: the high-Q limit.

[2]The exact hydrodynamics expression contains a small additional contribution which makes the Brillouin components asymmetric, as emphasized by Nichols and Carome (1968) and by Verkerk (2001). The resulting line shape can be easily recognized as the already mentioned damped harmonic oscillator, originally proposed within a solidlike picture (Fåk and Dorner, 1997), which can be actually retrieved by a liquidlike point of view within the memory function formalism, shown in Sec. II.F.2.

[3]In the case of copper, for instance, the distance to the Fermi surface is 2.3 eV. Thus electrons are promoted by energies associated with the blue-green end of the spectrum. As a result, red and orange light at the opposite end of the spectrum is reflected back and gives copper its characteristic color. With the alkali metals, the *s* electron is involved in promotion to the Fermi level. There is little overlap to the empty 3*p* and 3*d* orbitals that contribute to the conduction band. Therefore only radiation close to the ultraviolet region is absorbed and visible light is reflected, hence the silverlike appearance of the alkali liquid metals.

D. The short-wavelength limit

In the previous sections we examined the self- and collective motion at very small wave vectors and frequencies. In the opposite regime, i.e., at short distances and time scales, the particles of a fluid are expected to move as if they were free, as it happens in an ideal gas. Since in this case the behaviors of different particles are uncorrelated $[G_d(r,t)=0]$, the self- and collective dynamic structure factors coincide in this limit.

The correlation function of Eq. (3) can be easily calculated for a free particle, i.e., for $\mathbf{r}_i(t)=\mathbf{r}_i(0)+\mathbf{v}_i t$. The classical free particle correlation function is

$$F(Q,t)=\frac{1}{N}\sum_i \langle e^{-i\mathbf{Q}\cdot(\mathbf{p}_i/m_i)t}\rangle = \langle e^{-i\mathbf{Q}\cdot(\mathbf{p}/m)t}\rangle, \tag{19}$$

evaluating the thermal average one easily gets

$$F(Q,t)=\int e^{-p^2/2mk_BT}e^{-iQpmt}dp = e^{-k_BTQ^2t^2/2m}, \tag{20}$$

and the corresponding dynamic structure factor is

$$S(Q,\omega)=\sqrt{\frac{m}{2\pi k_BTQ^2}}e^{-m\omega^2/2k_BTQ^2}. \tag{21}$$

By virtue of the previously mentioned considerations, the van Hove self-correlation function reads

$$G_s(r,t)=\left(\frac{m}{2\pi k_BTt^2}\right)^{3/2}e^{-mr^2/2k_BTt^2}. \tag{22}$$

In the quantum case the correlation function (19) can be evaluated treating $\mathbf{r}_i$ and $\mathbf{p}_i$ as operators, and paying attention to the fact that, in this case, the product of the exponential in Eq. (3) cannot be reduced to a single exponential, as in the classical treatment. Invoking the identity $e^{\hat{A}}e^{\hat{B}}=e^{\hat{A}+\hat{B}+(1/2)[\hat{A},\hat{B}]}$, holding when, as in the present case, $[\hat{A},\hat{B}]$ is a number, one can write

$$\begin{aligned}\langle e^{-i\mathbf{Q}\cdot\mathbf{r}_i(0)}e^{i\mathbf{Q}\cdot\mathbf{r}_i(t)}\rangle &= \langle e^{i\mathbf{Q}\cdot[\mathbf{r}_i(t)-\mathbf{r}_i(0)]+(\mathbf{Q}^2/2)[\mathbf{r}_i(0)\cdot\mathbf{r}_i(t)]}\rangle \\ &= \langle e^{i\mathbf{Q}\cdot(\mathbf{p}_i/m)t-(\mathbf{Q}^2/2)[(\mathbf{p}_i/m)t,\mathbf{r}_i(t)]}\rangle \\ &= e^{i\hbar(Q^2t/2m)}\langle e^{-i\mathbf{Q}\cdot(\mathbf{p}/m)t}\rangle,\end{aligned}$$

and, using the result of Eq. (19), one obtains

$$F(Q,t)=e^{-(Q^2/2m)(k_BTt^2-i\hbar t)}, \tag{23}$$

the correspondent dynamic structure factor:

$$S(Q,\omega)=\sqrt{\frac{m}{2\pi k_BTQ^2}}e^{-(m/2k_BTQ^2)(\omega-\hbar Q^2/2m)^2}. \tag{24}$$

Summing up, the quantum dynamic structure factor for a free moving particle is a Gaussian with recoil energy $\omega_R(Q)=\hbar Q^2/2m$ and linewidth $\sigma=\sqrt{k_BT/M}Q$. It is worthwhile to point out that Eq. (24) satisfies the detailed balance condition $S(Q,\omega)=e^{\hbar\omega/k_BT}S(Q,-\omega)$ and coincides with the classical case for $\hbar\to 0$ or, equivalently, for $T\to\infty$. As far as the sound velocity is concerned, one can still define the apparent frequencies $\omega_l(Q)=\frac{1}{2}(\omega_R\pm\sqrt{8\sigma^2+\omega_R^2})$ as the positive and negative maxima of the longitudinal current $C_L(Q,\omega)=\omega^2S(Q,\omega)/Q^2$. In the classical case, the two values coincide and are $\omega_l(Q)=\sqrt{2}\sigma$.

E. The nonhydrodynamic region: Single particle

1. The Gaussian approximation

As can be easily noticed looking at the expressions (14) and (22), both the hydrodynamic and the ideal gas limit end up with the van Hove correlation functions that are Gaussian in r. On the basis of this observation it seems natural to assume the Gaussian dependence as valid in the whole dynamical range. In terms of the second moment of $G_s(r,t)$ one can write the following expression:

$$G_s(r,t)=\sqrt{\frac{3}{2\langle r^2(t)\rangle}}e^{-3r^2/2\langle r^2(t)\rangle}, \tag{25}$$

where $\langle r^2(t)\rangle$ is the mean-square displacement which in the hydrodynamic and single-particle approximations reads $\langle r^2(t)\rangle=6Dt$ and $\langle r^2(t)\rangle=(3KT/m)t^2$, respectively.

In the Gaussian approximation therefore the self-scattering function is related to the mean-square displacement which can be, for instance, inferred by molecular-dynamics simulations.

2. The jump diffusion model

The jump diffusion model was first introduced by Chudley and Elliot (1961). The particle is thought to live for a residence time τ_0 in the cage of its neighbors, and at some point to change cage. In some sense therefore it is the opposite of collisional models, where the free diffusion of a particle is sometimes interrupted by collisional events. The jump diffusion model sets a rate equation for the van Hove self-scattering function of the kind

$$\frac{\partial G_s(\mathbf{r},t)}{\partial t}=\frac{1}{\mathcal{N}\tau_0}\sum_{\mathbf{l}} G_s(\mathbf{r}+\mathbf{l},t)-G_s(\mathbf{r},t),$$

with $\mathcal{N}$ the number of available residence sites.

By Fourier transform in space and time one immediately gets

$$S_s(Q,\omega) = \frac{1}{\pi}\frac{f(Q)}{\omega^2 + f(Q)^2}, \tag{26}$$

which is a Lorentzian function with Q-dependent damping

$$f(Q) = -\frac{1}{n\tau_0}\sum_{\mathbf{l}} (e^{i\mathbf{Q}\cdot\mathbf{l}} - 1). \tag{27}$$

This latter can be conveniently estimated supposing that the vectors $\mathbf{l}$ have random and continuous orientations and distributions. In this case one can average Eq. (27):

$$f(Q) = -\frac{1}{\tau_0}\left[1 - \frac{1}{1 + Q^2 l_0^2}\right].$$

It can be easily shown that Eq. (26) tends to the Fick's free diffusion expression (13) (Egelstaff, 1967).

3. The mode coupling theory

The Laplace transform of the intermediate scattering function can be generally written as

$$\tilde{S}(Q,s) = \frac{1}{s + Q^2\tilde{U}(Q,s)},$$

$\tilde{U}(Q,s)$ being a generalized frequency and wave-vector-dependent diffusion coefficient. The mode coupling theory provides a self-consistent expression for $\tilde{U}_s(Q,s)$ (de Schepper and Ernst, 1979), and the resulting self-dynamic structure factor reads

$$S_s(Q,\omega) \approx \frac{1}{\pi}\frac{DQ^2}{\omega^2 + (DQ^2)^2} + \frac{1}{\pi DQQ^*}\,\mathrm{Re}\,G\left(\frac{i\omega + DQ^2}{\delta DQ^2}\right), \tag{28}$$

with

$$G(s) = \arctan\left(\frac{1}{\sqrt{s-1}}\right) - \frac{(s-2)\sqrt{s-1}}{s^2}, \tag{29}$$

where $Q^* = 16\pi m\rho D^2/k_B T$ and $\delta = D/(D+\nu)$, D being the diffusion coefficient and ν the kinematic viscosity.

An estimate of the FWHM can be numerically evaluated (De Jong, 1993), yielding

$$\Delta\omega \approx \left[1 - \frac{Q}{Q^*}H(\delta) + O(Q^{3/2})\right]DQ^2, \tag{30}$$

with

$$H(\delta) \approx 1.45\delta^{3/2}[1 - 0.73\delta - 0.15\delta^2 - O(\delta^3)]. \tag{31}$$

4. The Nelkin-Ghatak model

Nelkin and Ghatak have considered a dilute gas in which the atomic motion is dominated by binary collisions, with a distribution function obeying a linearized Boltzmann's equation, valid in a small disturbance limit, i.e., for arbitrary large fluctuations compared to the mean collision time. In terms of the reduced variables $x = -\omega/Qv_0$ and $y = \alpha/Qv_0$, with $v_0 = \sqrt{2KT/m}$ and α an adjustable parameter, and by introducing the real $[u(x,y)]$ and imaginary $[v(x,y)]$ parts of the probability integral for complex argument $z(x+iy) = \int_{-\infty}^{+\infty} e^{-t^2}(z-t)^{-1}dt$:

$$U(x,y) = \sqrt{\pi}yu(x,y), \tag{32}$$

$$V(x,y) = \sqrt{\pi}yv(x,y), \tag{33}$$

one gets the following expression for the incoherent scattering function (Nelkin and Ghatak, 1964):

$$S_s^{NG}(Q,\omega) = \frac{1}{\pi\alpha}\frac{U(1-U) - V^2}{(1-U^2) + V^2}. \tag{34}$$

It can be easily noticed that Eq. (34) has the correct low-Q (Lorentzian) and high-Q (Gaussian) limits: in the first case it is sufficient to pose $\alpha = v_0^2/2D$, while at high Q's one has that $y \to 0$ and the familiar Gaussian shape is recovered.

5. The memory function formalism

The easiest way to abandon the hydrodynamic region is to assume the frequency dependence of the transport coefficients, entering the so-called generalized hydrodynamics. The natural playground for performing such step is the memory function framework (Mori, 1965): we will recall here the basic formalism while a detailed treatment can be found in specialized books (Balucani and Zoppi, 1983; Hansen and McDonald, 1986). Let $\mathbf{M}^{(0)}$ be the correlation matrix of a given set of dynamical variables $\mathbf{A}$ $[M_{\nu\sigma}^{(0)} = \langle A_\nu^* A_\sigma(t)\rangle]$. The equation of motion of $\mathbf{M}^{(0)}(t)$ can be conveniently expressed in terms of a chain of arbitrary order n of integrodifferential equation involving appropriate memory functions $\mathbf{M}^{(i)}(t)$ for $i = 1, \ldots, n$:

$$\frac{d\mathbf{M}^{(i-1)}}{dt} - i\mathbf{\Omega}^{(i-1)}\mathbf{M}^{(i-1)} + \int_0^t \mathbf{M}^{(i)}(t-t')\mathbf{M}^{(i-1)}(t')dt' = 0, \tag{35}$$

with

$$i\mathbf{\Omega}^{(i-1)} = \dot{\mathbf{M}}^{(i-1)}(0)\cdot[\mathbf{M}^{(i-1)}(0)]^{-1}. \tag{36}$$

Here $\mathbf{\Omega}^{(i-1)}$ is a set of generalized frequency matrixes, while the memory kernels $\mathbf{M}^i(t)$ rule the dynamical evolution of the observables correlation matrix $\mathbf{M}^{(0)}$.

In the specific case of self-dynamics, as we have seen in Sec. II.B the relevant set of variables is given by the self-density only, therefore $M^{(0)}(t) = \phi_s(t)$. The equations of motion for the density correlation function are

$$\frac{d\phi_s(Q,t)}{dt} + \int_0^t M^{(1)}(Q,t-t')\phi_s(Q,t')dt' = 0, \tag{37}$$

$\Omega^{(0)} = 0$ being due to the orthogonality of ρ_s and $\dot{\rho}_s$.

A good description of the evolution of $\phi_s(Q,t)$ is normally gained utilizing the first two equations of the chain (35). In terms of Laplace transform it holds that

$$\tilde{\phi}_s(Q,t) = [s + \tilde{M}^{(1)}(Q,s)]^{-1} = \left[s + \frac{M^{(1)}(Q,t=0)}{s + \tilde{M}^{(2)}(Q,s)} \right]^{-1}. \tag{38}$$

The initial values $\mathbf{M}^{(i)}(t=0)$, can be easily obtained from the general relation

$$\mathbf{M}^{(i)}(0) = -\ddot{\mathbf{M}}^{(i-1)}(0) \cdot [\mathbf{M}^{(i-1)}(0)]^{-1} - [\mathbf{\Omega}^{(i-1)}]^2, \tag{39}$$

which, in turn, is obtained deriving Eq. (35) and exploiting Eq. (36). For the first two memory functions it holds therefore that

$$M^{(1)}(Q,0) = \frac{k_B T Q^2}{m} = \langle \omega^2(Q) \rangle_{S_s},$$

$$M^{(2)}(Q,0) = 2\langle \omega^2(Q) \rangle_{S_s} + \Omega_0^2 = \frac{\langle \omega^4(Q) \rangle_{S_s}}{\langle \omega^2(Q) \rangle_{S_s}} - \langle \omega^2(Q) \rangle_{S_s}. \tag{40}$$

Here $\langle \omega^n(Q) \rangle_{S_s}$ are the frequency moments of $S_s(Q,\omega)$ and the quantity Ω_0^2 is related to the mean-squared force $\langle |\mathbf{F}|^2 \rangle$ acting on the diffusing particle and, for a system of identical particle interacting via pairwise interactions potential $V(r)$, it holds that

$$\Omega_0^2 = \frac{\langle |\mathbf{F}|^2 \rangle}{3mk_BT} = \frac{\rho}{3m} \int \nabla^2 V(r) g(r) d\mathbf{r}, \tag{41}$$

where $g(r)$ is the pair distribution function.

It is worthwhile to stress that Eq. (38) is the exact solution of motion in which all the dynamics is detailed by the shape of the second-order memory function $M^{(2)}(Q,t)$. The most common way of solving the equation is making a guess on the shape of the memory function. A useful approximation is provided by the exponential shape, which has the advantage of being easily Laplace transformed:

$$M^{(2)}(Q,t) = \Delta_s^2(Q) e^{-t/\tau_s(Q)} = [2\langle \omega^2(Q) \rangle_{S_s} + \Omega_0^2] e^{-t/\tau_s(Q)}. \tag{42}$$

With such a choice it follows straightforward that

$$S_s(Q,\omega) = \frac{1}{\pi} \frac{\langle \omega^2 \rangle_{S_s} (2\langle \omega^2 \rangle_{S_s} + \Omega_0^2) \tau_s}{\omega^2 \tau_s (\omega^2 - 3\langle \omega^2 \rangle_{S_s} - \Omega_0^2)^2 + (\omega^2 - \langle \omega^2 \rangle_{S_s})^2}. \tag{43}$$

It is interesting now to look at the FWHM $\Gamma_s(Q)$ of Eq. (43). In the small-Q limit it is easy to show that

$$\frac{\Gamma_s(Q)}{DQ^2} = \frac{1}{\sqrt{1 + \frac{2k_BT}{m\Omega_0^2} Q^2}}. \tag{44}$$

The memory function approach with exponential kernel therefore predicts a quasielastic line shape narrower than the hydrodynamic one, a result which is in agreement with several experimental data. Contrarily, in the Gaussian approximation the linewidth is always larger than the hydrodynamic value.

Theoretical expressions have been proposed in the past for the memory function in terms of kinetic theory, splitting the memory function in a contribution due to uncorrelated binary collision, obtained by a Fokker-Plank equation, and a long time contribution representing the coupling of a tagged particle to the collective motion of the surrounding particles. This approach has been tested in hard spheres, Lennard-Jones, and alkali metals (Sjögren, 1979; Sjögren and Sjölander, 1979; Bengtzelius *et al.*, 1984).

F. The nonhydrodynamic region: Collective motion

1. The Langevin equation

The most reliable approach to the study of collective dynamics at finite wave vectors parallels the one adopted for the single particle in Sec. II.E, i.e., an extension of the classical hydrodynamics assisted by the formalism of the memory function ruling the Langevin equation of motion of the density fluctuations.

We will deal therefore with a 3×3 correlation matrix $\mathbf{M}^{(0)}$, and a set of n (with n arbitrary large) memory matrixes $\mathbf{M}^{(i)}$ with the same dimensionality and coupled by the chain of n equations (35). Actually, in order to work with an orthogonal set of variables (and energy and density are not), one normally prefers to replace the microscopic energy with the microscopic temperature $T(Q) = [1/m\rho c_V(Q)] \{E(Q) - [\langle E^*(Q)\rho(Q) \rangle / \langle \rho^*(Q)\rho(Q) \rangle] \rho(Q)\}$. With this choice, solving for $\phi(Q,t) = M^{(0)}_{\rho\rho}(Q,t)/M^{(0)}_{\rho\rho}(Q,0) = F(Q,t)/S(Q)$ in terms of Laplace transform one has

$$\tilde{\phi}(Q,s) = \cfrac{1}{s + \cfrac{\omega_0^2(Q)}{s + \tilde{M}^{(1)}_{JJ}(Q,s) - \cfrac{[\tilde{M}^{(1)}_{JT}(Q,s) - i\Omega^{(0)}_{JT}][\tilde{M}^{(1)}_{TJ}(Q,s) - i\Omega^{(0)}_{TJ}]}{s + \tilde{M}^{(1)}_{TT}(Q,s)}}}, \tag{45}$$

where

$$\omega_0^2(Q) = k_B T Q^2/mS(Q). \tag{46}$$

Recalling the definition of the isothermal sound velocity $c_t = \sqrt{1/\rho m \chi_T}$, and the expression for the low $Q \to 0$ limit of the static structure factor $S(0) = \rho \chi_T k_B T$ it seems natural to introduce a finite Q generalization of the isothermal sound velocity as $c_t(Q) = \omega_0(Q)/Q$.

It is easy to recognize in Eq. (45) the same structure of Eq. (38), once the following identification is made:

$$\tilde{M}^{(\mathrm{eff})}_{\rho\rho}(Q,s) = \tilde{M}^{(1)}_{JJ}(Q,s) - \frac{[\tilde{M}^{(1)}_{JT}(Q,s) - i\Omega^{(0)}_{JT}(Q)][\tilde{M}^{(1)}_{TJ}(Q,s) - i\Omega^{(0)}_{TJ}(Q)]}{s + \tilde{M}^{(1)}_{TT}(Q,s)}.$$

The effective memory function $\tilde{M}^{(\mathrm{eff})}_{\rho\rho}(Q,t)$ therefore can be formally considered as the second-order memory function of a chain of two equations for the single variable $\rho(Q,t)$:

$$\frac{dF(Q,t)}{dt} + \int_0^t M^{(1)}(Q,t-t')F(Q,t')dt' = 0,$$

$$\frac{dM^{(1)}(Q,t)}{dt} + \int_0^t M^{(2)}(Q,t-t')M^{(1)}(Q,t')dt' = 0, \tag{47}$$

which, as can be easily verified, corresponds to the single second-order integrodifferential equation:

$$\ddot{\phi}(Q,t) + \omega_0^2(Q)\phi(Q,t) + \int_0^t M(Q,t-t')\dot{\phi}(Q,t')dt' = 0. \tag{48}$$

From here on, to save writing, we define $M(Q,t) = M^{(2)}(Q,t) = \tilde{M}^{(\mathrm{eff})}_{\rho\rho}(Q,t)$.

From knowledge of $\tilde{\phi}(Q,s)$ one straightforwardly obtains $S(Q,\omega) = [S(Q)/\pi]\mathrm{Re}\{\tilde{\phi}(Q,s=i\omega)\}$ in terms of the real (M') and imaginary ($-M''$) parts of the Fourier-Laplace transform of the memory function:

$$S(Q,\omega) = \frac{S(Q)}{\pi} \frac{\omega_0^2(Q)M'(Q,\omega)}{[\omega^2 - \omega_0^2 - \omega M''(Q,\omega)]^2 + [\omega M'(Q,\omega)]^2}. \tag{49}$$

The spectral features of the dynamic structure factor can be characterized by its frequency moments $\langle \omega^n(Q) \rangle_S \equiv \int \omega^n S(Q,\omega) d\omega$, where, for a classical system, only the even frequency moments [such as $\langle \omega^0(Q) \rangle_s = S(Q)$ and $\langle \omega^2(Q) \rangle_s = (k_B T/m)Q^2$] are different from zero.

It can be easily proven that the dynamic structure factor is related to the longitudinal current spectrum through the relation $C_L(Q,\omega) = (\omega^2/Q^2)S(Q,\omega)$. The presence of the factor ω^2 wipes out the low-frequency portion of the dynamic structure factor, and consequently emphasizes the genuine inelastic features of $S(Q,\omega)$. After its definition and Eq. (38), it is readily seen that the Laplace transform $\tilde{C}_L(Q,s)$ satisfies

$$\tilde{C}_L(Q,s) = -s[s\tilde{F}(Q,s) - S(Q)] = \frac{k_B T}{m}\{s + [\omega_0^2(Q)/s] + \tilde{M}(Q,s)\}^{-1}. \tag{50}$$

Again, the spectrum $C_L(Q,\omega)$ can be expressed as $(1/\pi)\mathrm{Re}\{\tilde{C}_L(Q,s=i\omega)\}$. Then the position and the width of the inelastic peaks in $C_L(Q,\omega)$ are determined by the poles of $\tilde{C}_L(Q,s)$.

2. Collective memory function and hydrodynamics

The effective, second-order memory function $M(Q,t)$ accounts for all the relaxation mechanisms affecting collective dynamics and, consequently, is the central quantity in most theoretical approaches. In analogy with the single-particle case [Eq. (40)], the initial value of $M(Q,t)$ is related to the spectral moments of $S(Q,\omega)$ by

$$M(Q,0) = \frac{\langle \omega^4(Q) \rangle_S}{\langle \omega^2(Q) \rangle_S} - \langle \omega^2(Q) \rangle_S \doteq \Delta^2(Q). \tag{51}$$

Along the same line, relations similar to Eqs. (40) and (41) hold, and an explicit expression for $\langle \omega^4(Q) \rangle_S$ can be given, involving both the derivatives of the interparticle potential and the pair distribution function:

$$\frac{\langle \omega^4(Q) \rangle_S}{\langle \omega^2(Q) \rangle_S} = \frac{3K_B T Q^2}{m} + \frac{\rho}{m} \int \frac{\partial^2 V(r)}{\partial z^2}(1 - e^{-iQz})g(r)d^3r. \tag{52}$$

The second and fourth frequency moments are particularly significant, as they rule the sound velocity in the whole Q-ω domain. For sufficiently large s, indeed, $\tilde{M}(Q,s) \simeq M(Q,t=0)/s$ and Eq. (50) is seen to have poles at $s = \pm i\sqrt{\omega_0^2(Q) + \Delta^2(Q)} \doteq \pm i\omega_\infty(Q)$. This latter relation defines the frequency $\omega_\infty(Q)$ which characterizes the instantaneous collective response of the liquid at the wave vector Q and, in turn, defines the unrelaxed sound velocity as $c_\infty(Q) \equiv \omega_\infty(Q)/Q$. In the opposite limit, i.e., for small s, one easily verifies that $\tilde{M}(Q,s) \simeq \int M(Q,t)dt$. In this (relaxed) regime therefore the poles of the longitudinal current are located at $s = \pm i\omega_0^2(Q)$, i.e., the longitudinal modes propagate with the isothermal sound velocity $c_t(Q) = \omega_0(Q)/Q$. Summing up, whatever the details of the memory function are, in the presence of a relaxation process one observes a transition of the longitudinal sound velocity between two different regimes, associated with the evolution of the longitudinal current correlation maxima. It is interesting to study in a parallel way the evolution of $S(Q,\omega)$. In the low-frequency limit, Eq. (49) reduces to the spectrum of a damped harmonic oscillator (DHO) of characteristic frequency ω_0 (which, in general, does not coincide with the position of the inelastic maximum), with damping $\Gamma = \int M(Q,t)dt$:

$$\frac{S(Q,\omega)}{S(Q)} = \frac{1}{\pi}\frac{\omega_0^2(Q)\Gamma(Q)}{(\omega^2-\omega_0^2)+\omega^2\Gamma^2}. \quad (53)$$

In the opposite, high-frequency, limit, again Eq. (49) tends to a harmonic oscillator with no damping and with an higher characteristic frequency $\pm\omega_\infty(Q)$. Additionally, an elastic peak appears of area $\Delta^2(Q)/[\omega_0^2(Q)+\Delta^2(Q)]$. The same results can be directly retrieved in the time domain from Eq. (49), substituting the high-frequency limit (constant) and low-frequency limit (delta shaped) of the memory function, in turn, and taking the Fourier transform.

The memory function formalism leads, in the small-wave-vector limit, to the hydrodynamic prediction of Eq. (16). It can be easily proven, indeed, that the diagonal terms of the memory matrix appearing in Eq. (45) have a Q^2 dependence, while the cross terms follow a Q^4 dependence. For $Q\to 0$ therefore these latter can be neglected. Moreover, from the continuity equations (15) it follows that in the same limit the time dependence of the conserved quantities and their associated currents becomes increasingly slow. Consequently, one can model the decay of the terms $M^1_{JJ}(Q\to 0,t)$ and $M^1_{TT}(Q\to 0,t)$ as instantaneous, or, equivalently, constant in the Laplace domain. By making the identifications $\tilde{M}^1_{JJ}(Q\to 0,s)=D_V Q^2$ and $\tilde{M}^1_{TT}(Q\to 0,s)=\gamma D_T Q^2$, and computing $\Omega^{(0)}_{JT}(Q)\Omega^{(0)}_{TJ}(Q)=(\gamma-1)\omega_0^2(Q)$, from Eq. (45) one gets for the memory function

$$\tilde{M}(Q\to 0,s) = D_V Q^2 + \frac{(\gamma-1)\omega_0^2(Q)}{s+\gamma D_T Q^2},$$

$$M(Q\to 0,t) = 2D_V Q^2\delta(t) + \omega_0^2(Q)(\gamma-1)e^{-\gamma D_T Q^2 t}. \quad (54)$$

The dynamic structure factor can be obtained by substituting Eq. (54) in the general expression (49). In the $Q\to 0$ limit, moreover, one has $\omega_0 = c_t Q \gg \gamma D_T Q^2$. In this limit, $S(Q,\omega)$ is (i) a DHO function around the Brillouin peaks, which are located at $\omega_s=\sqrt{\gamma}c_t Q$ (adiabatic sound propagation) and have a linewidth $D_V Q^2+(\gamma-1)D_T Q^2$, (ii) a Lorentzian function around $\omega=0$, whose linewidth is $2D_T Q^2$. In the small damping limit, the DHO is well approximated by two symmetrically shifted Lorentzians, and the hydrodynamic limit of Eq. (16) is finally recovered.

The advantage of the memory function approach is, however, in providing a way to generalize the hydrodynamic result for wave-vector and frequency-dependent transport coefficients. To this purpose, from the very start it is convenient to separate in $M(Q,t)$ the decay channels which explicitly involve couplings to thermal fluctuations $[M_{\rm th}(Q,t)]$ from those directly associated with longitudinal density modes $[M_L(Q,t)]$.

3. Finite wavelengths generalization: Beyond hydrodynamics

A straightforward generalization of ordinary hydrodynamics at finite wave vectors suggests for the thermal contribution the following form:

$$M_{\rm th}(Q,t) \approx [\gamma(Q)-1]\omega_0^2(Q)\exp[-\gamma D_T(Q)Q^2 t], \quad (55)$$

where $D_T(Q)$ and $\gamma(Q)$ can be regarded as a finite Q *generalization* of the quantities $D_T=\kappa/nC_P$, being κ the thermal conductivity, and $\gamma=c_P/c_V$.

It must be stressed, however, how the extension to finite wave vectors, in the special case of highly conductive systems, requires attention to the physics behind this model. As pointed out by Faber (1972), in a liquid metal, due to the high thermal conductivity, the quantity $\gamma D_T(Q)Q^2$ may easily become larger than the Brillouin frequency as soon as $Q\approx c_t(Q)/D_T(Q)$.[4] Actually, both $c_t(Q)$ and $D_T(Q)$ are expected to decrease on approaching values comparable to the inverse mean interparticle distance, i.e., in coincidence with the first sharp rising edge of $S(Q)$. But assuming that the transition occurs below this edge, one finds the crossover condition $Q=c_t/D_T$ which, considering typical values of sound speed and thermal diffusivity of metals (a few thousand m/s and $\approx 50\ \mathrm{nm}^{-2}/\mathrm{ps}$, respectively), lies at wave vectors around $0.1-0.5\ \mathrm{nm}^{-1}$, which is indeed consistent with the initial assumption. In other words, on increasing the momentum transfer, the thermal peak broadens ultimately overlapping with the Brillouin lines, the sound propagation turns from adiabatic to isothermal, and independent thermal fluctuations become impossible. Using the memory function point of view, at wave vectors $Q \gg c/D_T$ (i.e., when the condition $\omega\tau_{\rm th}\ll 1$ holds), $M_{\rm th}$ decays instantaneously in a similar fashion to M_L. With this condition, the dynamic structure factor is a DHO with isothermal characteristic frequency, while the Brillouin damping is given by the area under the memory function which is $D_V Q^2+(\gamma-1)c_t^2/\gamma D_T$. The existence of this adiabatic to isothermal crossover is expected just below the lowest accessible values of momentum transfer of an inelastic scattering experiment ($\approx 1\ \mathrm{nm}^{-1}$ at present) and therefore has never been observed directly. Moreover, the magnitude of this effect is ruled by $\gamma-1$, which is normally very small. A remarkable exception to this latter condition is constituted by nickel (Bermejo *et al.*, 2000) ($\gamma=1.88$), which has been studied by INS, as it will be discussed in the next section.

Beside the thermal contribution, the viscous term D_V is also expected to exhibit a Q dependence. For simplified Lennard-Jones pairwise interaction a decay has been shown of $\eta_l(Q)$ of a factor of ten up to the main

[4]More specifically, the discrepancy observed in liquid lead between the sound velocity measured with ultrasound (adiabatic) and with inelastic neutron scattering has been tentatively assigned to the isothermal nature of the sound propagation at the wave vectors probed with neutrons.

peak of $S(Q)$, with η_B becoming negative over the same region (Tankeshwar, 1994).

4. Finite frequencies generalization: Viscoelasticity

A second important generalization of transport coefficients concerns their possible frequency dependence.

This latter case stems when the frequencies of the observed density fluctuations are high enough that their time scale competes with the one ruling the decay of M_L. In this condition, one has to drop the hypothesis on the instantaneous (Markovian) nature of the viscous term, and one has to introduce a finite time scale (τ) for the decay of M_L. As discussed at the beginning of this section, the time scale of M_L sets a new crossover between two different regimes, characterized by different sound velocities and attenuations.

The simplest practical way to go beyond the hydrodynamic result (54) is to allow for an exponential decay of $M_L(Q,t)$:

$$M_L(Q,t) = \Delta_L^2(Q) e^{-t/\tau(Q)}, \tag{56}$$

with $\Delta_L^2(Q) = \omega_L(Q)^2 - \gamma\omega_0(Q)^2$, in order to have the correct normalization of the whole $M(Q,t=0)$.

Although this has the advantage of analytical simplicity when dealing with Fourier transform, a drawback of this ansatz lies in the violation of some basic short-time features of the memory function (such as a zero derivative at $t=0$), causing the divergency of $\langle\omega^n\rangle_S$ for $n \geqslant 6$.

Neglecting thermal effects, Eq. (56) yields the so-called *viscoelastic model*[5] for $S(Q,\omega)$ (Lovesey, 1971). Since as $Q \to 0$, $\tilde{M}_L(Q,s=0)/Q^2$ can be written as $[c_\infty^2 - c_0^2]\tau(Q \to 0)$, the requirement that this coincides with η_L/nm shows that the time $\tau(Q)$ must be finite as $Q \to 0$. Such a connection with viscous effects justifies the physical interpretation of the rate $1/\tau(Q)$ as a parameter giving an overall account of all relaxation processes by which the longitudinal response of the liquid is affected by time-dependent disturbances. In particular, for slow perturbations developing over a time scale $t \gg \tau(Q)$ the system can adjust itself to attain local equilibrium and the usual viscous behavior holds. In contrast, for density fluctuations fast enough that $t \ll \tau(Q)$ the liquid responds instantaneously with a solidlike (elastic) behavior. The crossover between these limiting situations marked by frequencies ω such that $\omega\tau(Q) \approx 1$ is ultimately responsible for the gradual changes often detected in the sound dispersion of several liquids at increasing wave vectors.

Although appealing, the simplicity of the viscoelastic model can be deceptive. First of all, the model itself provides no clue for the physical origin of the decay mechanisms leading to the rate $1/\tau(Q)$.

[5]Actually, the viscoelastic model stems from the approximation (56), with the additional condition $\gamma=1$ $[M_{\text{th}}(Q,t)=0]$. Within the viscoelastic framework, indeed thermal effects are neglected, in the sense that the hydrodynamic limit is isothermal [i.e., $\Delta_L^2(Q) = \omega_L(Q)^2 - \omega_0(Q)^2$].

Actually, the situation is even more involved. In earlier molecular-dynamics studies of Lennard-Jones fluids, it was soon realized that the viscous dynamics in the microscopic regime (i.e., at wavelengths comparable with the inverse mean interparticle separation) proceeds through two distinct processes, characterized by two well separated time scales (Levesque *et al.*, 1973). More recently, the advent of inelastic x-ray scattering (IXS) provided the experimental evidence substantiating these speculations (Scopigno *et al.*, 2000b, 2001a; Scopigno, Balucani, *et al.*, 2002; Scopigno, Filipponi, *et al.*, 2002; Monaco *et al.*, 2004).

In view of these results, the obvious remedy is to modify the simple ansatz (56) by allowing a two-step decay of $M_L(Q,t)$:

$$M_L(Q,t) = \Delta_L^2(Q)\{[1-\alpha(Q)]e^{-\gamma_1(Q)t} + \alpha(Q)e^{-\gamma_2(Q)t}\}, \tag{57}$$

where the rate $\gamma_1(Q)$ is chosen to be larger than $\gamma_2(Q)$, so that the dimensionless factor $\alpha(Q)$ measures the relative weight of the "slow" decay channel. Besides being more flexible than the viscoelastic model, we shall see that the ansatz (57) has the much more important merit that the presence of two different time scales does in fact have a definite physical interpretation.

A simplified version of the previous ansatz has been implicitly introduced in the viscoelastic analysis of Brillouin light-scattering (BLS) spectra of glass-forming materials [see, for example, Li *et al.* (1992)]. In fact, in these works, the general expression of $M_L(Q,t)$ for a two times decay is always expressed as

$$M_L(Q,t) = 2\Delta_\mu^2(Q)\tau_\mu(Q)\delta(t) + \Delta_\alpha^2(Q)e^{-t/\tau_\alpha(Q)},$$

with explicit reference to the so-called α- (structural) relaxation process as responsible for the long lasting tail, and to the μ-microscopic process as additional, faster, relaxation dominant over a very short time scale (in the BLS window the condition $\omega\tau_\mu \ll 1$ holds).

On the contrary, in the above-mentioned IXS works it has been shown how this approximation is no longer tenable in the case of liquid metals at the IXS frequencies. In particular, it has been pointed out that the slower (α) relaxation time satisfies the condition $\omega_B(Q)\tau_\alpha(Q) \gg 1$, i.e., some part of the viscous flow is frozen. As a consequence, at the wave vectors typical of the IXS experiments ($Q=1$–20 nm^{-1}) the quasielastic spectrum acquires a component arising from this frozen structural relaxation.

The origin, at the atomic level, of this fast decay channel is still an open issue: the rapidly decaying portion of $M_L(Q,t)$ is customarily attributed to largely uncorrelated collisional events, similar to those occurring in a dilute fluid. In addition, at the high densities typical of the liquid state, non-negligible correlations among the collisions can be expected, making no longer valid an interpretation only in terms of "binary" collisions. Although the magnitude of the correlation effects is relatively small and their buildup slow, once established their decay is even slower, and for $t > 1/\gamma_1(Q) \equiv \tau_\mu(Q)$

this relaxation channel dominates the decay of $M_L(Q,t)$, which consequently may exhibit a small but long lasting "tail." The ansatz (57) can incorporate most of this physics: on the basis of the latter, one may reasonably anticipate that $\alpha(Q) \ll 1$, and that the time $1/\gamma_2(Q) \equiv \tau_\alpha(Q)$ is distinctly longer than $1/\gamma_1(Q) \equiv \tau_\mu(Q)$. In this picture, the best fitted values of the viscoelastic rate $1/\tau(Q)$ clearly represent some sort of "weighted average" between $\gamma_1(Q)$ and $\gamma_2(Q)$. Finally, we may argue that at increasing Q (namely, over a shrinking length scale) the magnitude $\alpha(Q)$ of correlation effects should decrease, and that at higher temperatures the value of $\alpha(Q)$ at a given wave vector should equally decrease. On a general basis, the requirement that $\lim_{Q\to 0} \tilde{M}_L(Q,s=0)/Q^2 \to \eta_L/nm$ now takes the form

$$(c_\infty^2 - c_0^2)\left[\frac{1-\alpha(Q\to 0)}{\gamma_1(Q\to 0)} + \frac{\alpha(Q\to 0)}{\gamma_2(Q\to 0)}\right] \to \eta_L/nm. \tag{58}$$

The refined model (57) yields a dynamic structure factor given by

$$S(Q,\omega) = \frac{S(Q)}{\pi}\mathrm{Re}\left\{\frac{\omega_0^2(Q)}{i\omega + \dfrac{\Delta_\mu^2(Q)}{i\omega+\gamma_1(Q)} + \dfrac{\Delta_\alpha^2(Q)}{i\omega+\gamma_2(Q)} + \dfrac{\Delta_{\mathrm{th}}^2(Q)}{i\omega+\gamma(Q)D_T(Q)Q^2}}\right\}^{-1}. \tag{59}$$

One of the major drawbacks of the expression (59) is that one normally overestimates the relaxation strength of the faster viscous process. Such a problem is somehow expected as one is trying to force an exponential dependence to reproduce the memory function at short times, which, instead, has a zero derivative in the $t\to 0$ limit. As a consequence, adjusting the characteristic time of the exponential memory on experimental data one can reproduce the decay of the true memory function but will overestimate the short time limit, due to the cusp behavior of the exponential at $t=0$.

One obvious remedy is a better choice of the memory function model. An alternative possibility could be a Gaussian shape. Also the sech function has been proposed as solution of the Mori equation (Tankeshwar and Pathak, 1994), but this latter case is of limited practical interest, as the Fourier transform is related to the digamma function and therefore the expression (59) must be numerically evaluated.

G. Kinetic theories: The hard-sphere approximation

Special attention has been devoted in the past to the theoretical and numerical study of the hard-sphere model, as it conveniently mimics the behavior of more realistic simple liquids (Lebowitz *et al.*, 1969; Furtado *et al.*, 1975). In the 1980s, transport coefficients (Alley and Alder, 1983) and neutron-scattering response (Alley *et al.*, 1983) have been evaluated by means of molecular dynamics. On the theoretical side, the dynamical properties have been investigated by a revisiting the so-called "Enskog fluid," i.e., by means of the spectral decomposition of the Enskog operator (de Schepper and Cohen, 1980; Cohen *et al.*, 1984; de Schepper *et al.*, 1984; Kamgar-Parsi *et al.*, 1987; Mryglod *et al.*, 1995). This latter approach turned out to be particularly useful to describe INS experimental data (Cohen *et al.*, 1987), and we will briefly recall the basics in this section.

The main idea beyond Enskog's theory is to evaluate the correlation functions (2) replacing the Liouville operator $\mathcal{L}$ and the dynamical variables $a_\alpha(Q)$, defined at the N-particle ensemble level, with the one-particle Enskog's operator L, and appropriate one-particle variables $\phi_\alpha(Q)$. It can be easily recognized, indeed, that

$$a_\alpha(Q) = \frac{1}{\sqrt{N}}\sum_j \phi_\alpha(\mathbf{v}_j)e^{-i\mathbf{Q}\cdot\mathbf{r}_j},$$

where, for the first three dynamical variables (1), it holds that

$$\phi_1(\mathbf{v}) = \frac{1}{S(Q)},$$

$$\phi_2(\mathbf{v}) = \sqrt{\frac{m}{k_BT}}\frac{\mathbf{Q}\cdot\mathbf{v}}{Q},$$

$$\phi_3(\mathbf{v}) = \frac{3 - mv^2/k_BT}{\sqrt{6}}.$$

For a hard-sphere system, a possible asymmetric representation of L reads (de Schepper *et al.*, 1984)

$$L(\mathbf{Q},\mathbf{v}_1) = -i\mathbf{Q}\cdot\mathbf{v}_1 + \rho g(\sigma)\Lambda(\mathbf{Q}) + \rho A(\mathbf{Q}), \tag{60}$$

where $g(\sigma)$ is the pair distribution function evaluated at the contact point between two spheres. The first term appearing in Eq. (60) is a free streaming contribution. The second term accounts for binary collisions through the operator $\Lambda(\mathbf{Q})$, defined through its action over a generic function of the velocity $f(\mathbf{v}_1)$:

$$\Lambda(\mathbf{Q})f(\mathbf{v}_1) = -\sigma^2 \int d\hat{\boldsymbol{\sigma}} \int d\mathbf{v}_2 \xi(v_2)\delta\theta(\delta) \times \{f(\mathbf{v}_1) - f(\mathbf{v}_1') + e^{-i\mathbf{Q}\cdot\hat{\boldsymbol{\sigma}}\sigma}[f(\mathbf{v}_2) - f(\mathbf{v}_2')]\}, \tag{61}$$

with $\xi(v)$ the normalized Maxwell distribution function, $\theta(x)$ the Heaviside step function, $\hat{\sigma}$ the unit vector, $\delta = (\mathbf{v}_1 - \mathbf{v}_2)\cdot\hat{\boldsymbol{\sigma}}$, and $\mathbf{v}_{1,2}' = \mathbf{v}_{1,2} \mp \delta\hat{\boldsymbol{\sigma}}$ the postcollision velocity. The third term, finally, is a mean-field operator defined through

$$\rho A(\mathbf{Q})f(\mathbf{v}_1) = [C(Q) - g(\sigma)C_0(Q)] \times \int d\mathbf{v}_2 \xi(v_2) i\mathbf{Q}\cdot\mathbf{v}_2 f(\mathbf{v}_2), \tag{62}$$

where $C(Q) = 1 - 1/S(Q)$ and $C_0(Q) = \lim_{\rho\to 0} C(Q)$.

An explicit expression for the dynamic structure factor can be easily retrieved through the spectral decomposition of L:

$$L(\mathbf{Q},\mathbf{v}_1) = -\sum_j |\Psi_j(\mathbf{Q},\mathbf{v}_1)\rangle z_j(Q) \langle\Phi_j(\mathbf{Q},\mathbf{v}_1)|,$$

in which z_j, Ψ_j, and Φ_j are eigenvalues, left, and right eigenfunctions of $-L$, respectively. $S(Q,\omega)$ then reads

$$\frac{\pi S(Q,\omega)}{S(Q)} = \mathrm{Re}\left\langle \frac{1}{i\omega - L(\mathbf{Q},\mathbf{v}_1)} \right\rangle_1 = \mathrm{Re}\sum_j \frac{B_j(Q)}{i\omega + z_j(Q)}, \tag{63}$$

with

$$B_j(Q) = \langle \Psi_j(\mathbf{Q},\mathbf{v}_1)\rangle_1 \langle \Phi_j^*(\mathbf{Q},\mathbf{v}_1)\rangle_1. \tag{64}$$

The subscript $\langle\cdots\rangle_1$ explicitly indicates that we are now dealing with single-particle averages over the Maxwell-Boltzmann velocity distribution function.

There are several approaches to determine the spectrum of L, but the main point is that different approximations can be performed according to the density and kinematic region of interest. These regions are marked by the values of the reduced density $V_0/V = \rho\sigma^3/\sqrt{2}$, V_0 being the closed-packed volume for spheres or radius σ, and the Enskog mean free path $l_E = l_0/\chi$ with l_0 the Boltzmann mean free path $l_0 = 1/\sqrt{2}\rho\pi\sigma^2$ and $\chi = g(\sigma)$ the pair distribution function evaluated at the contact point between two spheres.

The lower three eigenvalues of L always goes to zero with $Q \to 0$. In the same limit it can be shown that these latter eigenvalues are

$$z_1(Q) = z_h(Q) = D_{TE}Q^2,$$

$$z_{2,3}(Q) = z_\pm(Q) = \pm ic_0 Q + \Gamma_E Q^2, \tag{65}$$

and only the first three coefficients (64) are relevant, so that the eigenfunctions are linear combinations of the density, current, and energy variables. In other words, the hydrodynamic result of Eq. (16) is recovered, with the dynamic structure factor composed of three Lorentzian functions: a diffusive heat mode and two propagating modes with the adiabatic sound velocity, with dampings D_{TE} and Γ_E as given within Enskog's transport theory. The relative intensities of the thermal and acoustic contributions are ruled by the Landau-Placzek ratio.

This limit is practically attained at low densities ($V_0/V < 0.1$ and therefore $l_E \approx l_0$) and sufficiently small Q's ($Q\sigma \ll 1$), when the contribution (62) can be safely neglected and the term (61) can be replaced with $\Lambda(Q\sigma = 0)$. This normally occurs for the case of light scattering of dilute gases ($Ql_0 \approx 1$), and one speaks in terms of three extended hydrodynamic modes. Still in the same low density-momentum range, but at wave vectors $1 \leqslant Ql_0 \leqslant 3$ a description in terms of a few hydrodynamic modes is no longer allowed, while for $Ql_0 > 3$ one can evaluate the first-order corrections to the free-particle result of Eq. (21) which reads

$$S(Q,\omega) = \sqrt{\frac{m}{2\pi k_B T Q^2}}\left[e^{-m\omega^2/2k_BTQ^2} + \frac{S^B(\omega/Q)}{Ql_0} + O(1/Ql_0)^2 \right], \tag{66}$$

with $S^B(\omega/Q)$ the leading correction to the free streaming term $-i\mathbf{Q}\cdot\mathbf{v}_1$ of Eq. (60) due to a single binary collision event, which can be numerically estimated (Kamgar-Parsi *et al.*, 1987).

Conversely, for dense fluids ($V_0/V > 0.35$), the hydrodynamic scheme breaks down at $Ql_E > 0.05$. Above this value, only the extended heat mode is well separated from all the other modes. Still a description in terms of three *effective* hydrodynamic modes apply, and the low-Q limit of these modes is again coincident with the hydrodynamic result. For $0 < Ql_E < 1$ the free streaming and the mean-field contributions of the Enskog operator can be treated as perturbation to the binary collision term (61), and the following approximate expression for the extended heat mode can be given:

$$z_h(Q) = \frac{D_E Q^2}{S(Q)} d(Q), \tag{67}$$

in which

$$D_E = -\left\langle v_{1x} \frac{1}{\rho\chi\Lambda(Q\to\infty)} v_{1x} \right\rangle$$

is the Enskog diffusion coefficient and

$$d(Q) = -\frac{\left\langle v_{1x} \frac{1}{\rho\chi\Lambda(Q)} v_{1x} \right\rangle}{D_E} \approx \frac{\langle v_{1x}\Lambda(Q\to\infty)v_{1x}\rangle}{\langle v_{1x}\Lambda(Q)v_{1x}\rangle} = \frac{1}{1 - j_0(Q\sigma) + 2j_2(Q\sigma)} \tag{68}$$

can be approximated in terms of the first two even spherical Bessel functions. Enskog's diffusion coefficient is related to the Boltzmann diffusion coefficient:

$$D_0 = \frac{3}{8\rho\sigma^2}\sqrt{\frac{k_B T}{\pi m}} \approx \frac{0.216}{\rho\sigma^2}\sqrt{\frac{k_B T}{m}}$$

by the collision enhancing term $g(\sigma)$ as $D_E = D_0/g(\sigma)$. Using the analytic expression of $g(\sigma)$ for nonattractive hard spheres one finally gets an expression for D_E in terms of the packing fraction $\varphi = \pi\rho\sigma^3/6$:

$$D_E = \frac{1}{16}\sqrt{\frac{\pi k_B T}{m}}^3 \sqrt{\frac{6}{\pi\rho\varphi^2}}\frac{(1-\varphi)^3}{1-\varphi/2}.$$

As in the low-density case, for $Ql_E > 3$ the free streaming limit is recovered along with binary collisions corrections. In this case, however, a different approximation holds, since the binary collision term (61) is now replaced with the Lorentz-Boltzmann operator $\Lambda(Q \to \infty)$. One ultimately gets an expression similar to Eq. (66) in which $S^B(\omega/Q)$ is replaced with a different Lorentz-Boltzmann expression.

At intermediate densities, finally, again the hydrodynamic result does not hold for $Ql_E \gtrsim 0.05$. Moreover, in this regime three effective modes do not suffice and one has to extend the description with two additional kinetic modes, i.e., including the kinetic part of the z-z component of the stress tensor and the z component of the heat flux (Kamgar-Parsi *et al.*, 1987). As in the high-density case, for $1 < Ql_E < 3$ all modes are closely interwoven, while at larger Q's the free streaming limit with the Lorentz-Boltzmann correction is retrieved.

According to kinetic theory therefore $S(Q,\omega)$ in simple liquids not too far from the melting temperature (such as argon) should be described in terms of three Lorentzians up to relatively large wave vectors ($Q \approx 30\ \mathrm{nm}^{-1}$). Consequently, sound modes should exist even in a Q region where side peaks are not distinctly observable. In this respect, Lovesey argued that the extended hydrodynamic picture should break up above $Q \approx 3\ \mathrm{nm}^{-1}$, while above, a viscoelastic theory should be utilized (Lovesey, 1984).

Exploiting the previous results obtained for the coherent case, one can describe the incoherent dynamics via the Lorentz-Enskog operator:

$$L_s(\mathbf{Q},\mathbf{v}_1) = -i\mathbf{Q}\cdot\mathbf{v}_1 + \rho g(\sigma)\Lambda(\mathbf{Q}\to\infty). \tag{69}$$

As already mentioned, at large Q's the self- and collective dynamics coincide, and therefore the spectrum of L will tend to the one of L_s [$A(Q\to\infty)=0$]. In this limit the extended heat mode z_h will tend to the self-diffusion mode z_D. In the opposite, $Q\to 0$, limit, they both approach their hydrodynamic values: $z_h(Q\to 0) = D_{TE}Q^2$ and $z_D(Q\to 0) = D_E Q^2$, with D_{TE} and D_E the thermal diffusivity and the self-diffusion coefficient of Enskog's theory. At intermediates Q values, z_h oscillates around z_D, with a periodicity dictated by $S(Q)$ and $d(Q)$ according to Eq. (67).

Sears has calculated the moments of the self-part of the van Hove scattering function at large wave vectors (Sears, 1972). Starting from the general case of a velocity-independent central force field, he specialized the result to the hard-sphere case, evaluating the leading correction to the impulse approximation due to final-state interactions, which turns out to be Q^{-1}:

$$\omega_H(Q) \approx \sqrt{\frac{2k_B T \ln 2}{m}}Q\left(1 - \frac{0.27}{Ql_E} + O(Q^{-2})\right). \tag{70}$$

The transition from the Fickian to the Gaussian regime occurs in this case at $Ql_E \approx 1$.

Finally, it is worthwhile to recall here one of the most significant achievements of the mode coupling theory applied to hard-sphere fluids, but which has been shown to apply to a wider class of simple fluids. Ernst and Dorfman (1975) have shown how Eq. (65), which retrieves the hydrodynamic expression of the sound velocity and attenuation, is actually the leading term of an expansion of the kind

$$z_h(Q) = \alpha_h Q^2 - \beta_h Q^{5/2} + O(Q^{11/4}),$$

$$z_\pm(Q) = \pm ic_0 Q + \alpha_\pm Q^2 + (\pm i - 1)\beta_\pm Q^{5/2} + O(Q^{11/4}). \tag{71}$$

H. The ionic plasma

The dynamical descriptions given up to this point are extensions of models holding for ordinary fluids which, in some cases, are modified \ to account for the high thermal conductivity of liquid metals.

A totally different approach is to look at liquid metals, from the very start, as a one-component plasma, i.e., as an assembly of identical, pointlike charged particles (ions) embedded in a uniform background (the electrons) which neutralizes the total charge (Baus and Hansen, 1980). The long-ranged Coulomb interaction active in this case gives rise to peculiar phenomena such as screening effects and plasma oscillations.

The ionic number density $\rho(\mathbf{r},t)$ and the current density $\mathbf{j}(\mathbf{r},t)$ are related through the continuity equation

$$\frac{\partial\rho(\mathbf{r},t)}{\partial t} = -\nabla\cdot\mathbf{j}(\mathbf{r},t).$$

The Poisson equation, for a fluid with Ze charge, reads

$$\nabla\cdot\mathbf{E}(\mathbf{r},t) = 4\pi Ze\,\delta\rho(\mathbf{r},t),$$

in which $\delta\rho(\mathbf{r},t)$ is the deviation of the ionic density from its average value ρ (neutralized by the opposite uniform electronic density). Neglecting thermal conductivity effect (collisionless regime), from Newton's law for the equation of motion one can find a third equation and close the system. In the limit of large wavelength fluctuations (compared to the ionic size) one can write

$$m\frac{\partial\mathbf{j}(\mathbf{r},t)}{\partial t} = \rho Ze\mathbf{E}(\mathbf{r},t),$$

m being the ionic mass. Combining the previous equations one easily gets

$$\frac{\partial^2 \rho(\mathbf{r},t)}{dt^2} = -\Omega_p^2 \delta\rho(\mathbf{r},t),$$

which describes ionic plasma oscillation of characteristic Q independent frequency

$$\Omega_p^2 = \frac{4\pi\rho Z^2 e^2}{m}. \tag{72}$$

This simplified picture therefore contrasts with the experimental evidence of long-wavelength excitations whose frequency vanishes in the $Q \to 0$ limit. The commonly used remedy is to "dress" the plasma frequency accounting for the electron screening effect, i.e., to take into account that the background electrons have their own dynamics that can be described introducing the dielectric response $\epsilon(Q)$. In such a way the Coulomb interactions and, in turn, the plasma frequency are renormalized leading to the expression

$$\omega_p^2 = \frac{\Omega_p^2}{\epsilon(Q)}. \tag{73}$$

In the small wave-vector limit the Thomas-Fermi expression within the random-phase approximation (RPA, in which the system is assumed to have a free electron gas compressibility) yields the useful expression (March and Tosi, 1991)

$$\epsilon(Q) = 1 + \frac{Q_{\mathrm{TF}}^2}{Q^2}, \tag{74}$$

in which $Q_{\mathrm{TF}} = 6\pi e^2 \rho_e / E_F$, with $E_F = \hbar^2 (3\pi^2 \rho_e)^{2/3} / 2m_e$, ρ_e, and m_e the Fermi energy, the electronic density, and the electronic mass, respectively. At small Q values, Eq. (74), together with Eqs. (72) and (73), leads to the so-called Bohm-Staver expression, i.e., a dispersive excitation with sound velocity

$$c_{\mathrm{BS}} = \frac{\omega_p}{2} = \sqrt{\frac{m_e Z}{3m}} v_F, \tag{75}$$

in which v_F is the electron velocity at the Fermi level.

As we will show in the following, the experimental values for sound velocities in conductive liquids often contrast with the prediction of Eq. (75), especially at small electron density or, equivalently, at large values of the reduced ionic radius $r_s = (3/4\pi\rho_e a_0^3)^{1/3}$, where the Thomas-Fermi approximation is no longer valid.

The interplay between plasma oscillations and sound waves can be better accounted for within a two-component plasma (TCP) description in which nuclei and electrons are treated separately (Chihara, 1985), eventually exploiting the framework of Mori and Zwanzig (Hansen and Sjögren, 1982). The details of the two-component plasma are, however, beyond the scope of this review; the interested reader might want to consult more specialized literature.

III. EXPERIMENTAL STUDY OF THE MICROSCOPIC DYNAMICS

The main experimental ways to study microscopic dynamics in liquid metals are acoustic spectroscopy and inelastic-scattering experiments. These latter have to be necessarily performed with probes which can penetrate enough into the sample to give boundary-free information, a requirement which restricts the choice to neutrons and x-rays only. Actually, a few attempts have been performed by means of visible light scattering (Dil, 1982), for instance, on liquid mercury and gallium (Dil and Brody, 1976), but Brillouin scattering from opaque, liquid matter presents several difficulties, mainly associated with the ill definition of the exchanged momentum in absorbing media.

The basics of the neutron interaction with matter have been surveyed in many papers (Copley and Lovesey, 1975) and books (Egelstaff, 1967; Marshall, 1971; Lovesey, 1987) which provide exhaustive surveys of this issue. Inelastic x-ray scattering is a relatively newer technique, and therefore we will detail the basics of an IXS experiment recalling from time to time INS features for comparison.

A. The scattering problem

The measured signal in an inelastic-scattering experiment is determined by the double differential scattering cross section. Within the linear-response theory, where it is assumed that the coupling between the probe and the system is weak, this scattering differential cross section can be written quite generally as the product of three terms: (i) One term describes the intensity of the probe-sample coupling, and it is independent from the energy of the incident particle. (ii) A second one is a kinematic term related to the phase-space volumes of the incident and scattered particles. (iii) The third term is the space and time Fourier transform of the correlation function of the observable in the system that couples to the probe particle. This last quantity is the one related to the elementary excitations characteristic of the system.

1. The photon-electron interaction Hamiltonian

The actual expression for the scattering cross section can be derived by a perturbation expansion from the probe-system interaction Hamiltonian. In the case of the interaction of charges with the electromagnetic field, in the weak relativistic limit (i.e., to first order in v^2/c^2), neglecting the direct coupling of the field with the nuclei (i.e., to zero order in the electron-to-nuclei mass ratio m_e/m), and neglecting the magnetic terms (i.e., to the zero order in the electron spin) one gets

$$H_{\mathrm{INT}} = \frac{e^2}{2m_e c^2} \sum_j \mathbf{A}(r_j) \cdot \mathbf{A}^*(r_j) + \frac{e}{2m_e c} \sum_j \{\mathbf{A}(r_j), \mathbf{p}_j\}$$
$$\doteq H_{\mathrm{INT}}^{(1)} + H_{\mathrm{INT}}^{(2)},$$

where the symbol $\{\}$ denotes the anticommutator opera-

tor. The two "electric" terms $H_{\mathrm{INT}}^{(1)}$ and $H_{\mathrm{INT}}^{(2)}$ contain, respectively, two and one field operators $\mathbf{A}(r)$. It is clear therefore that—in a perturbation expansion treatment of the interaction Hamiltonian—the term $H_{\mathrm{INT}}^{(1)}$ will give rise to two-photon processes at first order while the term $H_{\mathrm{INT}}^{(2)}$ will give rise to one-photon processes at first order. To have the two-photon processes from the latter (the so-called $\mathbf{p}\cdot\mathbf{A}$ contribution), necessary to describe the scattering events, one must consider the second order in the perturbation expansion, which is consequently completely negligible in the off-resonance case. In the following therefore we will consider only the first charge scattering term.

2. The x-ray scattering cross section

The double differential cross section $\partial^2\sigma/\partial E\partial\Omega$ is proportional to the probability that an incident particle is scattered with a given energy and momentum variation within an energy range ΔE and a solid angle $\Delta\Omega$. In the process, a photon of energy E_i, wave vector $\mathbf{k}_i$, and polarization ϵ_i is scattered into a final state of energy E_f, wave vector $\mathbf{k}_f$, and polarization ϵ_f, and the electron system goes from the initial state $|I\rangle$ to the final state $|F\rangle$ (states with energies E_I and E_F, respectively). According to this definition, the double differential cross section can be related to the quantity $dP_{i\to f}/dt$ which is the probability rate per sample and probe unit that a probe particle makes the transition from the initial state to the final state:

$$\frac{\partial^2\sigma}{\partial E\partial\Omega}=\frac{dP_{i\to f}}{dt}\frac{1}{j}\frac{\partial^2 n}{\partial E\partial\Omega}.$$

In this equation j is the incident particle current density ($j=\rho v$, with ρ the particle density and v its velocity) and $\partial^2 n/\partial E\partial\Omega$ the density of states of the scattered particle. For zero-mass particles, the latter two quantities can be written as

$$j=\frac{c}{V_0}, \tag{76}$$

$$\frac{\partial^2 n}{\partial E\partial\Omega}=\frac{V_0}{8\pi^3}\frac{k_f^2}{\hbar c}. \tag{77}$$

Therefore the double differential cross section becomes

$$\frac{\partial^2\sigma}{\partial E\partial\Omega}=\frac{V_0^2}{8\pi^3}\frac{k_f^2}{\hbar c^2}\frac{dP_{i\to f}}{dt}. \tag{78}$$

The transition of the incident particles between states i and f involves, in general, different possible elementary excitations in the sample. This implies that, indicating with $dP_{i,I\to f,F}/dt$ the scattering probability involving the transition in the sample from the state $|I\rangle$ to the final state $|F\rangle$, the total probability $dP_{i\to f}/dt$ can be expressed as

$$\frac{dP_{i\to f}}{dt}=\sum_{F,I}\frac{dP_{i,I\to f,F}}{dt}.$$

Equation (78) is particularly useful, as the transition probability per unit time $dP_{i,I\to f,F}/dt$ can be calculated from the perturbation theory. To first order this quantity is written as (Fermi's golden rule)

$$\frac{dP_{i,I\to f,F}}{dt}=\frac{2\pi}{\hbar}|\langle i,I|H_{\mathrm{INT}}|f,F\rangle|^2\delta(E_i+E_I-E_f-E_F). \tag{79}$$

Inserting the term $H_{\mathrm{INT}}^{(1)}$ into Eq. (79), using Eq. (78), and considering the initial and final photon states as plane waves one gets

$$\frac{\partial^2\sigma^{(1)}}{\partial E\partial\Omega}=\left(\frac{e^2}{m_e c^2}\right)^2\frac{k_f}{k_i}(\epsilon_i\epsilon_f)^2\sum_{F,I}P_I\delta[E-(E_F-E_I)]\times\left|\langle F|\sum_j e^{i\mathbf{Q}\cdot\mathbf{r}_j}|I\rangle\right|^2, \tag{80}$$

where $Q=\mathbf{k}_i-\mathbf{k}_f$ ($E=E_f-E_i$) is the momentum (energy) transferred from the photons to the system. The sum over the initial and final states is the thermodynamic average, and P_I corresponds to the equilibrium population of the initial state.

Apart from the sum over the phase factors of the photons scattered from the different particles, whose interference gives rise to a truly Q dependent scattering signal, the energy- and angle-integrated cross section is of the order of the square of the classical electron radius $r_0=e^2/m_e c^2$.

3. The adiabatic approximation and the dynamic structure factor

From Eq. (80), which implicitly contains the correlation function of the electron density, one arrives at the correlation function of the atomic density on the basis of the following considerations: (i) One assumes the validity of the adiabatic approximation, and this allows one to separate the system quantum state $|S\rangle$ into the product of an electronic part $|S_e\rangle$, which depends only parametrically from the nuclear coordinates, and a nuclear part, $|S_n\rangle$: $|S\rangle=|S_e\rangle|S_n\rangle$. This approximation is particularly good for exchanged energies that are small with respect to the excitations energies of electrons in bound core states: this is indeed the case in basically any atomic species when considering values in the range of phonon energies. In metals we neglect the small portion of the total electron density in proximity of the Fermi level. (ii) One limits to consider the case in which the electronic part of the total wave function is not changed by the scattering process, and therefore the difference between the initial state $|I\rangle=|I_e\rangle|I_n\rangle$ and the final state $|F\rangle=|I_e\rangle|F_n\rangle$ is due only to excitations associated with atomic density fluctuations. Using these two hypotheses we then obtain

$$\frac{\partial^2\sigma}{\partial E\partial\Omega} = \left(\frac{e^2}{m_e c^2}\right)^2 \frac{k_f}{k_i}(\epsilon_i\epsilon_f)^2 \sum_{F_n,I_n} P_{I_n}\delta[E-(E_F-E_I)] \times \left|\langle F_n|\sum_j f_j(Q)e^{i\mathbf{Q}\cdot\mathbf{R}_j}|I_n\rangle\right|^2, \quad (81)$$

where $f_j(Q)$ is the atomic form factor of the jth atom at R_j and the sum is now extended to all the atoms (molecules) of the systems. Assuming that all the scattering units in the system are equal, this expression can be further simplified by the factorization of the form factor of these scattering units, and by the introduction of the dynamic structure factor $S(Q,E)$ defined as

$$S(Q,E) = \sum_{F_n,I_n} P_{I_n}\delta(E-E_F+E_I)\left|\langle F_n|\sum_j e^{i\mathbf{Q}\cdot\mathbf{R}_j}|I_n\rangle\right|^2.$$

By representing the δ function above as a time integral, indicating by $\langle\cdots\rangle$ the thermal average $\langle o\rangle = \Sigma_I P_I\langle I|\hat{o}|I\rangle$ and using the completeness operator $\Sigma_{F_n}|F_n\rangle\langle F_n| = 1$ the dynamic structure factor can be also written in the following more familiar form:

$$S(Q,E) = \frac{1}{2\pi E}\int dt e^{iEt/h}\sum_{j,k}\langle e^{i\mathbf{Q}\cdot\mathbf{R}_j(t)}e^{-i\mathbf{Q}\cdot\mathbf{R}_j(0)}\rangle,$$

where N is the number of particles in the system and the sum over (j,k) extend over these N particles. The double differential cross section can then finally be rewritten as

$$\frac{\partial^2\sigma}{\partial E\partial\Omega} = \left(\frac{e^2}{m_e c^2}\right)^2 \frac{k_f}{k_i}(\epsilon_i\epsilon_f)^2|f(Q)|^2 S(Q,E). \quad (82)$$

In the limit $Q\to 0$, the form factor $f(Q)$ is equal to the number of electrons in the scattering atom, i.e., $f(Q) = Z$. For increasing values of Q, the form factor decays almost exponentially with the decay constants determined by the size of the radial distributions of the electrons in the atomic shells of the considered atom. At Q values large with respect to the inverse of these dimensions therefore the inelastic x-ray scattering from density fluctuations is strongly reduced.

The cross section derived so far is valid for a system composed of a single atomic species. This derivation, however, can be easily generalized to molecular or crystalline systems by substituting the atomic form factor with either the molecular form factor or the elementary cell form factor, respectively. The situation becomes more involved if the system is multicomponent and disordered. In this case the factorization of the form factor is still possible only assuming some specific distribution among the different atoms. In the limiting case that such a distribution is completely random, an incoherent contribution appears in the scattering cross section.

4. From cross section to count rate

The Z dependence of the Thomson scattering cross section seems to imply a facilitation in studying systems with high Z. In reality, this is no longer true when the effect of photoelectric absorption is taken into consideration. Indeed, neglecting multiple-scattering events, the signal detected in an IXS experiment from an infinitesimal slab of thickness δx orthogonal to k_i can be written as

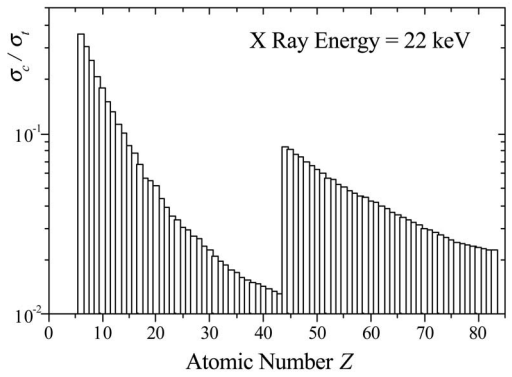

FIG. 1. Ratio between the total number of photons scattered by the Thomson process and those lost through all the other processes, among which is photoelectric absorption, in a sample of length μ^{-1} calculated as a function of the atomic number Z for photons of incident energy of ≈22 keV.

$$dN = N_0\left(\frac{\partial^2\sigma}{\partial E\partial\Omega}\right)\Delta E\Delta\Omega\rho dx, \quad (83)$$

where N_0 is the flux of the incident photons, N is the flux of scattered photons in an energy interval ΔE and in a solid angle $\Delta\Omega$, ρ is the number of scattering units per unit volume, and μ is the total absorption coefficient. Dealing with a macroscopic sample of length L, in the relevant case of a nearly forward scattering geometry, Eq. (83) becomes

$$dN(x) = N_0 e^{-\mu x}\left(\frac{\partial^2\sigma}{\partial E\partial\Omega}\right)\Delta E\Delta\Omega\rho dx e^{-\mu(L-x)}, \quad (84)$$

which, integrated over the whole sample length, yields

$$N = N_0\left(\frac{\partial^2\sigma}{\partial E\partial\Omega}\right)\Delta E\Delta\Omega\rho L e^{-\mu L}. \quad (85)$$

Let us discuss the L dependence of this function. It is obvious that N attains a maximum (the optimal sample length) when $L=\mu^{-1}$, and that the value of N at this maximum point is proportional to μ^{-1}. Considering an x-ray energy of approximately 20 keV and $Z>3$, μ is almost completely determined by the photoelectric absorption process. This process gives approximately $\mu \approx Z^4$ with modifications at energies close to electron absorption thresholds. Consequently, the effective scattering volume is very much reduced in materials with a high Z (as Z^4), while the cross section increases as Z^2, making the study of these materials by all means more difficult than for those with low Z. The behavior of the optimal signal intensity as a function of atomic number in monatomic systems with sample length $L=1/\mu$ can be deduced from the data reported in Fig. 1. There we show the quantity $\sigma_c\rho/\mu$, with $\sigma_c=(r_0Z)^2$, which gives directly a measure of the efficiency of the method at the considered photon energy: in this example we took an

incident photon energy of 22 keV. The quantity $\sigma_c\rho/\mu$ is by definition the ratio between σ_c and σ_t, where σ_t is the (measured) total x-ray cross section of the considered atom. This analysis is useful, however, only when it is possible to study samples of optimal length. In cases where the sample size is limited either by its availability or by the sample environment (extreme pressure, high or low temperature, high magnetic field, etc.) it is obvious that one has great advantages in studying high-Z materials.

Equation (85) accounts for single scattering events only. An estimate for the two-scattering process intensity can be obtained by invoking the forward scattering approximation again, indeed, the ratio of the two over the one-scattering rates $N^{(2)}/N^{(1)}$ reads

$$\frac{N^{(2)}}{N^{(1)}} = \frac{\pi\rho h r_0^2 \int_0^\pi [f(\theta)s(\theta)]^2 d\theta}{Z^2 S(0)},$$

where h is the sample transverse dimension traversed by the incident beam. The integral accounts for all possible two-scattering processes leading to final forward scattering. This expression shows that to suppress multiple scattering one has to reduce the transverse beam dimension. A similar estimate for neutron scattering is prevented by much more complicated scattering paths, since, within a similar Q range, the scattering angle in INS is normally much larger. However, it can be noted that in the case of neutrons the typical transverse beam size is much larger (≈10–100 mm) than the IXS ones (≈100 μm), thus resulting in a more important contribution requiring accurate corrections.

5. Kinematics of the scattering processes

Another important difference between x-ray and neutrons scattering lies in the kinematics of the scattering processes. The momentum and energy conservation laws impose that

$$\mathbf{Q} = \mathbf{k}_i - \mathbf{k}_f,$$

$$E = E_f - E_i,$$

$$Q^2 = k_i^2 + k_f^2 - 2k_i k_f \cos\theta,$$

where θ is the scattering angle between the incident and scattered particles. The relation between momentum and energy in the case of photons is given by

$$E(k) = hck$$

and therefore one obtains

$$\left(\frac{Q}{k_i}\right)^2 = 1 + \left(1 - \frac{E}{E_i}\right)^2 - 2\left(1 - \frac{E}{E_i}\right)\cos\theta. \tag{86}$$

Considering that the energy losses or gains associated with phononlike excitations are always much smaller than the energy of the incident photon ($E \ll E_i$), this relation reduces to

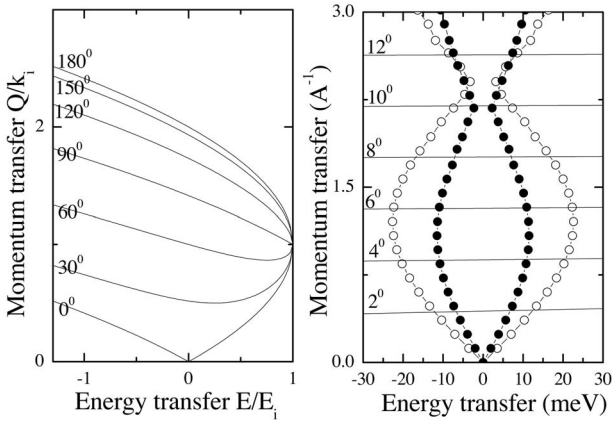

FIG. 2. Kinematic region accessible to IXS in reduced E/E_i and Q/k_i units (left panel). The right panel shows the realistic cases of molten lithium (open circles) and sodium (full circles) for an incident energy of 25 keV.

$$\left(\frac{Q}{k_i}\right) = 2\sin\frac{\theta}{2} \quad (E \ll E_i).$$

This last relation shows that, in the limit of small energy transfers, the ratio between the exchanged momentum and the incident photon momentum is completely determined by the scattering angle, as shown in Fig. 2. Therefore in inelastic x-ray scattering there are basically no limitations in the energy transfer at a given momentum transfer for phononlike excitations.

6. X rays vs neutrons

At variance with the previous equation, if the probe particles have mass m_p

$$E(k) = \frac{h^2k^2}{2m_p}$$

and therefore

$$\left(\frac{Q}{k_i}\right)^2 = 1 + \left(1 - \frac{E}{E_i}\right) - 2\sqrt{1 - \frac{E}{E_i}}\cos\theta. \tag{87}$$

In the case of thermal neutron scattering, the approximation $E \ll E_i$ no longer holds, and the kinematics of the scattering experiments is determined by Eq. (87). As an example, in Fig. 3 we report the accessible kinematics regions in the E/E_i vs Q/k_i plane for two different incident energies, indicating paths at constant scattering angles. In the same figure, similarly to Fig. 2, we also report the approximate dispersion curves for liquid lithium and sodium. In the best situation, i.e., in forward scattering where the accessible region is as wide as possible, the limiting curve is linear around $Q=0(E=0)$, and its tangent is $E/E_i=2Q/k_i$. Recalling that $E_i=\hbar^2k_i^2/2m_p$, one gets $E=v_N\hbar Q$, with v_N the velocity of the incoming neutron. As the dispersion relation for acoustic phonon is linear, $E=v_s\hbar Q$, with v_s the velocity of sound, it is clear that whenever v_s is larger than v_N the excitation peaks lie outside the accessible region and therefore when $v_s > v_N$ the neutron technique cannot be applied to

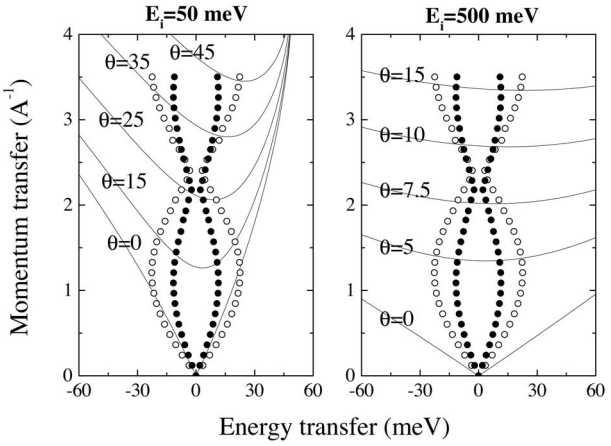

FIG. 3. Kinematic region accessible to neutron-scattering experiments for incident energies $E_i=50$ meV (left panel) and $E_i=500$ meV (right panel), reported for different scattering angles. Open and full circles are the (approximated) sound dispersion of molten lithium and sodium, respectively.

study the acoustic branch. This limitation does not apply to the case of x rays, as, according to Eq. (86), there are basically no limits to the energy region accessible at a given scattering angle.

As discussed before, the presence of relevant absorption phenomena is the main effect that determines the scattering volume in an IXS experiment. This implies therefore that the probability that a photon is scattered from the sample is small, and this strongly suppresses multiple-scattering processes. In IXS experiments, indeed, multiple scattering can be disregarded, thus avoiding the use of correction procedures. This is therefore an important advantage with respect to the neutron case, where, on the contrary, the sample length is determined by the scattering (rather than absorption) length. In Fig. 4 are reported for comparison the (coherent) scattering lengths of the elements for the x-ray and neutron cases.

Finally, it is worthwhile to compare the double differential scattering cross section for x rays obtained before [Eq. (82)] with a similar quantity derived for neutron scattering (in the hypothesis of fully coherent scattering). The latter quantity is not derived here for brevity and can be found in many textbooks (Egelstaff, 1967; Marshall, 1971; Lovesey, 1987). The two cross sections read as

$$\frac{\partial^2}{\partial E \partial \Omega} = \begin{cases} r_0^2 \dfrac{k_f}{k_i} (\boldsymbol{\epsilon}_f \boldsymbol{\epsilon}_i)^2 |f(Q)|^2 S(Q,E) & \text{x ray}, \\ b^2 \dfrac{k_f}{k_i} S(Q,E) & \text{neutron}. \end{cases} \tag{88}$$

Besides the proportionality of both the cross section to the dynamic structure factor, it is worth to underline the following:

(1) The two cross sections are proportional to a characteristic scattering length squared (r_0 in the case of x ray and b in the case of neutrons) that are comparable in magnitude (see Fig. 4). The form factor $|f(Q)|^2$ ($\propto Z^2$ for small Q's) in the case of x rays does not increase the actual signal in the experiment because, as discussed before, increasing Z also limits the optimal scattering volume due to the increase of the photoelectric absorption.

(2) In both cases the phase space of the incident and final plane waves gives rise to the factor k_f/k_i, however, while in the x-ray case $k_f \approx k_i$, and this factor is very close to 1, in the neutron case this term gives rise to a Q dependence of the scattered intensity.

(3) No polarization terms are present in the cross section for neutrons, while in the case of x rays the term tells us that the Thomson scattering arises from a scalar interaction and therefore the polarizations of the incident and scattered photons must be parallel.

(4) Finally, the x-ray scattering cross section contains the form factor $f(Q)$, i.e., the Fourier transform of the charge-density spatial distribution. As the charge density is localized around nuclei in a space region of typical dimension of a few tenths to a few hundredths of nm, the function $f(Q)$ decreases appreciably on a Q range of several inverse nm^{-1}, thus it does not depress too much the scattering cross section in the mesoscopic region of interest. In the case of neutrons this form factor is not present (actually it is equal to 1) as neutrons interact with the nuclear matter, localized in a typical dimension of 10^{-6} nm. The neutron form factor is therefore constant in the whole accessible Q region.

From the discussion so far, it should be now quite easy to understand how important is the development of the x-ray method, which can access, in principle, an extremely large region of the E-Q plane. Particularly important is the small Q region, where the acoustic excitations have energies which are not of easy access to neutron spectroscopies.

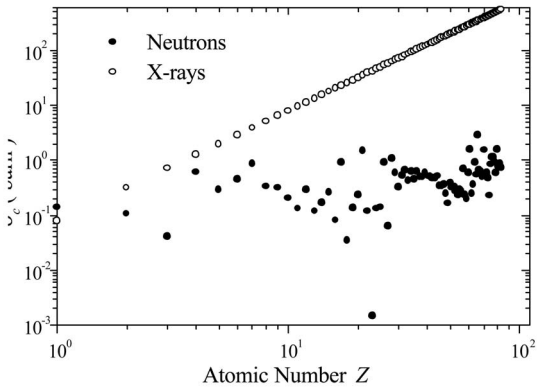

FIG. 4. The coherent scattering cross section of the elements for x ray (open circles) and for neutrons (full circles) reported as a function of the atomic number Z.

B. From the experimental data to the dynamical quantities

In order to extract quantitative information from the experimental intensity, i.e., to perform measurements of $S_q(Q,\omega)$ on an absolute scale, the most direct way is to use a reference scatterer and this is customarily done in neutron experiments. In IXS, for instance, such a procedure can be quite difficult because of the Q dependence of the form factor and of the analyzer's efficiencies. For these reasons an indirect method is always preferred. One possibility is to exploit the lowest-order sum rules of $S_q(Q,\omega)$ (Scopigno *et al.*, 2000a): in particular, for the first two frequency moments one has

$$\langle\omega^0\rangle_{S_q} = \int S_q(Q,\omega)d\omega = S(Q),$$

$$\langle\omega^1\rangle_{S_q} = \int \omega S_q(Q,\omega)d\omega = \hbar Q^2/2m,$$

where the second equality follows from Eq. (8) applied for $n=1$. The measured raw intensity is related to the dynamic structure factor through

$$I(Q,\omega) = A(Q)\int d\omega' S_q(Q,\omega')R(\omega-\omega'), \tag{89}$$

where $R(\omega)$ is the experimental resolution function and $A(Q)$ is a factor taking into account the scattering geometries, the experimental setup, and the atomic form factor. The first moments of the experimental data, $\langle\omega^0\rangle_I$ and $\langle\omega^1\rangle_I$, and those of the resolution function, $\langle\omega^0\rangle_R$ and $\langle\omega^1\rangle_R$, are related to $\langle\omega^0\rangle_S$ and $\langle\omega^1\rangle_S$ by

$$\langle\omega^0\rangle_I = A(Q)\langle\omega^0\rangle_{S_q}\langle\omega^0\rangle_R,$$

$$\langle\omega^1\rangle_I = A(Q)(\langle\omega^0\rangle_{S_q}\langle\omega^1\rangle_R + \langle\omega^1\rangle_{S_q}\langle\omega^0\rangle_R).$$

From the previous equation one derives that

$$S_q(Q) = \frac{\hbar Q^2}{2M}(\langle\omega^1\rangle_I/\langle\omega^0\rangle_I - \langle\omega^1\rangle_R/\langle\omega^0\rangle_R)^{-1}. \tag{90}$$

This procedure therefore can been adopted to establish an absolute scale for $S_q(Q,\omega)$ using the experimentally determined $I(Q,\omega)$ and $R(\omega)$.

C. Handling liquid metals

Working with liquid metals poses several practical problems. In particular, alkali metals are highly reactive and need to be kept under a protective atmosphere. A relatively small impurity (less than 100 ppm) in Ar or nitrogen will cause a film to form on the surface of the liquid metal.

In addition, glass is often limited in its use as a container for most liquid metals. Liquid metals are often strongly reducing. Glass, composed chiefly of silicon dioxide, is penetrated by the metal atoms, which can reduce the silicon by forming a metal oxide. As a result, the glass becomes discolored and brittle. For these reasons Pyrex cannot be used above 600 K and pure quartz above 900 K.

Preferred materials for working with liquid metals are refractory metals. This refers to the titanium group (Ti, Zr) as well as the vanadium and chromium groups. These transition metals are much less likely to undergo reduction and be solvated by liquid metals. The disadvantage in addition to cost is that the refractory metals have certain properties that make fabrication difficult. A tradeoff is to use iron plated with chromium. Other less reactive transition metals, such as the noble metals, are soluble in many liquid metal solutions. Austenitic stainless steel can be suitable up to 1000 K.

Liquid metals also share a common chemistry. The increasing electropositivity of the metals composing the liquid metal solution will determine the liquid's reactivity. Mercury, which is not very electropositive, is stable in air. Alkali metals, which are the most electropositive group of elements, are air sensitive. Li reacts slowly with air, yet dissolves and reacts quite readily with nitrogen. The other alkali metals are insensitive to nitrogen but react with other gases. All alkali metals violently react with water on the basis $\mathrm{Cs}>\mathrm{Rb}>\mathrm{K}>\mathrm{Na}\gg\mathrm{Li}$ (Ohse, 1985). The hydrogen generated in the water-alkali reaction can, in turn, react explosively with oxygen.

Reactivities reflect those of the solid material. The more reactive liquid metals, usually alkali ones, often develop a film if exposed to air. The high surface tensions of many liquid metals enable this film to remain in place. However, rates are greatly increased if turbulence is introduced because the protective coating is often dissolved into the liquid metal. Products of reaction, such as hydrides and oxides, are often redissolved into the liquid metal solution.

By virtue of the previously mentioned difficulties, experiments with alkali metals are often very hard to perform. In the case of inelastic x-ray scattering, in particular, such difficulties are enhanced by sample dimension requirement. As we have seen in Sec. III.A.4, indeed, in an optimal IXS experiment the sample length has to be comparable with the absorption length. With a few exceptions (Li and Na) this typically means submillimeter sample thickness. Common choices are therefore sample cells made of compatible metals provided with sealed sapphire or diamond windows.

Large efforts have been made recently to overcome the difficulty of performing x-ray experiments on liquid metals, the most remarkable example being the so-called Tamura-type cells made with a single-crystal sapphire with Be windows pressurized under He (Tamura *et al.*, 1999), performing up to 1900 K and 2 Kbars. More recently, a new sample environment especially tailored for alkali metals has been proposed (Matsuda *et al.*, 2004). In this case the cell is entirely made of molybdenum, with the windows made by single-crystal disks of controlled orientation electrolytically thinned at $\approx 40\ \mu$m.

A totally different approach is the one of contactless techniques. In this case the sample is levitated either

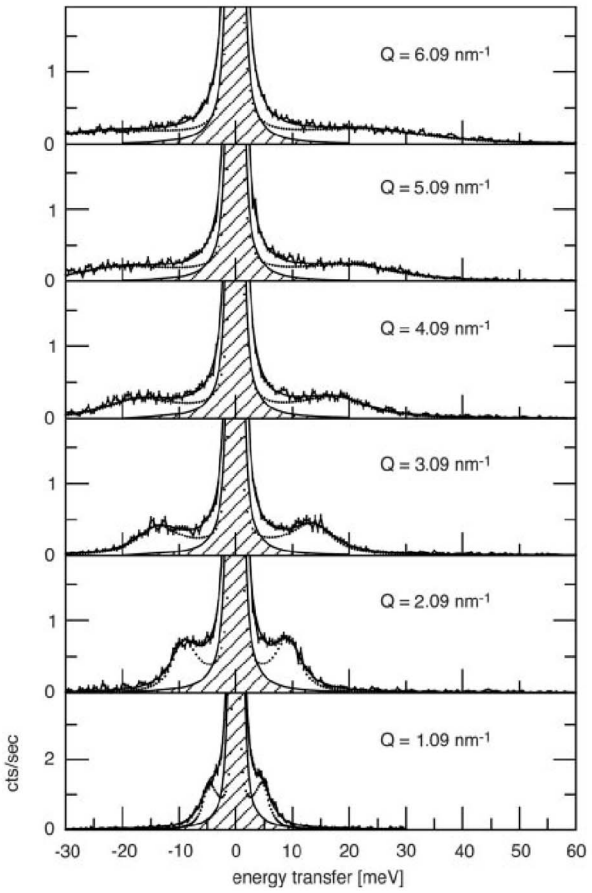

FIG. 5. Coupling IXS with levitation techniques: constant Q spectra of liquid alumina. From Sinn *et al.*, 2003.

electrostatically or by means of a controlled gas jet. The main difficulty in this technique is related to the sample stability in the x-ray beam, but recent impressive advancement has been done in this field. A new beamline for electrostatic levitation (BESL) has been developed at the Argonne Advanced Photon Source (APS), and the relevance of icosahedral ordering in the supercooling capabilities of liquid metals has been investigated (Kelton *et al.*, 2003). Another example is a recent x-ray scattering experiment performed on liquid Al_2O_3 in which alumina droplet of 3–4 mm diameter have been levitated by gas jet flow on the inelastic scattering beamline 3ID-C (Sinn *et al.*, 2003) (see Fig. 5).

IV. EXPERIMENTAL RESULTS

In this section we review, to the best of our knowledge, the experimental results reported so far, ordered according to the sample group in the periodic table. No results are available so far for elements belonging to group II.

A. Alkali metals

Alkali metals do not occur freely in nature, they are very reactive and can explode if exposed to water. These metals have only one electron in their outer shell and, as with all metals, they are malleable, ductile, and good conductors of heat and electricity. Alkali metals are softer than most other metals. Among the metallic elements they share the simplest pairwise interaction potential, which is also the closest to the Lennard-Jones one. As a consequence, their structural properties are also particularly simple, with a structure factor resembling the one of hard spheres. Also the dynamics therefore is expected to mimic the theoretical and numerical results achieved for Lennard-Jones and hard-sphere systems.

1. Lithium

Liquid lithium is probably the system which better reveals the complementarity of neutrons and x rays as far as inelastic scattering is concerned. Due to the high absorption cross section of the ^{6}Li isotope (σ_a=940 b) neutron-scattering experiments must necessarily be performed on ^{7}Li enriched samples, which is the dominant specie in the natural abundance. The high sound velocity ($c_t \approx 4500$ m/s), and the almost equivalent neutron scattering cross sections (σ_i=0.68 b,σ_c=0.62 b for ^{7}Li), pose severe limitations to the use of INS aiming at the deter-

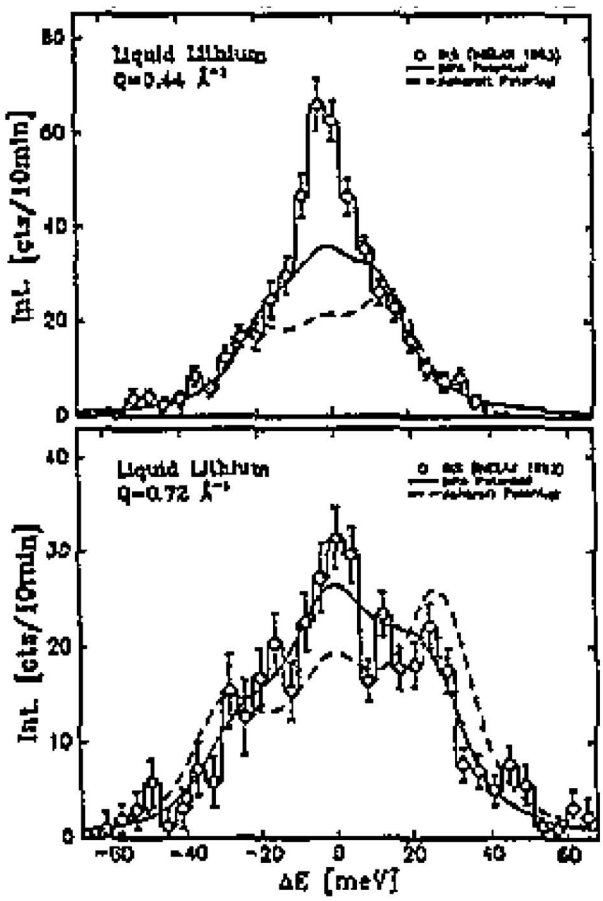

FIG. 6. Pioneering (1991) low-resolution IXS determination of the dynamic structure factor in liquid lithium with INELAX. From Burkel and Sinn, 1994.

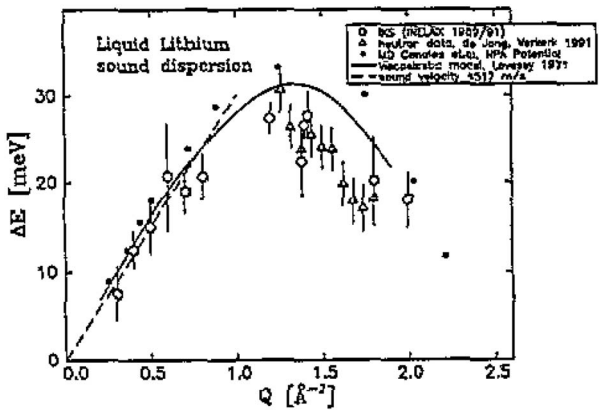

FIG. 7. Dispersion curve of liquid lithium achieved with IXS at INELAX. Theoretical predictions and INS results at higher Q's are also reported. From Burkel and Sinn, 1994.

mination of collective properties, while this technique turns out to be extremely useful for the investigation of single-particle motion. The first INS studies on this system can be traced back to the work of De Jong and Verkerk (Verkerk *et al.*, 1992; De Jong, 1993; De Jong *et al.*, 1993), who showed the presence of collective modes with a series of accurate experiments. Though they had to face the above-mentioned drawbacks, indeed, they were able to point out some significant issues: by modeling the coherent contribution with the extended hydrodynamic model [see Eq. (63) of Sec. II.G] they measured the dispersion curve above $Q_m/2$ (see Fig. 7) and they reported deviations from the Landau-Plazek ratio, which is expected to hold in the hydrodynamic regime [see Eq. (18) of Sec. II.C]. On the other side they shed light on the single-particle motion, accurately determining the incoherent contribution to the dynamic structure factor within the framework of Sec. II.G [Eqs. (28)–(31)]. They corroborated the mode coupling predictions (de Schepper and Ernst, 1979), extracting values of the diffusion coefficient and determining its temperature dependence.

An exhaustive characterization of the coherent dynamics was provided by the advent of inelastic x-ray scattering developed in the early 1990s, and liquid lithium has been the benchmark of such development. Being the lightest of the liquid metals, indeed, lithium played a privileged role in IXS, for the favorable signal-to-noise ratio and for the high sound velocity which allowed one to resolve the inelastic spectral component minimizing the initial difficulty of achieving energy resolutions comparable to neutrons.

Since the pioneering work of Burkel (1991) with the INELAX instrument (see Figs. 6 and 7), a decisive step forward achieved with the advent of the third generation sources which, combined with a brilliant technique for manufacturing silicon crystal analyzers, allowed one to

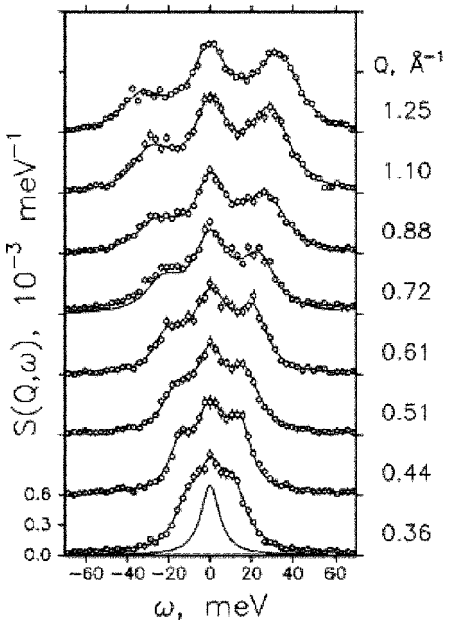

FIG. 8. First IXS measurements on liquid lithium performed on a third generation source (ESRF). Energy resolution is $\delta E = 11$ meV. The continuous line is the best fit according to the extended hydrodynamic model of Eq. (63). From Sinn *et al.*, 1997.

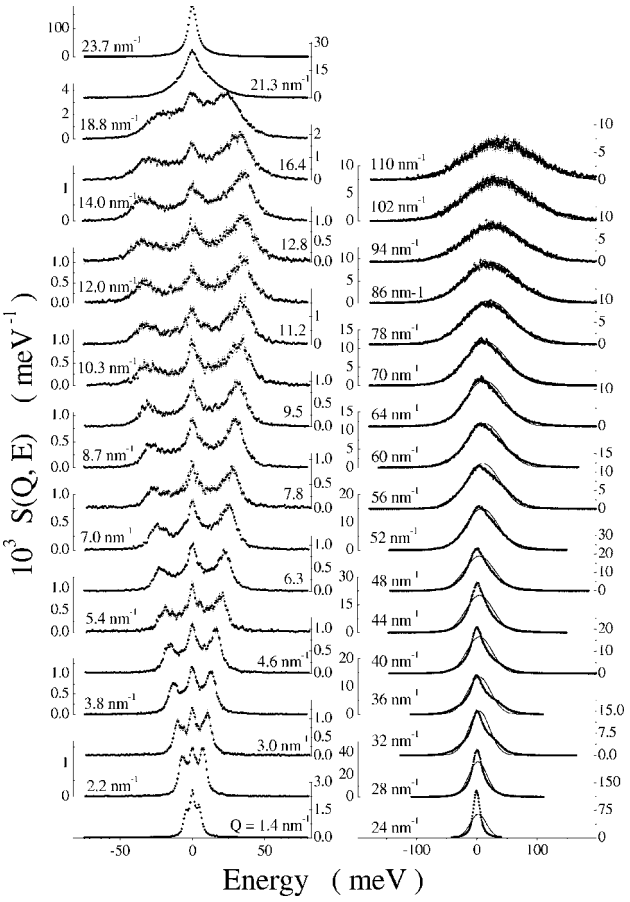

FIG. 9. IXS measurement of liquid lithium in a wide energy-momentum region. The transition from hydrodynamic to Gaussian-like response (continuous line in the right panel) can be clearly noticed. Energy resolutions are 1.5, 3.0, and 7.0 meV, increasing with the exchanged momentum. From Scopigno, Balucani, Cunsolo, *et al.*, 2000.

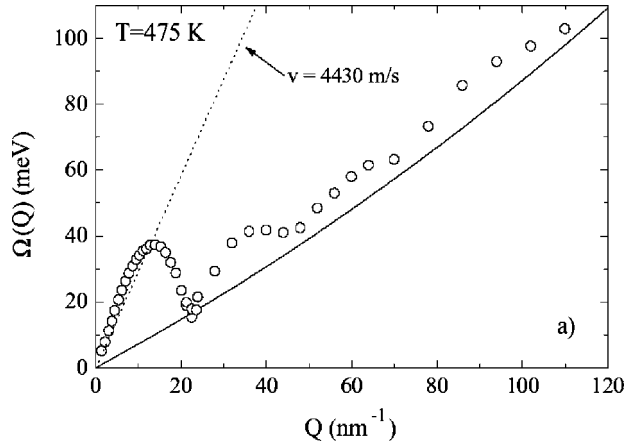

FIG. 10. Sound velocity as deduced by the maxima of the current correlation spectra, from the best fit with quantum corrected and resolution convoluted models.

exploit IXS to gather insight into the microscopic dynamics of disordered systems.

The first remarkable result on a third generation facility (ESRF) was provided by Sinn *et al.* (1997) (see Fig. 8) who, measuring energy spectra at fixed wave vectors, reported clear evidence of collective modes, being able to give significant hints for the choice of the most appropriate pseudopotential to describe liquid metals in numerical simulations (Canales *et al.*, 1994). In the same work, following the extended hydrodynamic model outlined in Sec. II.G (de Schepper and Cohen, 1980; de Schepper *et al.*, 1983), evidence was also reported for positive dispersion, i.e., for a sound velocity value exceeding the hydrodynamic one. This phenomenon was ascribed to a transition from a liquid to a solidlike response.

Following the development of the IXS technique, new experiments have been more recently performed on liquid Li in the extended region 1.4–110 nm^{-1}, corresponding to $Q/Q_m \approx 5\times10^{-2}$–5, which are reported in Fig. 9.

In Fig. 10 the dispersion relation is reported, determined in the same energy–wave-vector region, and the transition between the two distinct dynamical regimes is evidenced here by the sound velocity behavior. Beyond the first quasihydrodynamic region (an initial nearly linear dispersion), structural effects take place suppressing the sound propagation around $Q_m/2$ due to strong negative interference. With increasing Q values, the points in Fig. 10 show a second pseudo-Brillouin zone, followed by a series of oscillations that damp out with increasing Q—here, $\omega_l(Q)$ is approaching the single-particle behavior. These oscillations are in antiphase with those of $S(Q)$ and are therefore associated with the local order in the liquid.

While at low Q's the dynamic structure factor is qualitatively described by an extended hydrodynamic treatment [Eq. (63) of Sec. II.G], at wave vectors distinctly larger than Q_m the single-particle response is attained

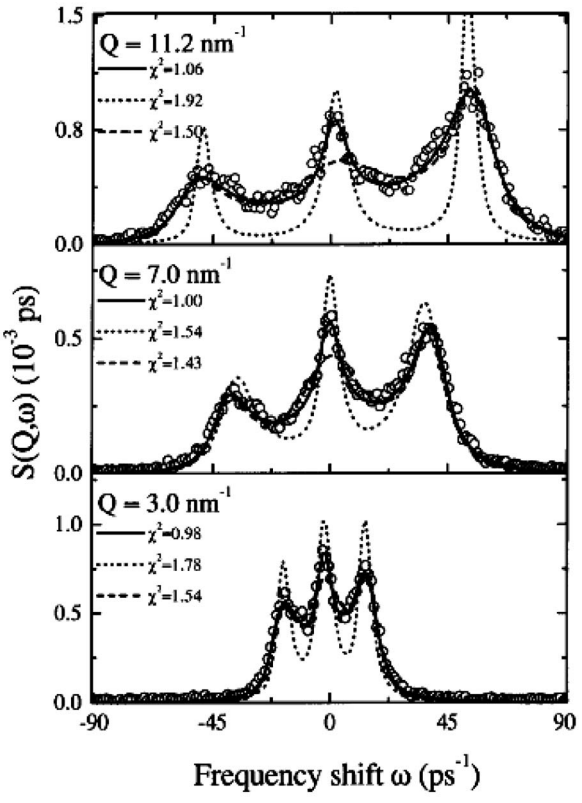

FIG. 11. Memory function at work: refined line-shape analysis of high-resolution IXS spectra. Both thermal and viscous channel are taken into account, mimicking this latter with single [Eq. (56), dotted line] or two [Eq. (59), continuous line] exponential processes.

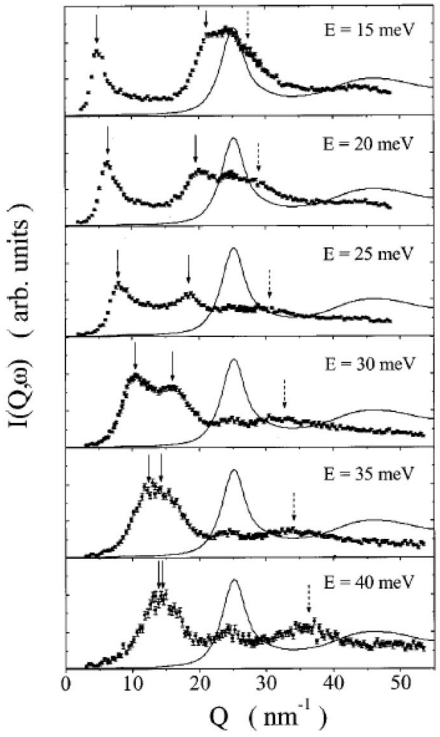

FIG. 12. Constant energy slices of the dynamic structure factor determined by IXS. Umklapp modes are visible on the sides of the main structure factor peak.

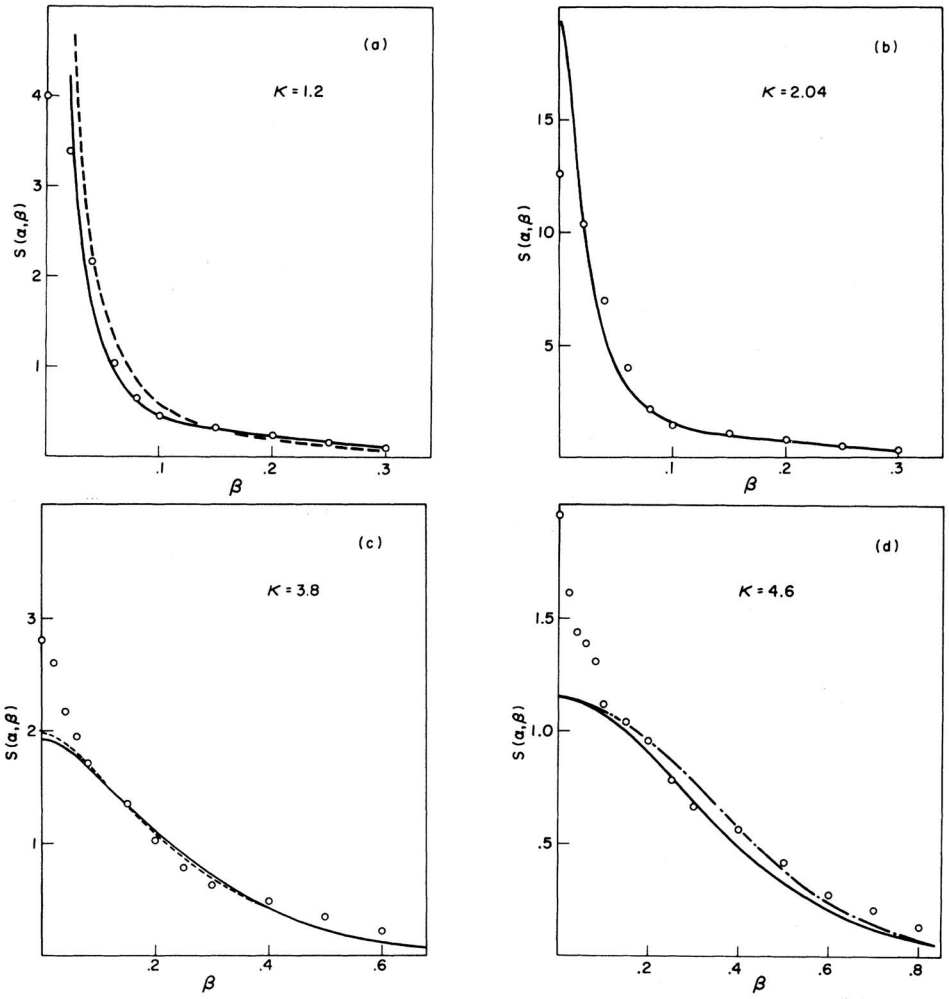

FIG. 13. Randolph's measurement (Randolph, 1964) of the dynamic structure factor of liquid sodium in reduced units, $\alpha = \hbar^2 Q^2/2mT$ and $\beta = \hbar\omega/T$, for four different values of momentum transfer. Line-shape analysis according to different models (Desai and Yip, 1969) Continuous line: EMA +calculated MSD. Short dashed line: EMA+computer simulation computation of the MSD. Long dashed line: hydrodynamic prediction. Dot-dashed line: free streaming limit.

through the mechanism described in Sec. II.D, ultimately leading to expressions well accounted by a combination of Eq. (24) accounting for each of the two isotopes ^{6}Li and ^{7}Li.

Due to an improvement in the energy resolution, which is nowadays comparable to the one of INS spectrometers in the same energy–wave-vector domain (1.5 meV at present), an approach based on the generalized hydrodynamics has been developed, which allowed one to point out the presence and the role of relaxation processes driving the collective dynamic at the microscopic probed wavelengths (Scopigno *et al.*, 2000a, 2000b). Within a memory function framework (Mori, 1965), the presence of two distinct viscous relaxation channels have been ascertained (see Fig. 11) beyond thermal relaxation, clarifying the origin and the nature of sound dispersion and attenuation properties in simple fluids. Of the two processes, active over well separated time scales, one is related to the well-known transition between a low-frequency, liquidlike response to a high-frequency, solidlike response. The second mechanism is instead a general relaxation process peculiar of the vibrational dynamics which is present regardless of the thermodynamic state of the system. In this context, positive dispersion has been shown to be strongly related to this latter process, the solidlike response being already attained over the wave-vector range probed in IXS (or INS) experiments.

An alternative route to the investigation of collective dynamics, which is dual to the one followed in the above-mentioned experiments and which is easily achievable through IXS, is the determination of the dynamic structure factor performing Q scan for fixed values of the energy transfer, reported in Fig. 12 for the case of lithium (Scopigno, D'astuto, *et al.*, 2001). In this way, one is able to have a direct sight over the so-called umklapp modes, i.e., excitations characterized by wave vectors which differ by a multiple of the reciprocal-lattice spacing, which have been early reported by means of INS in liquid lead (Cocking and Egelstaff, 1965a; Dorner *et al.*, 1965; Randolph and Singwi, 1966).

2. Sodium

Pioneering experimental determinations of the scattering law in liquid sodium can be traced back to the time of the IAEA symposium held in Chalk River (Cocking, 1963; Randolph, 1964). In this system the ratio between the incoherent to coherent cross section is very close to 1 (see Table I), therefore the separation between

TABLE I. Summary of some physical properties of liquid metals relevant for the dynamics.

Sample	T (K)	γ	c_s (m/s)	c_t (m/s)	max$\{c_l\}$ (m/s)	$\sigma_{inc}/\sigma_{coh}$	D_T (nm^2/ps)
Li	453	1.08[a,b] 1.065[c]	4554[c]	4466[d]	5762[d]		19.1[e]
	488				5423[f,g]		
	500						20.3[e,h]
	600	1.092[c]		4356[d]	5560[d]		
						0.99[h] 1.1[g]	
Na	371	1.12[i] 1.091[c]	2531[c]				68.8[e]
	388	1.11[a,b]	2514[j]		3160[j]		
	390				2930[k]		
	500						68.4[e]
	773		2310[j]		2881[j]		
	1073		2150[j]		2577[j]		
	1173		2093[j]		2492[j]		
						0.84[l] 1.006[m] 0.976[j]	
Mg	923	1.29[a]	4070[a]				37[e]
	973		4038[n]		4380[n]		
	1000						39.8[e]
						0.06[h]	
Al	933	1.4[a]	4750[a]				35.2[e]
	1000			4670[o]	7075[o]		36.4[e]
Si	1683	1.57[a]	3977[a]				9.4[e,p]
	1753		3952[q]		4597[q]		
						0.05[h]	
K	336.7	1.11[i] 1.102[c]	1880[c]				81.4[e]
	343	1.105[c]	1877[c]	1605[r] 1710[s]	2352[s] 2260[r]		
	350				2360[t]		
						0.20[h] 0.16[r]	
Fe	1808	1.8[a]	4000–4400[a]				7.3[e]
Co	1700						7.8[e,p]
	1765	1.8[a]	4033–4090[a]				
Ni	1500						16[e,p]
	1728	1.98[a]	4036–4045[a]				9.6[a]
	1763	1.88[u]	4280[u]	3121[u]	3855[u]		
						0.35[h] 0.30[u]	
Cu	1356	1.33[a]	3440–3485[a]		4230[v]		42.1[e]
						0.06[h]	
Zn	693	1.25[i] 1.26[a]	2835–2850[a]				15.7[e]
Ga	303	1.08[i]					11.6[e]
	315		2930[w]	2600[x]	3050[y]		
	326	1.08[x]			3240[x]		
	350						13.6[e]
						0.07[x] 0.02[h]	
Ge	1253	1.18[a,z]	2682[z]		2682[z]		
	1063						8–9[e]
						0.006[h]	
Rb	312	1.15[i] 1.097[c]	1260[c]				61.5[e]
	320		1370[aa]		1420[aa,f]		

TABLE I. (*Continued.*)

Sample	T (K)	γ	c_s (m/s)	c_t (m/s)	max$\{c_l\}$ (m/s)	$\sigma_{inc}/\sigma_{coh}$	D_T (nm^2/ps)
						0.00055[h]	
Ag	1233	1.32[a]	2710–2770[a]				66.5[e]
						0.125[h]	
Cd	594	1.25[a] 1.25[i]	2235–2255[a]				39.8[e,p]
						2.3[h]	
Sn	505	1.11[i]					17.3[e]
	593	1.09[a,bb,b]	2443[bb]		2736[bb]		
	1273		2228[bb]		2362[bb]		
						0.01[bb] 0.007[h]	
Sb	904	1.21[a]	1893–1900[a]				15.5[e]
						0.046[h]	
Te	723	1.033[a]	889[a]				0.8–1.3[e]
						0.05[h]	
Cs	302		967[c]				44.6[e]
	308	1.102[cc]	965[cc]		1140[cc]		
		1.099[c]					
						0.0596[cc]	
Au	1336	1.28[a]	2560[a]				40.4
						0.06[h]	
Hg	234						3.62[e]
	293	1.14[dd]	1451[ee]		2100[c] 1800[ff]		4.41[e]
	300						4.41[e]
						0.324[dd] 0.31[h]	
Tl	576	1.143[a]	1665[a]				25.2[e]
						0.025[h]	
Pb	600						9.89[e]
	623	1.19[a,b]	1770[gg]				9.89[e]
	700						11.4[e]
						0.000088[f]	
Bi	544	1.15[i]					8.09[e]

[a]Iida and Guthrie, 1993.
[b]Hultgren *et al.*, 1973.
[c]Ohse, 1985.
[d]Scopigno *et al.*, 2000.
[e]Touioukiam and Ho, 1973.
[f]From the max of S.
[g]Sinn *et al.*, 1997.
[h]Mughabghab, 1984.
[i]Kleppa, 1950.
[j]Pilgrim *et al.*, 1999.
[k]Scopigno, Balucani, *et al.*, 2002.
[l]Desai and Yip, 1969.
[m]Morkel and Gläser, 1986.
[n]Kawakita *et al.*, 2003.
[o]Scopigno *et al.*, 2001a.
[p]Solid.
[q]Hosokawa, Pilgrim, *et al.*, 2003; Hosokawa *et al.*, 2003a.
[r]Cabrillo *et al.*, 2002.
[s]Monaco *et al.*, 2004.
[t]Bove *et al.*, 2003.
[u]Bermejo *et al.*, 2000.
[v]Cazzato, 2005.
[w]Inui *et al.*, 1992.
[x]Bermejo *et al.*, 1997.
[y]Scopigno, Filipponi, *et al.*, 2002.
[z]Hosokawa *et al.*, 2001.
[aa]Copley and Rowe, 1974.
[bb]Hosokawa *et al.*, 2003b.
[cc]Bodensteiner *et al.*, 1992.
[dd]Badyal *et al.*, 2003.
[ee]Bove *et al.*, 2002a.
[ff]Hosokawa *et al.*, 2002.
[gg]Söderström *et al.*, 1980.

the two contributions is of crucial importance. Soon after Randolph's experiment, his data were analyzed in terms of mean-square displacement of an atom (Desai and Yip, 1969). This framework (described in Sec. II.E.1) poses on the Gaussian assumption for the incoherent cross section, while the coherent contribution was evaluated according to the effective-mass approximation (de Gennes, 1959):

$$S_s(Q,\omega) = \frac{1}{\pi}\int_0^\infty dt\,\cos(\omega t)\exp\left[-\frac{Q^2\langle r^2(t)\rangle}{6}\right],$$

$$S(Q,\omega) = \frac{1}{\pi}\int_0^\infty dt\,\cos(\omega t)\exp\left[-\frac{Q^2\langle r^2(t)\rangle}{6S(Q)}\right].$$

The mean-square displacement was then determined describing the atomic motion in terms of independent harmonic oscillators of frequency ω_0 and lifetime τ_0, which, in turn, are related to the spectral density of the velocity autocorrelation function $f(\omega)$:

$$\omega_0^2 = \int_0^\infty d\omega\omega^2 f(\omega) = \frac{\langle(\vec{\nabla}U)^2\rangle}{3m},$$

$$\tau_0 = \frac{T}{mD\omega_0^2},$$

$$f(\omega) = \frac{2}{\pi}\frac{\omega_0^2/\tau_0}{(\omega^2-\omega_0^2)^2+(\omega^2/\tau_0)^2}.$$

The basic ingredients of this approach are therefore the knowledge of the static structure factor, of the macroscopic diffusion coefficient, and of the mean-squared force $\langle(\vec{\nabla}U)^2\rangle$. The results of this description are tested against the experimental data in Fig. 13. From the same figure, it emerges how the single-particle regime is already attained at the lowest reported Q value, i.e., $Q = 12$ nm^{-1}, while the low-frequency discrepancy has been tentatively ascribed to finite instrumental resolution and to multiple-scattering effect.

Twenty years later, new INS data were reported (Söderström and Dahlborg, 1984; Morkel and Gläser, 1986), addressing in more detail the incoherent scattering contribution and showing how the diffusion process is actually more complex. Morkel and Gläser, following for the coherent contribution the Lovesey's prescription (Lovesey, 1971), and adopting for the incoherent part the Nelkin-Gatak model (Nelkin and Ghatak, 1964) described in Sec. II.E.4, extracted the reduced half width $\omega_{1/2}$ of the incoherent contribution finding a crossover between the hydrodynamic (Lorentzian) and single-particle (Gaussian) regimes. In Fig. 14 the linewidth $\omega_{1/2}/DQ^2$ is reported, and it clearly emerges how the single-particle limit ($\omega_{1/2}/DQ^2 \propto 1/Q$) is not yet attained even at $Q \approx 40$ nm^{-1}, which contrasts with the earlier assumptions of Desai and Yip. After a low-Q diffusion retardation the mobility increases in the transition region and finally tends to the free gas limit. The whole Q dependency is well described within the Enskog's hard-sphere gas (Sears, 1972), in terms of the expression (70). An alternative description of single-particle dynamics can be recovered within the memory function approach, though it fails in the high-Q region (Götze and Zippelius, 1976).

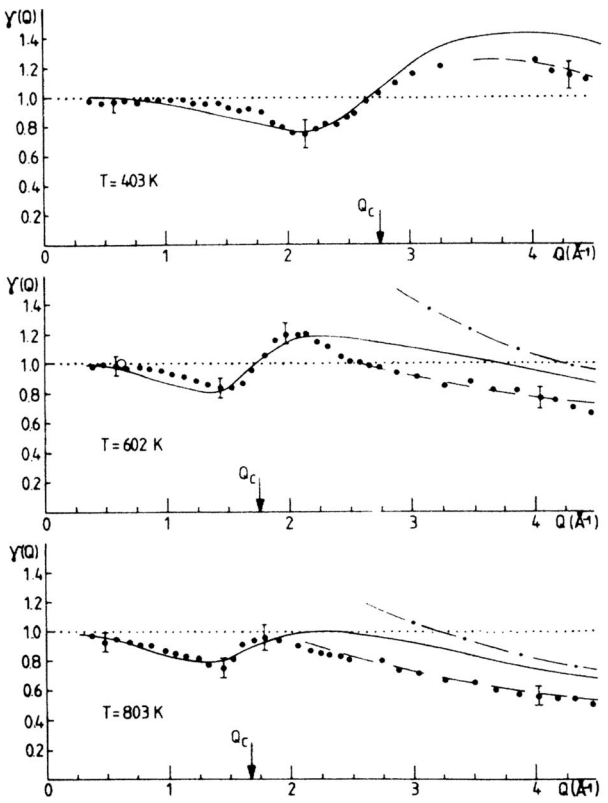

FIG. 14. Reduced quasielastic linewidth $\omega_{1/2}/DQ^2$ in liquid sodium at three different temperatures (Morkel and Gläser, 1986). The dotted line is the Fickian limit while the dash-dotted line is the perfect gas behavior ($\propto 1/Q$). The dashed line is the hard-sphere prediction (Cohen *et al.*, 1987), while the continuous line is the result obtained with mode coupling theory (Götze and Zippelius, 1976).

The first IXS determination of the collective dynamics in liquid sodium is due to Pilgrim and collaborators (1999), see Fig. 15. In this work, the coherent dynamic structure factor was measured at several temperatures, and analyzed according to the extended hydrodynamic model previously applied in liquid lithium (Sinn *et al.*, 1997). The take-home message is the presence of a positive dispersion effect which does not show significant temperature dependence. This result seems to rule out an interpretation of positive dispersion in terms of an activated process, as is the case in hydrogen bonding systems (Monaco *et al.*, 1999).

IXS experiments on liquid lithium were then repeated with increased energy resolution (Scopigno, Balucani, Cunsolo, *et al.*, 2002), and analyzed within the same two viscous relaxation processes proposed for liquid lithium (Scopigno *et al.*, 2000b). The same data have also been interpreted within the framework of the scale invariance of relaxation processes (Yulmetyev *et al.*, 2003), a theory

originally developed for liquid cesium (Yulmetyev *et al.*, 2001), which has been recently shown to be equivalent to the memory function approach in the sense that one solves the chain of Eqs. (35) with some *ad hoc* closure relation.

3. Potassium

The first experimental data on liquid potassium appeared surprisingly late relative to the other liquid metals (Novikov, Ivanovskii, *et al.*, 1996; Novikov, Savostin, *et al.*, 1996; Novikov *et al.*, 1997). Moreover, the kinematic region Q-E spanned in this experiment was quite narrow ($10 < Q < 13$ nm^{-1}) and only partial information on the microscopic dynamics could be obtained.

Very recently, two sets of INS experiments have been reported in molten K just above the melting temperature, one at the ISIS source (Cabrillo *et al.*, 2002), and the other at the ILL (Bove *et al.*, 2003). In the first case, two time-of-flight spectrometers were utilized (IRIS and MARI) aiming at a combined study of the dynamic structure factor with different energy resolutions for the narrow quasielastic and the broader inelastic component. The experiment of Bove *et al.* has been instead performed on the triple axis spectrometer IN1 optimized to access a broader kinematic region, as shown in Fig. 16 where a detail of the energy-momentum region accessed in the two experiments is shown.

The data taken on IRIS allowed for an accurate, high-resolution, determination of the diffusive processes underlying the incoherent dynamics. The results support the hydrodynamics predictions corrected by the mode coupling terms [see Eqs. (28)–(31) of Sec. II.E.3], as reported in Fig. 17. Beyond the diffusive mode, Cabrillo *et al.* identify a second contribution, coherent in nature according to the authors, which is weaker, broader, and almost Q independent up to $Q \approx Q_m$, while it becomes narrower above Q_m. The Q dependence of this coherent mode is rationalized in terms of extended heat mode [Eq. (67) of Sec. II.G] but its ultimate origin is rather ambiguous, especially in view of the INS measurements taken at IN1 and MARI.

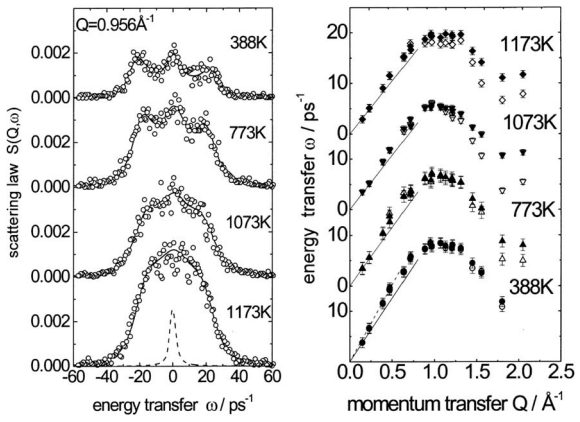

FIG. 15. Left panel: IXS determination of the $S(Q,\omega)$ in liquid sodium for selected temperatures. Right panel: dispersion curves at different temperature.

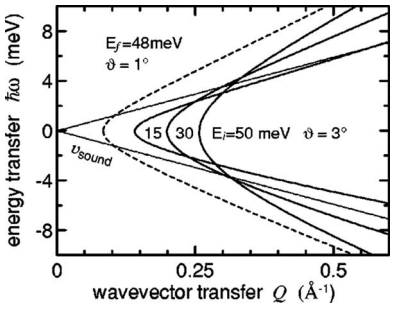

FIG. 16. Sketch of the kinematic regions accessed in the experiments of Bove *et al.* (dashed line) and Cabrillo *et al.* (continuous lines). Linear sound dispersion is also reported.

The results of these two experiments are reported in Fig. 18 for similar fixed Q values (Cabrillo *et al.*, 2002; Bove *et al.*, 2003). As can be easily noticed the possibility (offered by IN1) of extending the INS measurements at low Q is paid in terms of resolution. In both cases, however, evidence for inelastic coherent scattering is reported, though incoherent scattering largely dominates in the region where collective modes are more visible. The two sets of data have been analyzed according to different approaches by the respective authors. Cabrillo *et al.* utilized a memory function approach truncating the continued fraction at $n=2$, motivating this assumption as necessary to account for the nearly Q independence of the coherent quasielastic contribution reported in Fig. 17. Oddly enough, as evinced from Fig. 18 (left panel), neither the inverse relaxation time nor the raw quasielastic width that they extract with this model favorably compare with the coherent linewidth reported in Fig. 17.

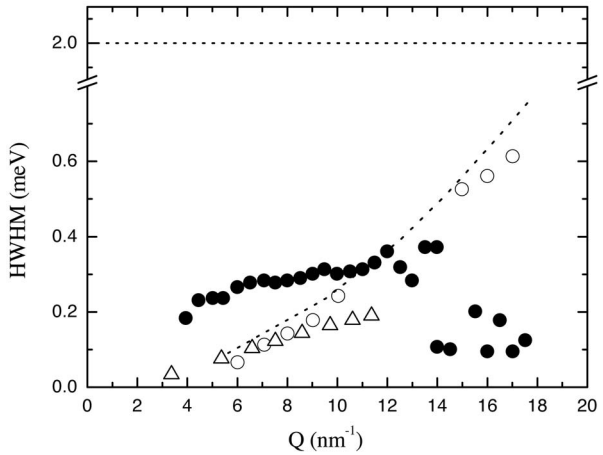

FIG. 17. Quasielastic linewidth according to recent INS measurements. Full and open circles are the coherent and incoherent contributions, respectively, determined with time of flight (Cabrillo *et al.*, 2002). Open triangles are the incoherent linewidth as measured with triple axis spectrometer (Bove *et al.*, 2003), the observed 2-meV coherent contribution is also indicated. The lower dotted line indicates the Fickian approximation.

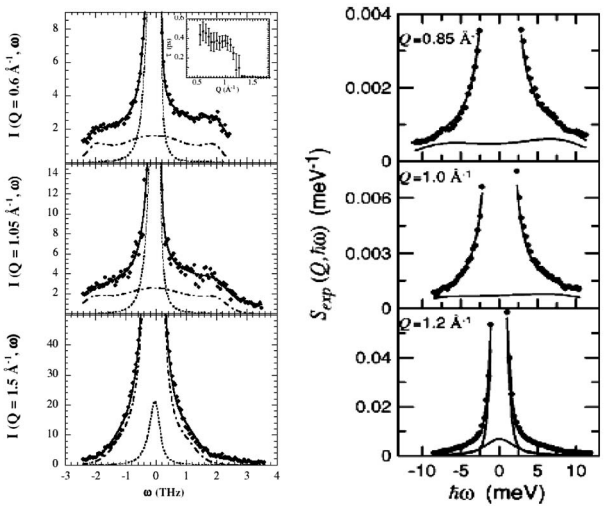

FIG. 18. Left panel: time-of-flight determination of the DSF in liquid potassium (circles) (Cabrillo *et al.*, 2002). The dash-dotted line depicts the coherent contribution. Right panel: triple axis spectrometer measurements in a similar momentum transfer region (circles) (Bove *et al.*, 2003). The continuous line is the inelastic contribution to the collective dynamics.

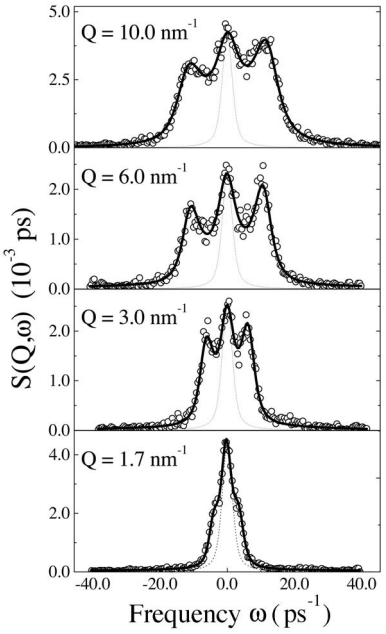

FIG. 19. High-resolution IXS measurements in liquid potassium (open circles) (Monaco *et al.*, 2004). The continuous line is the line-shape description according to a multiple relaxation memory function model (see text).

Bove *et al.*, on the other side, utilize a damped harmonic oscillator for the *purely* inelastic term and two Lorentzian for the quasielastic coherent and incoherent contributions, respectively. The results for the incoherent part, achieved within the jump diffusion model described in Sec. II.E.2, are consistent with the high-resolution measurements (IRIS) of Cabrillo *et al.* (see Fig. 17). On the other side, the coherent contribution turns out to be much broader (FWHM$\approx$4 meV, i.e., a relaxation time $\tau\approx$0.32 ps), in contrast with the data of Cabrillo *et al.* reported in Fig. 17 (full circles), but in qualitative agreement with the quasielastic linewidth and the relaxation time of the same authors' measurements reported in Fig. 18.

Both experiments extract the dispersion curves, in one case following the exact hydrodynamic prescription as the maxima of the current correlation function (Cabrillo *et al.*, 2002) and in the other (Bove *et al.*, 2003) as the damped harmonic oscillator (DHO) frequency, which coincides with the current correlation maximum if the presence of the quasielastic coherent term is neglected. The two independent determinations are indeed in good agreement, except at large wave vectors where the data of Bove *et al.* are systematically higher though with some scattering. The sound velocity values exhibit the usual excess with respect to the hydrodynamic value. This high-frequency sound is ascribed by both studies as a reminiscence of solidlike behavior, i.e., as the upper edge of a transition occurring from the low-Q, hydrodynamic domain to the high-frequency regime. This claim stems on the basis of the similarity of the sound velocity value of molten potassium with the value for crystalline acoustic phonons along the [1 0 0] direction.

A recent IXS experiment on molten K (Monaco *et al.*, 2004) contributed to shed some light on some aspects of the collective dynamics, giving a coherent picture in terms of relaxation processes which is common to several other simple fluids and, more generally, to glass forming materials and molecular liquids (see Fig. 19).

First, it has been shown how the coherent dynamics is driven by thermal and viscous processes. These latter, which are dominant, proceed over two different time scales. Consequently, the FWHM of the quasielastic (coherent) contribution is not *per se* directly associated to any relevant time scale. The thermal process, indeed, is characterized by a time scale largely exceeding the Brillouin frequency, while both the viscous processes control

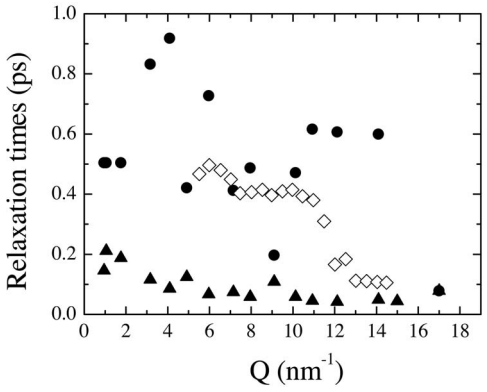

FIG. 20. Viscous relaxation times as measured by means of IXS (Monaco *et al.*, 2004). Circles: structural relaxation time. Triangles: microscopic relaxation time. The relaxation time obtained by means of INS is also reported (Cabrillo *et al.*, 2002), showing how it averages between the two mechanisms reported by IXS.

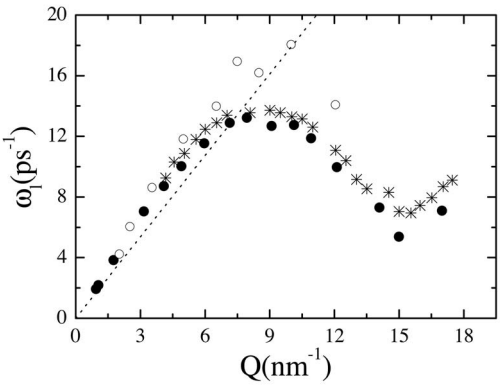

FIG. 21. Dispersion curves (maxima of the current correlation function) measured by INS [open circles (Bove *et al.*, 2003), stars (Cabrillo *et al.*, 2002)] and IXS [full circles (Monaco *et al.*, 2004)].

the quasielastic width. The corresponding relaxation times can instead be determined within the memory function formalism of Eq. (59), obtaining the results reported in Fig. 20. In the same plot, the relaxation time obtained by Cabrillo *et al.* (consistent with the determination of Bove *et al.*) is also reported (see Fig. 21). As one might expect, this value is somehow averaging between the two distinct viscous processes. More specifically, at low Q the single time approximation of Cabrillo *et al.* seems to mimic the slower process, while at higher Q the faster process is described. This hypothesis is consistent with the observation, reported in other alkali metals, of a decreasing weight of the slow relaxation process on increasing the wave vector (Scopigno *et al.*, 2000a). As far as the sound propagation properties are concerned, the IXS experiment analyzed in terms of generalized hydrodynamics suggests a minor role of the structural process, which accounts for approximatively 10% of the whole positive dispersion effect, which is dominated by the faster process (see Fig. 22). This observation, already reported for many other simple liquids, poses against the commonly invoked explanation of the positive dispersion in terms of transition from a liquidlike to solidlike regime (structural relaxation).

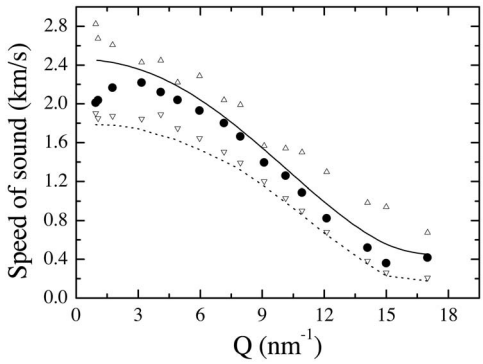

FIG. 22. Sound velocities as determined by IXS: apparent [circles, from the maxima of $C_L(Q,\omega)$], isothermal (dotted line), and infinite frequency limit (continuous line) determined from Eqs. (46) and (52). The unrelaxed sound velocity values, due to the structural relaxation only (down triangle) and to the whole relaxation process (uptriangle), are also reported as estimated by the fitting.

4. Rubidium

Liquid rubidium has been the first of the alkali metals to be addressed by a very famous neutron-scattering experiment (Copley and Rowe, 1974), immediately substantiated by molecular-dynamic simulations (Rahman, 1974) (see Fig. 23). The reason for such interest lies in the possibility of extracting information on the collective dynamics, given the almost negligible incoherent cross section ($\sigma_i/\sigma_c \approx 10^{-4}$) and the relatively low sound velocity value. The result of this experiment contributed to open the route to the understanding of the collective dynamics in simple liquids, showing that the presence of a high-frequency inelastic mode is an intrinsic property of alkali metals not related to quantum properties or critical thermal population effect as suggested by earlier works on liquid hydrogen (Carneiro *et al.*, 1973). Though the experiment was affected by an elaborated multiple-scattering subtraction (due to the lack of an absolute normalization), which leads to a possibly unreliable quasielastic spectral component, some other chords of

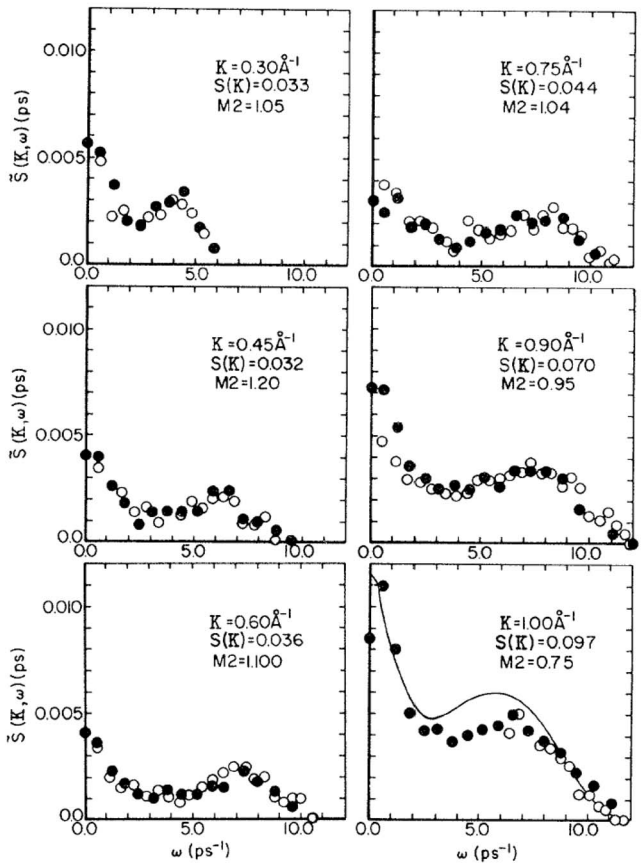

FIG. 23. The experimental determination of constant Q slices of the DSF by means of INS scattering in liquid rubidium. A new era for the study of collective properties in simple liquids. From Copley and Rowe (1974).

interest were hit. At variance with earlier results on liquid lead (Dorner *et al.*, 1967), no evidence of secondary modes of transverse nature was reported in this system. Finally, a mild positive dispersion effect was observed [though Copley and Rowe looked at the maximum of $S(Q,\omega)$ rather than to the maximum of $J(Q,\omega)$] which was tentatively ascribed to the distinction of zero sound and first sound as discussed by Egelstaff (1967).

More recently, an inelastic-scattering experiment was performed with cold neutrons (Chieux *et al.*, 1996) aiming at the determination of the dynamic scattering law in an extended temperature region beyond the one explored by Copley and Rowe. The kinematic accessed region is above $Q=9$ nm^{-1}, and therefore the observed excitations lies beyond the linear dispersion region. This work has the merit to stress the importance of the choice of the appropriate dynamical variable and of the fitting model to determine the dispersion curve.

The old data of Copley and Rowe have been more recently reanalyzed in terms of generalized hydrodynamics (Morkel and Bodensteiner, 1990), comparing the results to the ones obtained in molten cesium, which are discussed in Sec. IV.A.5.

To our knowledge no IXS measurements have been reported on liquid rubidium. The main difficulties for such an experiment would be the very small absorption length (about 200 μm) and the quite low sound velocity value ($\approx$1400 m/s) which would confine the elastic modes on the tail of the resolution function.

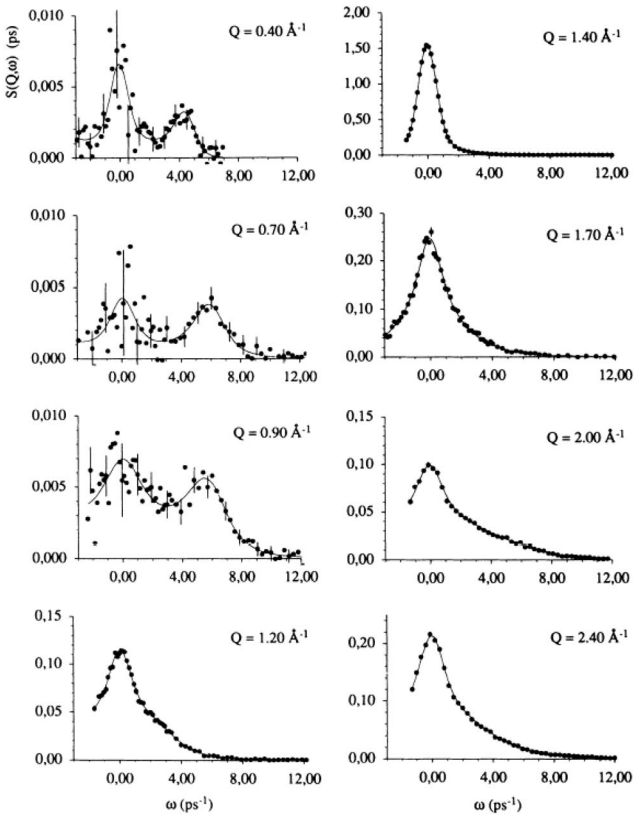

FIG. 24. Dynamic structure factor of cesium at the melting point (circles). The continuous line is the viscoelastic approximation. From Bodensteiner *et al.*, 1992.

5. Cesium

The experimental determination of the dynamic scattering law in liquid cesium is dated to the early 1990s (Gläser, 1991; Bodensteiner *et al.*, 1992) (see Fig. 24). Due to the relatively small incoherent cross section and to the low sound velocity value, after rubidium liquid Cs is the most favorable alkali metal aiming at the study of collective dynamics by means of INS. Despite its late outlet, the work of Gläser and Bodensteiner reports an impressive state-of-the-art triple axis experiment, and a robust data reduction performed with innovative algorithms (Bodensteiner, 1990).

The experiment is focused on the determination of the collective properties and, though a careful subtraction of the incoherent contribution is performed, once more the intrinsic difficulty of determining the quasielastic part of the coherent spectrum emerges. This notwithstanding, the data clearly show the departure of the collective dynamics from the strict hydrodynamic region and the evolution toward the free streaming limit. This effect is quantified by the behavior of the FWHM of the quasielastic line reported in Fig. 25: while the hydrodynamic prediction, based on purely adiabatic thermal fluctuations, predicts $\omega_{1/2}=D_T Q^2$, the actual linewidth is always below this limit in the whole explored region, indicating the dominant presence of viscous processes in the quasielastic spectrum, as recently pointed out in other alkali metals and liquid aluminum (Scopigno and Ruocco, 2004) against an opposite interpretation in terms of linearized hydrodynamic models (Singh and Tankeshwar, 2003, 2004). The de Gennes (1959) narrowing was also observed, and the Q dependence of the linewidth was described within the hard-sphere extended mode approximation [Eq. (67), Sec. II.G]. The free streaming limit is not yet attained at wave vectors as large as twice the position of the main peak of the static structure factor (Bodensteiner *et al.*, 1992). The lineshape analysis was performed with several approaches,

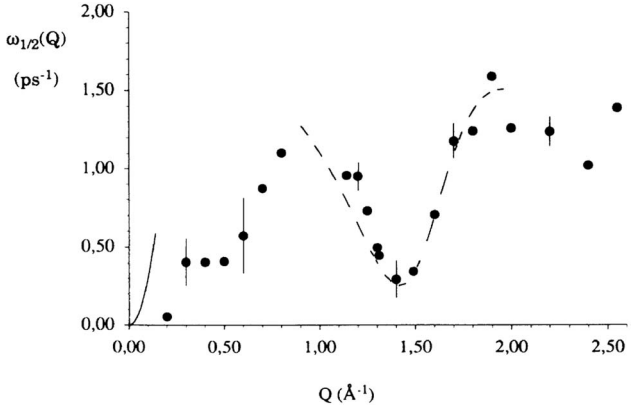

FIG. 25. Linewidth of the coherent quasielastic spectral component in molten cesium (circles). The continuous line is the thermal value $D_T Q^2$, while the dashed line is the hard-sphere prediction from Eq. (67). From Bodensteiner *et al.*, 1992.

within the extended hydrodynamic model (de Schepper and Cohen, 1980), with the viscoelastic model (Lovesey, 1971), and with two relaxation times accounting for both viscous and thermal processes. In this latter case was found a negligible role of the thermal process on approaching the first maximum of the structure factor, though the fitted values of the thermal relaxation time were in significant disagreement with the expected values $1/D_T Q^2$ [Fig. 9 of Gläser (1991)]. It was then pointed out the impossibility of discriminating the different models, given the signal-to-noise ratio of the available data. The Q dependence of the longitudinal viscosity, extracted from the $S(Q,\omega=0)$ value (according to the prescription of generalized hydrodynamics), showed a decreasing behavior previously observed in Lennard-Jones systems (Ailawadi *et al.*, 1971; Tankeshwar, 1994) and more recently in several other liquid metals (Scopigno, Filipponi, *et al.*, 2002; Monaco *et al.*, 2004). Finally, the maxima of current correlation spectra showed the usual positive dispersion effect, which was interpreted as precursor of the solidification according to the usual idea of a transition between a liquidlike and solidlike regime.

Neutron-scattering data on liquid cesium have also been used as a benchmark to develop an approach based on the idea of time-scale invariance of the relaxation processes (Yulmetyev *et al.*, 2001). Within the Zwanzig-Mori projector formalism, one can construct an infinite, non-Markovian, set of interconnected kinetic equations relating each memory function with the one of higher order (Mori, 1965):

$$\frac{dF(Q,t)}{dt} = -\Omega_1^2 \int_0^t d\tau M_1(Q,\tau) F(Q,t-\tau),$$

$$\frac{dM_1(Q,t)}{dt} = -\Omega_2^2 \int_0^t d\tau M_2(Q,\tau) M_1(Q,t-\tau),$$

$$\vdots$$

$$\frac{dM_i(Q,t)}{dt} = -\Omega_{i+1}^2 \int_0^t d\tau M_{i+1}(Q,\tau) M_i(Q,t-\tau), \quad (91)$$

where $F(Q,t)$ is the normalized density correlation function and Ω_i are characteristic frequencies of the process. Following the Bogoliubov approach of the reduced description, one hypothesizes the time-scale invariance of the relaxation processes beyond a certain level, defining a closure level $M_{i+1}(t) \approx M_i(t)$ and thus getting an explicit expression for the DSF in terms of the spectral moments.

To our knowledge no IXS experiments on liquid Cs have been reported, for the same kind of difficulties as in liquid Rb.

B. Alkaline-earth elements

1. Magnesium

Magnesium is one of the simplest divalent elements. The coherent dynamic structure factor has been recently determined at the SPring8 IXS beamline (Kawakita *et al.*, 2003). The dispersion curve shows a 8% deviation from the adiabatic sound velocity, with a maximum value lying halfway in the hydrodynamic and the c_∞ value. An average relaxation time was determined ($\tau=0.094$ ps), which is about one-third of the one of the neighboring alkali element liquid Na (Pilgrim *et al.*, 1999). The analysis of the quasielastic line revealed a Q^2 broadening in the quasihydrodynamic regime, while around the de Gennes narrowing region the linewidth was successfully reproduced by the de Schepper and Cohen model (de Schepper *et al.*, 1984), i.e., through Eq. (67). Molecular-dynamics simulations have been recently performed in this system by both classical molecular dynamics and orbital free *ab initio* simulations (Alemany *et al.*, 1997; Gonzalez *et al.*, 2001). The two approaches give very similar results as far as the phonon dispersion is concerned, while the quasielastic contribution is less pronounced in the *ab initio* calculation. In this respect, a comparison with the experimental data (Kawakita *et al.*, 2003) would be extremely interesting, though one should first convolute the calculated $S(Q,\omega)$ with the instrumental IXS resolution and take into account the quantum correction arising from the detailed balance condition.

C. Group-III elements

1. Aluminum

One of the most puzzling results of early neutron spectroscopy is the striking similarity between the spectra of polycrystalline and liquid aluminum observed in Stockholm in 1959 and published in the final form a few years later (Larsson *et al.*, 1965). In this experiment time-of-flight data were collected on a cold neutron spectrometer, but at those times multiple-scattering corrections were almost impossible and therefore the spectra did not obtain a detailed explanation. A second time-of-flight experiment was performed in the same period, but again the results were lacking a detailed interpretation (Cocking, 1967b). Fifteen years later the original experiment of Larsson was revisited, in an effort to reanalyze the results in the light of up to date theoretical developments. More specifically, the experimental results were used to test the old convolution approximation (Vineyard, 1958), mean-field approaches (Singwi *et al.*, 1970), and kinetic theory (Sjögren, 1978; Sjögren and Sjölander, 1978). Nevertheless, these data have been collected at very large energy and wave-vector value and always presented as a time-of-flight scan, and therefore they are not very helpful to establish the existence of collective modes in this system. Aluminum, indeed, is an almost purely coherent scatterer, but the high sound velocity value prevents the study of acoustic modes by means of INS (see Table I). This is testified by a more recent INS experiment performed at IN4 (ILL) (Eder *et al.*, 1980). Although multiple-scattering correction and constant-Q cut reductions have been performed in this case, no evidence of collective modes could be reported

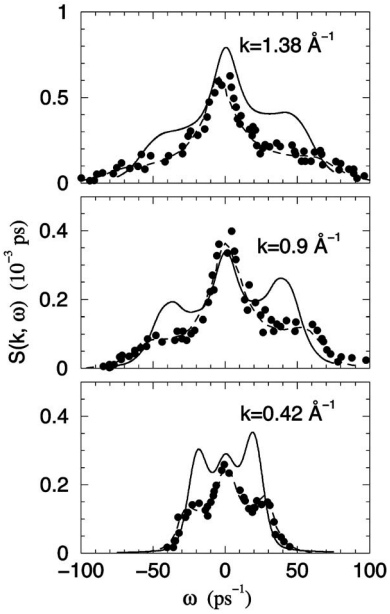

FIG. 26. Dynamic structure factor of molten aluminum. Comparison between the OF-AIMD calculation (continuous line) (Gonzalez *et al.*, 2002) and the experimental IXS values with their fitting based on generalized hydrodynamics (Scopigno *et al.*, 2001a). From Gonzalez *et al.*, 2001.

due to the restricted kinematic region corresponding to the slow neutrons utilized (≈55 meV).

Much of the knowledge about the microscopic dynamics in liquid Al relies, in fact, on the numerical work of Ebbsjö *et al.* (1980), who calculated the dynamic structure factor utilizing two different local pseudopotentials and the local pseudopotential originally developed by Ashcroft (1966). The dynamic structure factor has been shown to be somehow reminiscent of the viscoelastic model with the addition of a Gaussian term, accounting for the approach to the high-Q, free streaming limit. He was then able to predict the existence of collective modes for $Q<10$ nm^{-1}, though he reported sound velocity values distinctly larger then the adiabatic value over the whole explored range ($Q>3$ nm^{-1}). Triggered by this observation, a modified version of the viscoelastic approach was developed (Gaskell, 1986) and tested against the data of Ebbsjö. At the same time, a single relaxation process scenario has been proposed based on a sech memory function shape within the Mori-Zwanzig scheme (Tankeshwar *et al.*, 1988).

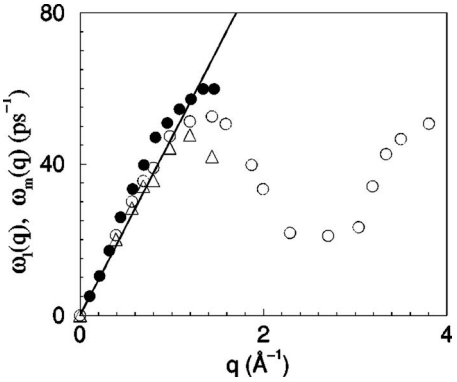

FIG. 27. Sound dispersion of liquid aluminum from the maxima of the current correlation function: open circles, OF-AIMD calculation (Gonzalez *et al.*, 2002); full circles, IXS experimental values (Scopigno *et al.*, 2001a). Dispersion from the maxima of the dynamic structure factor numerically evaluated is also reported (open triangles), as well as the hydrodynamic value (continuous line). From Gonzalez *et al.*, 2002.

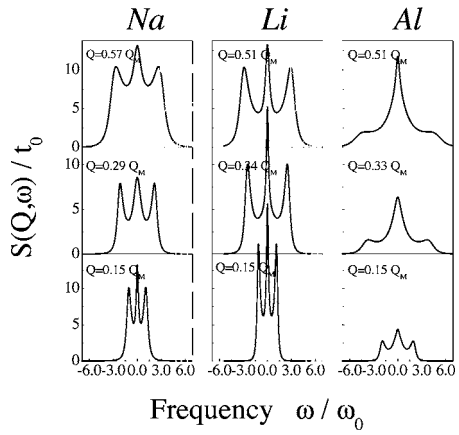

FIG. 28. Resolution deconvoluted, classical line shape utilized to described the IXS spectra of molten Li (Scopigno *et al.*, 2000b, 2001a; Scopigno, Balucani, *et al.*, 2002), Na, and Al, reported on relative momentum and energy scale (see text).

The first experimental observation of collective modes in liquid Al has been reported much more recently by means of IXS (Scopigno *et al.*, 2001a). A high-frequency regime has been observed for $Q>5$ nm^{-1}, while below this value the dynamics approaches the hydrodynamic limit, though the transition is not fully accomplished at the lowest investigated wave vector, $Q=1$ nm^{-1}. The scenario arising from the IXS study is quite similar to the one characterizing alkali metals, though with significant quantitative differences such as a more intense quasi-elastic component testifying a more important role of the structural relaxation in this system.

The IXS data have been recently used to test orbital free *ab initio* calculations (OF-AIMD) (Gonzalez *et al.*, 2001, 2002) (see Fig. 26). The overall agreement is quite satisfactory though the numerical calculations show somehow lower sound velocity value and tend to overemphasize the inelastic components. From Fig. 27 one can argue the importance of the dynamical variable representing the sound velocity. The presence of positive dispersion, in particular, is strongly affected by the choice of the maxima of $C_L(Q,\omega)$ rather than the maxima of $S(Q,\omega)$.

In Fig. 28, finally, we report a comparison of the line shape obtained from the resolution-deconvoluted, classical line shape utilized to fit the IXS spectra of liquid lithium, sodium, and aluminum at the same reduced values of momentum (Q/Q_M) and energy ($\omega t_0=\omega/\omega_0$, with $t_0=\sqrt{m/k_BT_m}/Q_M$) transfer. As can be clearly evinced, the attitude of alkali metals to sustain density fluctua-

tions is much more pronounced than in other simple liquid metals.

2. Gallium

Among simple liquid metals, Ga is endowed with peculiar structural and electronic properties. In addition to the low melting point (T_m=303 K), it shows an extended polymorphism in the solid phase with complex crystal structures where a competition between metallic and covalent bindings takes place. Despite the nearly free electron electronic DOS anomalies associated with some covalency residue are present. Moreover, the first peak of $S(q)$ presents a hump characteristic of non-close-packed liquid structures (Bellissent-Funel *et al.*, 1989).

Early inelastic scattering experiments on liquid Ga were performed at the beginning of the 1970s with neutrons (Gläser *et al.*, 1973; Löffler, 1973; Page *et al.*, 1973; Bosio *et al.*, 1976). Due to the quite large sound velocity value, compared to the available kinematic range, these studies were mainly addressed to the investigation of the quasielastic part of the dynamic structure factor.

Twenty years later, another series of INS experiments were performed on a triple axis instrument (Bermejo *et al.*, 1994) with the aim of ascertaining the presence of low-Q collective modes just above the melting temperature. Indeed, although by virtue of the above-mentioned anomalies liquid Ga seems to elude the picture of the high-frequency dynamics emerging in all monatomic liquids, on the basis of the shape of the interaction potential evidence for collective modes should be expected below $Q_m/2$. Quite surprisingly, no evidence of an inelastic signal was reported in the region were longitudinal modes were expected on the basis of the hydrodynamic sound velocity. This result was interpreted as an overdamping effect traced back to the high value of longitudinal viscosity ($\approx$10 cP). Additionally, by comparing a constant energy scan (see Fig. 29) to the expression of Buchenau for acousticlike plane-wave excitations in amorphous solids (Buchenau, 1985), an excess of scattering was reported for frequency distinctly larger then the maximum frequency of the acoustic branch. This result was interpreted as the fingerprint of the presence of high-energy opticlike modes.

A few years later, then, a new set of experiments were performed at higher temperatures by the same authors (Bermejo *et al.*, 1997), and a contrasting behavior with the previous findings was reported. More specifically, the appearance of nonoverdamped sound modes was reported, accompanied by a second, higher frequency mode of presumably optical origin. The discrepancy between the low- and high-temperature experiments was ascribed to a viscosity drop of a factor $\approx$7 and therefore to a narrowing of the acoustic mode according to the hydrodynamic expression (17).

The presence of a higher frequency mode appearing in the constant Q scan for wave vectors larger then Q_m seems to corroborate the presence of an opticlike excitation suggested by the previously mentioned constant energy scans (Bermejo *et al.*, 1994).

A recent IXS experiment performed on liquid gallium just above the melting point (Scopigno, Filipponi, *et al.*, 2002) portraits the collective dynamics in a quite similar fashion to the one of alkali metals and of liquid Al, thus removing the anomaly suggested by the neutron experiments. Collective modes, in fact, have been unambiguously observed in the low-temperature region where neutrons suggested an overdamped regime. This result suggests the inadequacy of Eq. (17) to estimate Brillouin linewidths, which can be easily understood in terms of generalized hydrodynamics results reported for alkali metals (Scopigno *et al.*, 2000a): outside the truly hydrodynamic region, the viscous relaxation dynamics proceeds over two distinct physical mechanisms, the structural relaxation and the short-lived rattling dynamics. In the high-frequency region of interest, structural relaxation is frozen (the system is responding as a solid) and therefore the viscosity associated to this process does not contribute to the sound damping. Moreover, the thermal contribution in Eq. (17) might not be correct at wave vectors as large as a few nm^{-1}, since the adiabatic regime could be replaced by as isothermal one, as already pointed out (Scopigno and Ruocco, 2004). Consequently, Eq. (17) is an overestimate of the actual linewidth [which in the case of liquid lithium has been quantified as a factor of 2 (Scopigno, Filipponi, *et al.*, 2000a)]. In Fig. 30 we report the two experiments for similar values of the momentum transfer. The viscoelastic prediction (Lovesey, 1971; Bermejo *et al.*, 1994) is also reported, showing how it clearly underestimates the quasielastic contribution, though it provides a reasonable estimate of the genuine inelastic mode. The IXS findings have been recently corroborated by a new accurate INS experiment, used to test the reliability of a model interaction potential by comparing the dynamic structure factors (Bove *et al.*, 2005).

Summing up, the lack of low-temperature collective excitations reported in this system with neutrons is probably due to the difficulty of a reliable extraction of the coherent part of the scattering function. On the other side, the interesting observation of possibly opticlike high-frequency modes certainly calls for further investigation although, in our opinion, does not justify *per se* a description of the acoustic dynamics in terms of crystalline reminiscent dynamics. The analogy with several IXS results on different systems suggests a prominent role of the topological disorder in characterizing the acoustic branch.

Very recently, an IXS experiment explored the high-Q region [$20<Q<70$ nm^{-1}, i.e., length scales smaller than the size of the first coordination shell (Scopigno *et al.*, 2005)]. While generalized hydrodynamics provides a coherent picture of the dynamics in the lower Q region, not much is known about collective dynamics at such short length scales. For hard spheres, Enskog's kinetic theory predicts in this region the dominant effect of a generalized heat mode (see Fig. 31). Liquid gallium, however, by no means can be modeled as a hard-sphere fluid, for the above-mentioned structural and electronic properties. Surprisingly, it turned out that a description

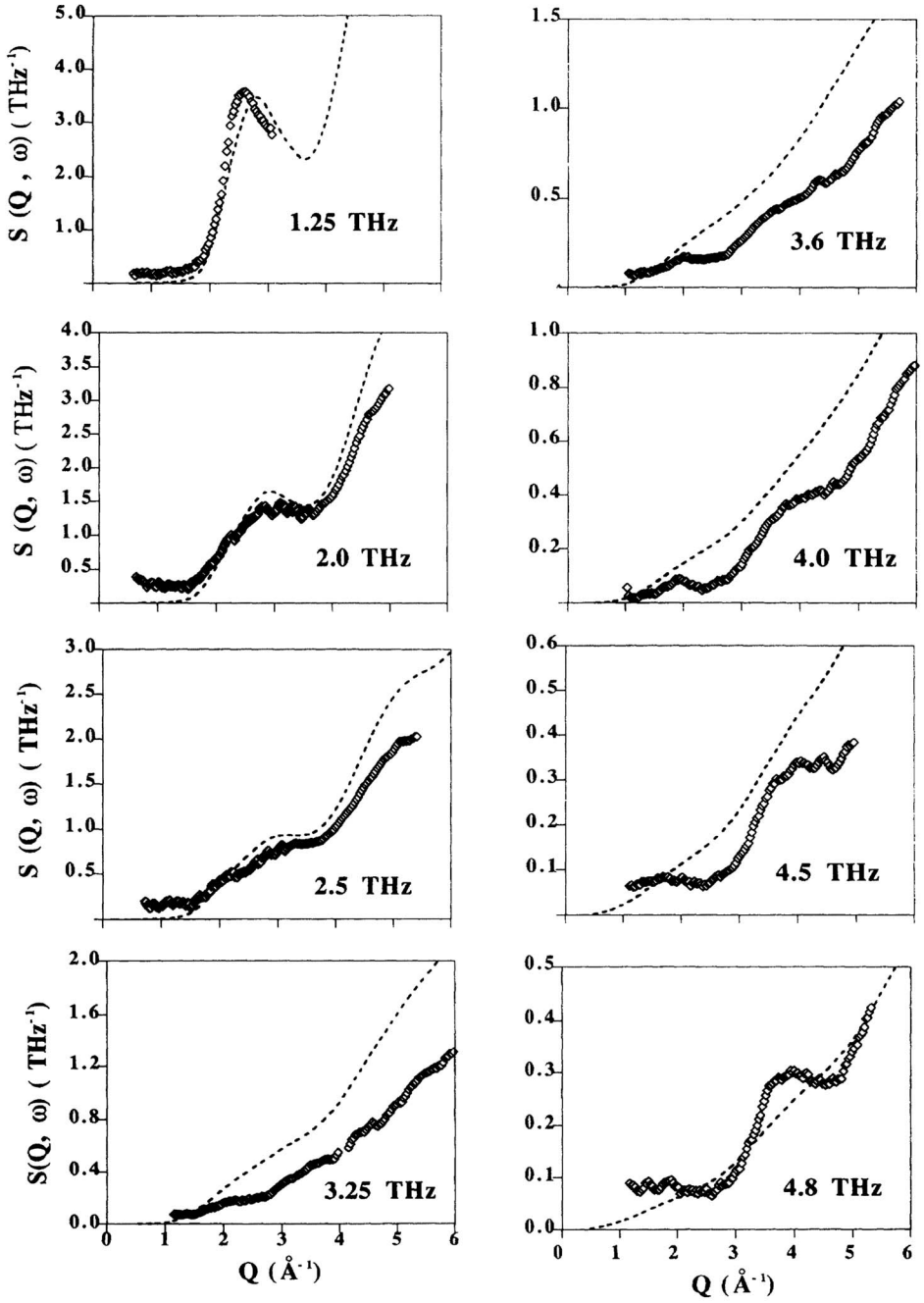

FIG. 29. INS constant energy scans (circles) compared to the model of Buchenau for plane-wave excitations in solids (Buchenau, 1985). From Bermejo *et al.*, 1994.

in terms of heat mode [Eq. (67)] still applies, at the price of introducing an *effective* hard-sphere diameter [larger than the one associated to the first $S(Q)$ maximum], which probably accounts for the associative tendency of this liquid (dimerlike structures).

D. Group-IV elements

1. Silicon

Due to its several unusual properties, liquid Si is always classified as a nonsimple liquid. While in the crystalline phase Si is a diamond structure semiconductor, it undergoes a semiconductor-metal transition upon melting, which is accompanied by a density increases of about 10%, and by significant structural changes (the coordination number grows from 4 in the solid state to about 7 in the liquid). Similarly to gallium, the static structure factor $S(Q)$ exhibits a shoulder on the high Q side of the first peak (Waseda and Suzuki, 1975), a feature that cannot be reproduced using a simple hard sphere model, appropriate for alkali metals.

No neutron-scattering data exist to the best of our knowledge, while very recently two inelastic x-ray scattering experiments have been performed at both the ESRF (Hosokawa *et al.*, 2003a) and SPring8 (Hosokawa, Pilgrim, *et al.*, 2003) (see Fig. 32).

In the first of the two above-referenced experiments, a positive dispersion of 15% has been found. In the sec-

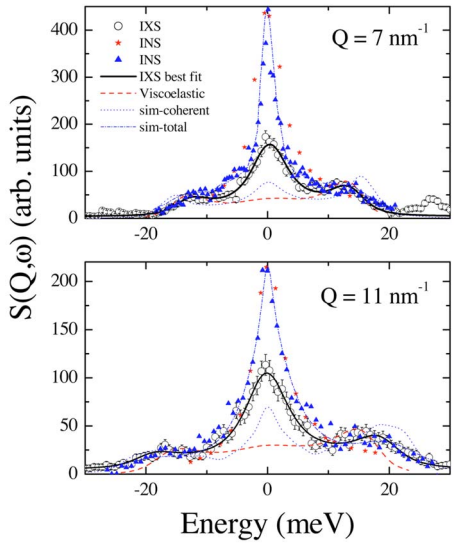

FIG. 30. (Color online) Comparison between the INS [stars (Bermejo *et al.*, 1994) and triangles (Bove *et al.*, 2005)] and IXS [open circles with error bars (Scopigno, Filipponi, *et al.*, 2002)] determinations of $S(Q,\omega)$ in gallium at the melting temperature, for two different values of the (constant) momentum transfer. The dotted line is the viscoelastic prediction (Bermejo *et al.*, 1994) (convoluted with the INS instrumental resolution and accounting for the detailed balance condition), while the continuous line is the best fit to the IXS data utilizing a memory function accounting for the thermal relaxation and two viscous processes (see text). Molecular-dynamics simulations for the coherent (dotted line) and total (dash-dotted line) $S(Q,\omega)$, convoluted to the INS resolution, are also reported (Bove *et al.*, 2005).

ond experiment, a higher resolution and more accurate study has been carried out, allowing one to follow the transition from the high-frequency to low-frequency regimes. The data were analyzed in terms of the damped harmonic oscillator model for the inelastic component and Lorentzian for the quasielastic, and no significant quantitative differences were detected utilizing the same memory function scheme proposed for other IXS studies on liquid metals (Scopigno *et al.*, 2000a).

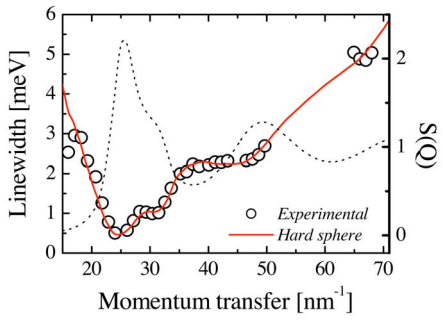

FIG. 31. (Color online) Half width at half maximum of the dynamic structure factor as determined by IXS in the kinetic regime (open circles). The prediction according to Enskog's theory is also shown (continuous line) (Scopigno *et al.*, 2005).

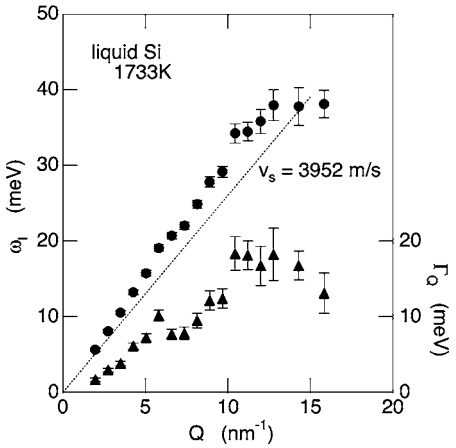

FIG. 32. Sound velocity and attenuation in molten silicon (Hosokawa, Pilgrim, *et al.*, 2003).

In the vicinity of the main peak of the static structure factor, the Lorentzian shape for the quasielastic component turned out to be inadequate, and has been replaced by a combination of Lorentzian and Gaussian contributions (pseudo-Voigt).

2. Germanium

Liquid Ge shares the same peculiarities as liquid silicon, though with some slight quantitative differences.

IXS data on liquid Ge have been recently obtained (Hosokawa *et al.*, 2001), and they show evidence for collective propagating modes. An analysis based on a Lorentzian shape for the quasielastic and a damped harmonic oscillator for the inelastic modes, revealed the absence of positive dispersion effects in the investigated Q range (2–28 nm^{-1}). In our opinion, this result calls for further investigations, as this is an almost unique feature in respect to the other monoatomic liquid metals investigated so far (especially silicon, which has very similar structural properties). The de Gennes narrowing has been analyzed in terms of an extended hydrodynamic heat mode, utilizing the analytical expression obtained within the hard-sphere approximation (Cohen *et al.*, 1987), but the quite large error bars and the limited spanned Q range prevents one to draw a final conclusion.

3. Tin

Tin is the heaviest of 4B elements. Its structural properties are quite similar to those of alkali metals, with a coordination number close to 12 but with the typical shoulder on the high-Q side of the main $S(Q)$ peak (Waseda and Suzuki, 1975) which is typical of Si, Ge, and Ga.

The first INS experiments in liquid tin have to be traced back to the early 1960s. Similarly to other early neutron-scattering experiments no clear picture of the microscopic dynamics could be outlined. In one case (Palevsky, 1961) the Vineyard approximation (Vineyard, 1958) was used to analyze the data, while in another

study an experimental strategy for suppressing multiple scattering was tested (Brockhouse *et al.*, 1963). Although a wave-vector–energy plot was obtained from raw time-of-flight data (Cocking and Egelstaff, 1965b), according to Copley and Lovesey no side peaks should be observed transforming time-of-flight data to $S(Q,\omega)$ on constant Q slices (Copley and Lovesey, 1975).

Constant Q IXS spectra of liquid tin have been very recently reported for low ($T=593$ K) and high ($T=1273$ K) temperatures at the ESRF (Hosokawa *et al.*, 2003b). The sound velocity seems to exceed the hydrodynamic value at both temperatures of 6% and 12%, respectively. This notwithstanding, these quantitative estimates must be taken with care, due to the quite large error bars. Moreover, the dispersion curves have been determined from the damped harmonic oscillator frequency, neglecting the effect of the quasielastic component. For Q values close to the main peak of the structure factor, as in the case of liquid Si (Hosokawa, Pilgrim, *et al.*, 2003), the line shape of $S(Q,\omega)$ turned out to be empirically described by a combination of Lorentzian and Gaussian contributions or, equivalently, by a memory function analysis similar to the one reported for alkali metals (Scopigno *et al.*, 2000b). As a matter of fact, at such large-Q values, as previously observed for liquid lithium (Scopigno, Balucani, Cunsolo, *et al.*, 2000; Scopigno *et al.*, 2000a), the microscopic dynamics undergoes a transition from the (generalized) hydrodynamic behavior to the free streaming limit and a detailed description of such transition is still missing.

4. Lead

Molten lead has been one of the first metals to be investigated by inelastic neutron scattering, as the first experiment can be traced back to the 1950s (Egelstaff, 1954; Brockhouse, 1955). Details of the experiments performed up to 1975 (Dorner *et al.*, 1965, 1967; Randolph and Singwi, 1966; Cocking and Egelstaff, 1968) have been exhaustively reviewed by Copley and Rowe (Copley and Lovesey, 1975). One of the most interesting results has been the evidence of both a longitudinal and a transverse branch in the dynamic structure factor, though this result was presented with some caution as the transverse mode could be an artifact arising from multiple-scattering effects.

In the early 1980s new INS studies performed with both triple axis spectrometer and time-of-flight spectrometers appeared (Söderström *et al.*, 1980; Söderström, 1981), aiming to validate the presence of a dispersion relation and of a transverse branch. A longitudinal mode compatible with the higher frequency excitation previously reported by Dorner *et al.* (1967) was reported, whose sound velocity is consistent with hydrodynamic value. The accessible kinematic range is too limited to assess any evidence of positive dispersion effect. No evidence for a lower frequency excitation was instead reported, corroborating the hypothesis that such a feature is an artifact stemming from multiple scattering.

Liquid lead has recently been the focus of molecular-dynamic simulations aiming to describe collective dynamics in terms of generalized kinetic modes (Bryk and Mryglod, 2001a, 2001b). Beyond the hydrodynamic region, different branches corresponding to sound and heat waves have been identified, and their nature has been extensively discussed.

E. Group-V elements

1. Bismuth

The first inelastic scattering investigation of molten bismuth was originally reported by Cocking (1967a), who reported a dispersion curve extracted by time-of-flight neutron spectra. At the IAEA symposium of 1968 two experiments Bi were presented: in one case two dispersion branches were obtained from time-of-flight data (Tunkelo *et al.*, 1968), though the low-frequency excitation was probably due to an artifact of a missing multiple-scattering correction. In the second study data were converted to constant Q spectra (Mateescu *et al.*, 1968).

Liquid Bi has been recently the subject of new INS investigations (Dahlborg and Olsson, 1982) (see Fig. 33). Measurements were performed just above melting at T

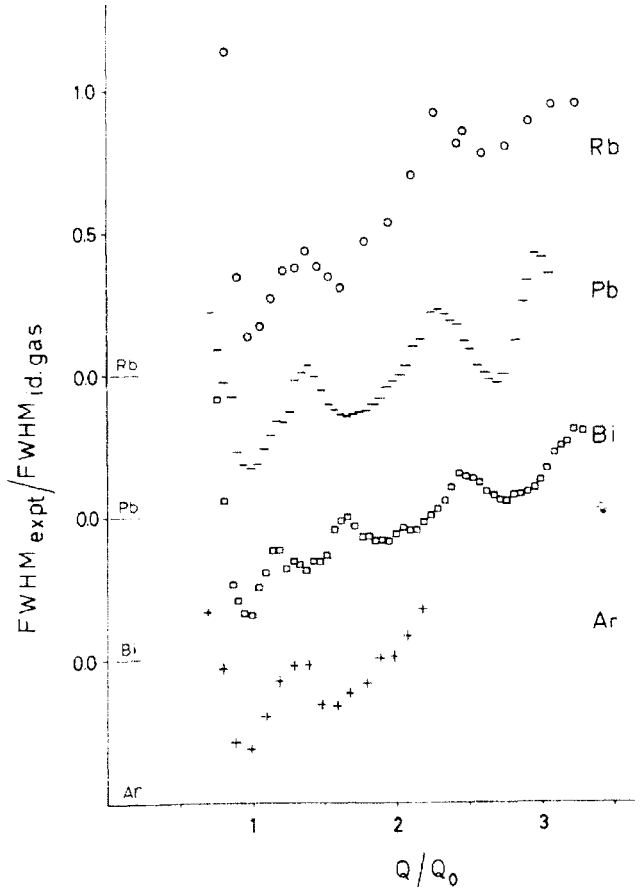

FIG. 33. FWHM of molten Bi compared to other simple liquids. It can be noted the presence of an intermediate minimum between the first two maxima which is not present in the other simple fluids. From Dahlborg and Olsson, 1982.

=578 K, in a wave-vector region spanning from just below the first maximum in $S(Q)$ up to wave vectors as high as 70 nm^{-1}. This kinematic region lies above the region were collective modes could be expected, so the study mainly deals with the quasielastic spectral component. Generalized hydrodynamics models based upon a single relaxation time were tested against the experimental data utilizing different approximation for the memory function shape (Ailawadi *et al.*, 1971; Lovesey, 1971). Experimental data were then unfolded by instrumental resolution modeling the quasielastic shape as Lorentzian and the resolution as Gaussian. The main point of the paper is the determination of the Q dependence of the spectral FWHM, which is also compared to other systems. In particular, it is pointed out how, beside the expected de Gennes narrowing occurring at Q_m, the FWHM shows a minimum rather then the expected maximum at $Q \approx 1.5 Q_m$ (which characterize the dynamics in several simple liquids such as Pb, Rb, and Ar). This anomaly is related by the authors to the shoulder observed in the static structure factor just above Q_m, and therefore identified as a nonsimple nature of liquid Bi.

The kinetic region has been investigated in liquid Bi within the generalized collective mode approach (Bryk and Mrygold, 2000). The presence of high-frequency kinetic branches has been ascertained, and it has been pointed out that their weight is too small to make them visible in the dynamic structure factor. This result seems to be in agreement with recent IXS findings on a very similar system, namely, liquid Ga, in which only acoustic modes were reported (Scopigno, Filipponi, *et al.*, 2002).

F. Transition metals

1. Mercury

Experimental studies of microscopic dynamics in liquid mercury are very recent compared to the systems reviewed so far, and they were presented at the LAM XI Conference (Yokohama, Japan). The first investigation was obtained by means of INS at the IN1 facility of the ILL (Bove *et al.*, 2002a, 2002b) (see Fig. 34). In this work, a detailed investigation of the dynamic structure factor is undertaken at room temperature, and presented as constant Q cuts in the range 2.5–12 nm^{-1} with a high-energy resolution of $\delta E \approx 1$ meV. The data are analyzed with an empirical model consisting of a damped harmonic oscillator for the purely inelastic part and the sum of two Lorentzian functions accounting for the quasielastic contribution. While the inelastic component is no doubt of coherent nature, the narrower of the two Lorentzians is ascribed to incoherent scattering, and modeled as a simple diffusive term of linewidth DQ^2. Given the values of D, this results in a quasielastic contribution which could not be resolved by the much broader resolution function. The linewidth of the broader Lorentzian is almost Q independent, and its origin is ascribed by the authors to an incoherent process, on the basis of the coincidence of the damped harmonic

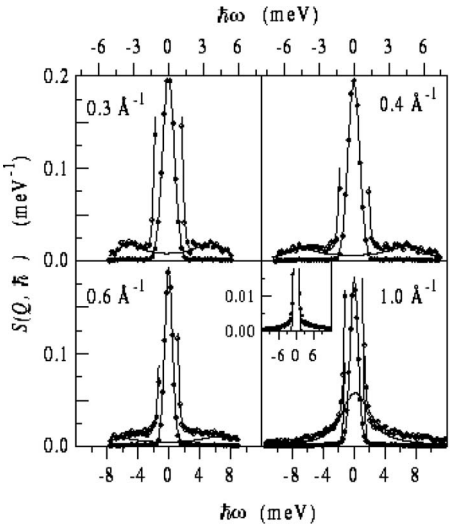

FIG. 34. DSF of molten Hg measured by means of INS at the indicated Q values. The inelastic and quasielastic components, modeled with two Lorentzians and a DHO, respectively, are also shown. From Bove *et al.*, 2002a.

oscillator area with independent (static) structure factor determinations. Turning our attention to the collective dynamics, the extrapolated high-frequency value of the sound velocity $[c_\infty(Q \to 0) = 2100 \pm 80$ m/s], obtained by the damped harmonic oscillator frequency parameter (therefore approximately equal to the maximum of the current correlation function, the difference being due to potential quasielastic coherent contribution), turns out to largely exceed the hydrodynamic value (c_s =1451 m/s), suggesting a huge positive dispersion effect close to 50% largely exceeding similar effects reported in other metals. This result is rationalized in terms of the Bohm-Staver model, which provides an expression, Eq. (75), for the sound velocity yielding, for molten Hg, $c_l(Q \to 0) \approx 2090$.

Nearly in coincidence with the neutron experiment of Bove *et al.*, an IXS study of the coherent dynamics in liquid Hg appeared (Hosokawa *et al.*, 2002), in which the dynamic structure factor is examined in a wave-vector region extended up to $Q_m \approx 25$ nm^{-1}, with a factor of 2 worse resolution, but in a significantly larger energy region (see Fig. 35). As in the work of Bove *et al.*, the genuine inelastic features of the data are modeled with a damped harmonic oscillator function, but it appears clearly from the raw data that a coherent quasielastic term dominates the $\omega \approx 0$ region. This latter contribution is modeled with a Lorentzian shape. Although the authors neglect the presence of this quasielastic term in the calculation of the sound velocity value, taking the damped harmonic oscillator frequency as the relevant parameter they obtain a value of $c_\infty(Q \to 0) = 1840$ m/s, an estimate which is directly comparable with the corresponding INS determination. This discrepancy, which may be due to the limited energy range at the low Q's of the INS experiment, as well as to the non-negligible resolution effect on the lowest Q's of the IXS experi-

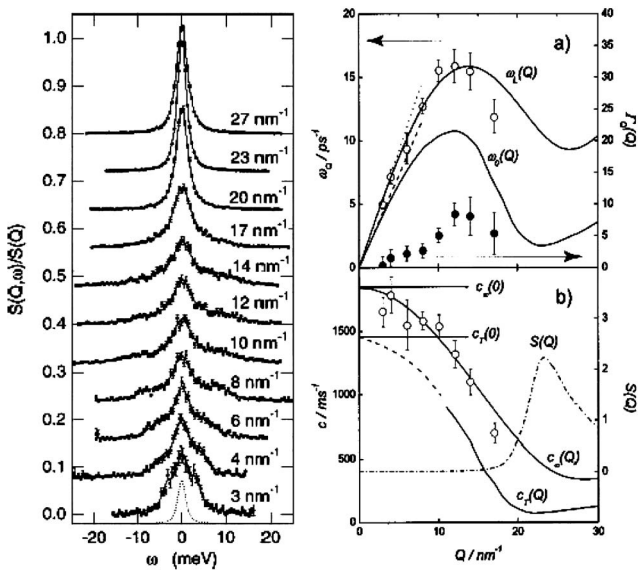

FIG. 35. Left panel: IXS determination of the DSF in Hg near the melting temperature. Right upper panel: dispersion relation and sound attenuation properties as deduced by a DHO +one Lorentzian fit. The low- and high-frequency limits are also reported. Right lower panel: Corresponding sound velocities. From Hosokawa *et al.*, 2002.

ment, calls in our opinion for further investigations and suggests to take with some care any interpretations in terms of the Bohm-Staver model of positive dispersion at least with a quantitative point of view. Hosokawa *et al.*, on the other hand, cast the anomalous dispersion in the usual framework of the shear relaxation. The IXS work also confirms the non-negligible presence of a quasielastic signal in the coherent dynamic structure factor, suggesting that it should also be taken into account in INS data treatment. We expect that the broader Lorentzian contribution reported by Bove *et al.* for example, could be at least partially coherent in nature.

A more recent INS study contributed to shed some light on the possible origin of the quasielastic spectral components (Badyal *et al.*, 2003). The experiment has been performed on the time-of-flight spectrometer MARI, optimized to access a restricted kinematic region ($-6<\omega<6$ meV at the lowest accessed momentum transfer $Q\approx 4$ nm^{-1}) with an energy resolution sufficient to study the diffusive dynamics ($\delta E=0.4$ and $\delta=0.8$ meV at the two incident energy utilized). The narrower incoherent contribution (self-diffusion), resolution limited in the experiment of Bove *et al.* was now detected with a procedure similar to the one applied in liquid potassium (Cabrillo *et al.*, 2002), i.e., fitting the data with two Lorentzian in a restricted wave-vector region where the two quasielastic features are well separated, determining the analytical Q dependence of the FWHM of the diffusive term, and finally focusing on the broader component over the whole momentum transfer region keeping all the parameters of the diffusive term fixed. With this procedure, the narrower Lorentzian is confirmed to be incoherent in nature, and well described by Fick's law properly modified according to the revised Enskog's theory (Kamgar-Parsi *et al.*, 1987). As far as the broader component is concerned, the authors point out that more than one Lorentzian is needed to describe it at increasing wave vector, then they discuss its possible origin. First, they point out that the thermal origin of this broad component is ruled out by its low-Q intensity, which is by far larger than the one expected by the Landau-Plazeck ratio. Moreover, the linewidth reaches a constant value on decreasing wave vector, instead of following the Q^2 dependency of the heat mode. Second, they examine the possibility of a cage diffusion mechanism, as proposed in molecular-dynamics simulations (Bove *et al.*, 2002c). In this respect, they point out how the experimentally observed mode intensity is larger than expected, but they propose an enhancement mechanism based on valence fluctuations which could be active at low wave vectors amplifying the expected intensity.

Very recently, new state-of-the-art IXS experiments have been reported in expanded mercury near the critical point ($T_c=1751$ K, $P_c=1673$ bars, and $\rho_c=5.8$ g cm^{-3}), aiming at the investigation of collective dynamics at the metal-nonmetal transition (Ishikawa *et al.*, 2004). Despite extremely difficult experimental conditions, the speed of sound has been accurately measured and no significant changes have been observed in the transition from the metallic ($m\rho_c=13.6$ g cm^{-3}) to the insulating ($m\rho_c=9.0$ g cm^{-3}) phase, while the ultrasonic sound velocity exhibits a significant drop across the same thermodynamic point (Yao *et al.*, 1996). Only upon further expansion in the insulating phase the high-frequency sound velocity ultimately drops reaching the adiabatic value. This result seems to indicate the presence of very large positive dispersion as peculiar of the metal-nonmetal transition, opening a new experimental route to the investigation of the interplay between acoustic and transport properties.

Summing up, though the microscopic dynamics in molten Hg has been the subject of deep investigations in the last few years, some aspects still remain controversial. The sound velocity as determined by INS and IXS are not fully consistent with each other, though both techniques show a positive dispersion effect the INS result show a very large effect never observed so far. On the one side has been emphasized the role of electronic properties (Bove *et al.*, 2002a), while, on the other side, the collective dynamics as determined by IXS closely resemble one of several other simple fluids (Hosokawa *et al.*, 2002). The most intriguing aspect concerns, however, the interpretation of the quasielastic component of $S(Q,\omega)$. Neutron-scattering data suggest a negligible effect of thermal fluctuations (Badyal *et al.*, 2003), adding a piece of information to a recently debated issue (Singh and Tankeshwar, 2003, 2004; Scopigno and Ruocco, 2004). On the other side, the IXS data unambiguously show the presence of a coherent quasielastic dynamics, which no doubt has to show up in the neutron experiment as well. The broad quasielastic component as observed with two different experiments show, however,

opposite Q trends, monotonically increasing (Bove *et al.*, 2002a) and decreasing (Badyal *et al.*, 2003), respectively. Badyal *et al.* suggest a cage diffusion process, enabled by the valence fluctuations mechanism. We believe that the broad mode observed in INS could be closely related to the coherent quasielastic scattering reported in the IXS data. In this case, the similarity with several other investigated systems would suggest an interpretation in terms of a high-frequency structural relaxation process (Scopigno *et al.*, 2000b, 2001a; Scopigno, Balucani, *et al.*, 2002; Scopigno, Filipponi, *et al.*, 2002; Monaco *et al.*, 2004). Very recent IXS investigations, however, suggest an enhancement of positive dispersion at the metal-nonmetal transition, pointing out how changes in electronic transport properties dramatically affect acoustic properties (Ishikawa *et al.*, 2004).

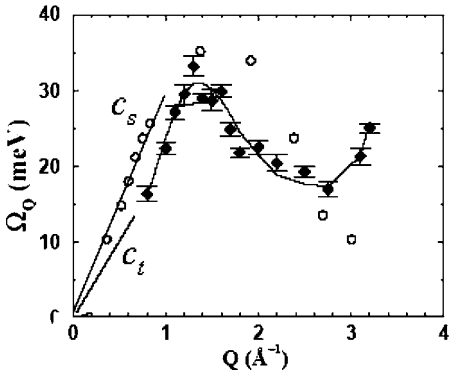

FIG. 36. Sound velocity in liquid nickel determined by INS (full circles) and MD (open circles). The isothermal (c_t) and adiabatic (c_s) values are also indicated.

2. Nickel

Early investigations in liquid nickel have been reported in 1977 with the time-of-flight technique (Johnson *et al.*, 1977). Two different isotopic concentrations, one with the natural abundance ratio and the other a wholly incoherent mixture, were chosen in order to study separately the coherent and incoherent scattering contributions. These latter, in turn, have been related to each other through the Vineyard approximation (Vineyard, 1958). The spectral density $g(\omega)$ was then extracted from the low-Q limit of the self-dynamic law. Coherent functions $S(Q,\omega=0)$ were reported for wave vectors above $Q=22$ nm^{-1}, therefore beyond the first Brillouin pseudozone. Consequently, this study was not able to ascertain the existence of low-Q collective modes.

A neutron-scattering experiment has been recently performed at the IN1 facility of the ILL (Bermejo *et al.*, 2000). Constant Q spectra have been collected from $Q=8$ nm^{-1} all the way up to wave vectors as high as twice the main peak in the static structure factor. The data have been analyzed utilizing two Lorentzian terms for the quasielastic (coherent and incoherent) contribution and one damped harmonic oscillator function for purely inelastic spectral features. Evidence of collective modes has been reported in the investigated Q domain, despite the relatively high viscosity value ($\eta_s \approx 5.7$ mPa s, i.e., one order of magnitude larger than the typical values for alkali metals). The reason for this apparent oddness can be traced back to arguments similar to the case of gallium, i.e., to the freezing of the diffusional motion over the probed high-frequency regime, which reduces the effective Brillouin damping in respect to the hydrodynamic prediction of Eq. (17).

More interestingly, the low-Q limit of the sound velocity seems to approach the isothermal and not the adiabatic value, as shown in Fig. 36. It is worthwhile to stress how, given the large value of γ (and therefore the large differences between c_t and c_s), this observation strikingly holds beyond the reported experimental error. If confirmed, this result would substantiate the hypothesis of an intermediate isothermal domain bridging the hydrodynamic limit and the high-frequency regime, which has been recently a matter of debate (Singh and Tankeshwar, 2003, 2004; Scopigno and Ruocco, 2004). On the other side, previous molecular-dynamics simulations indicate higher values of the sound velocity which agree quite well with the adiabatic response (Alemany *et al.*, 1998). Summing up, liquid Ni seems to be an ideal system to test the evolution of the thermal relaxation once the hydrodynamic limit is abandoned. An IXS investigation would be helpful to clarify this issue, though the small absorption length, the high melting temperature, and the reactivity of Ni pose severe experimental challenges.

3. Copper

Time-of-flight neutron-scattering data have been reported for this system a long time ago in the solid and liquid phases. The accessed kinematic range was quite broad ($Q>10$ nm^{-1} and $E<30$ meV) and the data have been analyzed with pioneering models (Egelstaff and Schofield, 1962). More recently, an IXS experiment has been performed at the ESRF, though this work is still in progress and a very preliminary estimate of the sound velocity gives a value of 4230 ± 70 m/s, well above the hydrodynamic value.

G. Solutions of metals

Alkali metals easily dissolve in water, molten alkali halides, and ammonia, resulting in a free electron and a positively charged ion. Given the relatively low electronic concentration of the saturated solutions, these are ideal systems to challenge the validity extents of plasma-based theories introduced in Sec. II.H, and the relative approximations for the dielectric function. Models such as the RPA, indeed, are expected to hold in systems with low r_s (or, equivalently, high electronic density) such as bulk metals, while they reach their limits on increasing the r_s value.

A second interesting aspect concerns the presence in liquid metals of the so-called Kohn anomaly, i.e., a kink in the dispersion curve occurring at $Q=2k_F$ and reflect-

ing a singularity of the dielectric function which is observed in metallic crystals, but which is not yet established in the disordered phase. The high-frequency dynamics of metal-ammonia systems, in particular, have been recently investigated by means of x rays and neutrons. High-resolution IXS performed in lithium-ammonia solutions allowed one to detect high-frequency excitations, softening at twice the Fermi wave vector k_F (Burns *et al.*, 2001). Unfortunately, at the investigated concentrations $2k_F$ is close to $Q=Q_m$, i.e., the main peak of the static structure factor. This coincidence generates an ambiguity in the interpretation of the observed dip in the sound dispersion, as it is not clear whether this feature is related to the structural periodicity as in nonordinary fluids or has to do with a purely electronic effect. The reported sound velocity values are intermediate between the bare ion values and the value appropriate for the $Li(NH_3)_4$ vibrating network, though close to the latter. In a later study (Said *et al.*, 2003), collective excitations are rationalized in terms of ionic plasma oscillations, and the sound velocity values measured at several metal concentrations are compared with the prediction of the Bohm-Staver expression (75), taking as the relevant mass either the bare ionic value or the metal-ammonia unit. In both cases the predictions do not agree with the measured values, and this seems to be a signature of the well-known failure of the RPA approximation in the low-density regime, where electron-electron interactions are relevant. A contemporary INS study on deuterated ammonia (Sacchetti *et al.*, 2003) also addresses the deviations from the Bohm-Staver model. In this case an improvement is achieved accounting for both the finite ionic size and electron-electron interactions. As far as the first aspect is concerned, an alternative renormalization of the free ionic plasma frequency is undertaken, while an expression for the dielectric screening function, going beyond the RPA approximation of Eq. (74) and accounting for local fields effects, is proposed. As far as the Kohn anomaly is concerned, this study suggests that the value of $2k_F$ (≈ 10 nm^{-1} in saturated lithium-ammonia solutions) has to be compared with $Q \approx 20$ nm^{-1}, which is actually the second peak of $S(Q)$, related to the N-N periodicity, rather than with the first peak ($Q_m \approx 20$ nm^{-1}) related to the $Li(NH_3)_4$ periodicity. This might arise from the different x-ray and neutrons cross sections: while in the first case the two peaks have similar intensities, the neutron diffraction strongly enhance the N-N peak. A later study has shown how an unambiguous separation between $2k_F$ and Q_m occurs in low-density solutions, although in this case the

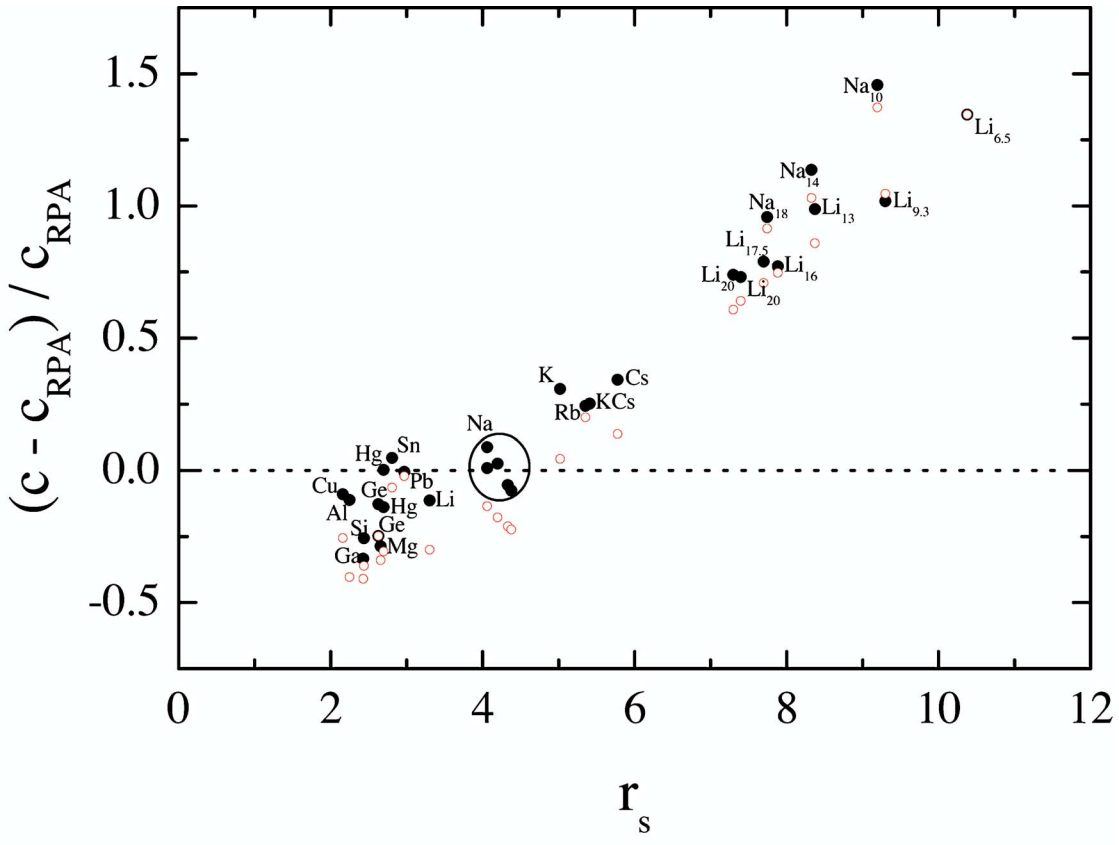

FIG. 37. (Color online) Random-phase approximation at work: data taken from Table I and Bove *et al.* (2005) for pure elements and from Giura *et al.* (2003) and Said *et al.* (2003) for alkali-ammonia solutions, with the BS values estimated through Eq. (75). Full circles: the measured sound velocity c is the maximum high-frequency value determined over the Q range probed by inelastic-scattering techniques, i.e., includes the positive dispersion effect. Open circles: c is the adiabatic value. The subscript of Li and Na indicates the concentrations in ammonia solutions. The Na group is relative to several different temperatures.

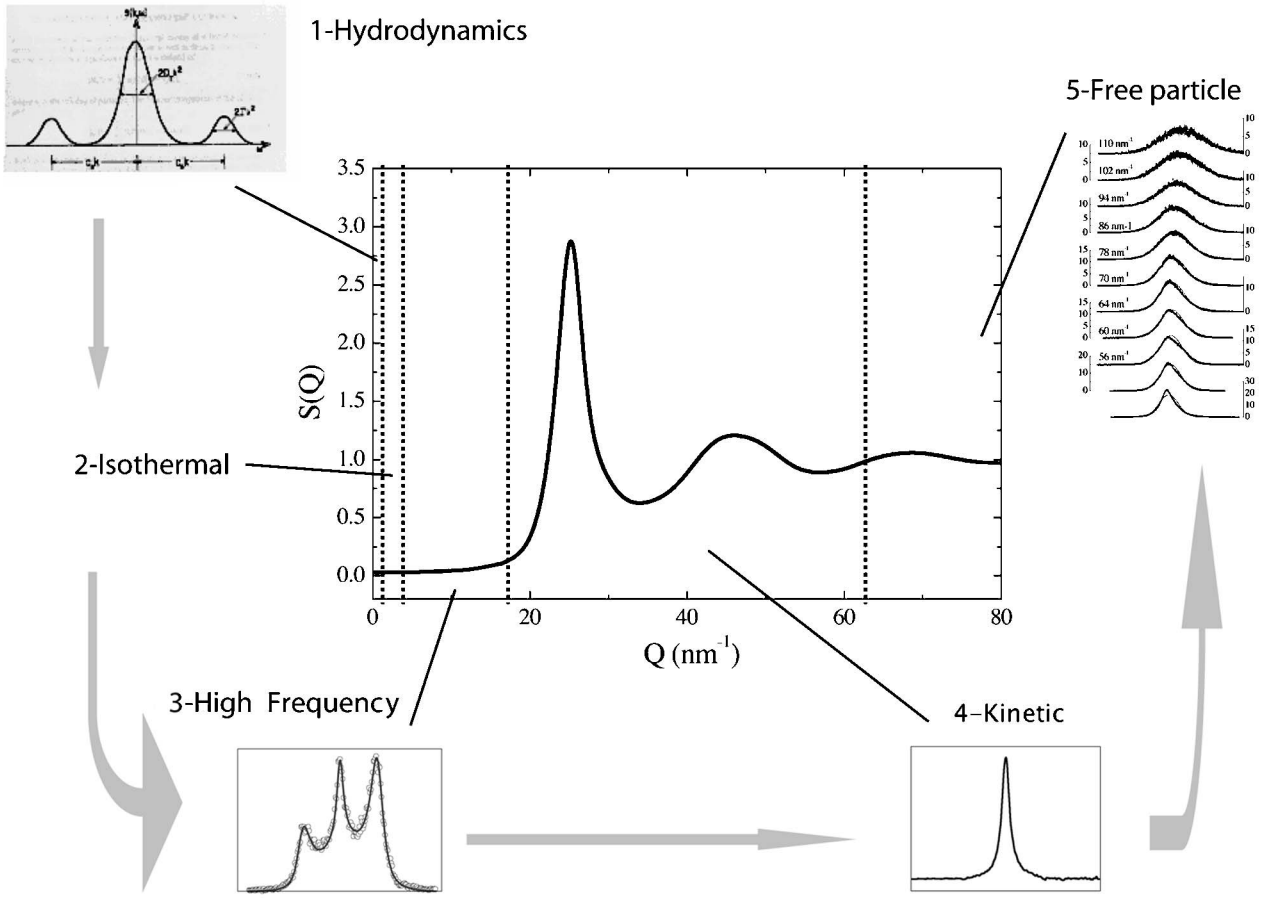

FIG. 38. Sketch of the different dynamical regimes on decreasing the wavelength.

kink observed in the dispersion curve is almost within the error bars (Giura *et al.*, 2003). Further studies therefore seem to be necessary to draw a conclusive picture about the presence of the Kohn anomaly in metallic fluids.

The validity extent of the RPA approximation for the determination of the sound velocity via the Bohm-Staver expression (75) is depicted in Fig. 37, in which we report the relative deviations of the Bohm-Staver calculated values (c_{RPA}) from the experimental ones, for systems of different r_s, ranging from pure metals to alkali-ammonia solutions. In the latter case ($r_s > 6$) the Bohm-Staver predictions underestimate more than 50% the calculated values. The deviations, however, show a trend which monotonically decreases towards low-r_s elements and finally get negative for r_s values close to 2.

A final remark concerns the choice of the dynamical variable to calculate the sound velocity when one is looking at subtle effects as in the present case. First, according to the hydrodynamic definition of sound velocity in liquids, one should look at the maxima of the current correlation spectra. While the difference with the maxima of $S(Q,\omega)$ is usually negligible in crystals, indeed, there can be a significant discrepancy in strongly overdamped cases such as the one metallic solutions. In this respect, the choice of the damped harmonic oscillator to describe $S(Q,\omega)$ implicitly overcame this problem, as the characteristic frequency of this model coincides indeed with the maxima of $C_L(Q,\omega)$. Second, in all the reported studies, the "phonon" velocity is extracted through *ad hoc* models (damped harmonic oscillator, extended hydrodynamic model, etc.) looking only at the genuine inelastic component. Again, in liquids, the full $C_L(Q,\omega)$ spectrum should be considered, as when $S(Q,\omega)$ has a significant quasielastic contribution this latter can affect the peak positions of $C_L(Q,\omega)$ (see, for instance, Fig. 27 for the aluminum case).

Inelastic x-ray scattering, with lower energy resolution (a few hundreds of meV) and in a broader energy range (up to a few eV), allows one to study electronic excitations (plasmons). In this case the plasma oscillation is brought about by free electrons, while the background is constituted by the ionic network. Some recent studies (Burns *et al.*, 1999; Burns, Giura, *et al.*, 2001) point out a decrease of the plasmon dispersion at low metal concentrations, which, in turn, is ascribed to the failure of the RPA approximation (see Fig. 38).

V. SUMMARY AND PERSPECTIVES

In this section we will try to summarize the scenario arising from the measurements reported so far. In re-

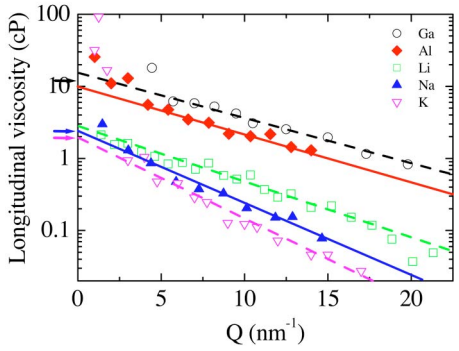

FIG. 39. (Color online) Generalized longitudinal viscosities for a collection of liquid metals, extracted by the experimental data throughout a memory function approach. The long-wavelength limit, determined by ultrasonic measurements, is also reported for K, Na, and Ga (bottom to top).

spect to the collective properties, it seems useful to discuss the different dynamical regimes probed at different wave vectors and frequencies. Although the two domains are in principle independent (as testified, for instance, by the two separate generalization of the classical hydrodynamics introduced in Sec. II.F), the existence of a dispersion relation ultimately allows one to think in terms of wavelengths only. From our point of view, though precise boundaries cannot be traced, one can identify in liquid metals the following dynamical regimes:

- The hydrodynamic, $Q \to 0$ limit, that, in liquid metals, basically means $Q \lesssim 0.1$ nm^{-1}. In this region simple hydrodynamic treatment based on three microscopic dynamical variables (density, current, energy) provides an exhaustive description of the main features. Although not accessible by neutron and x-ray spectroscopic techniques, the hydrodynamic predictions are in very good agreement with acoustic measurements of sound velocity and attenuation properties. Moreover, the strict analogy of long-wave-length fluctuations in conductive and ordinary liquids (accessible via light scattering) corroborates the validity of the simple hydrodynamic theory. This region is characterized by *adiabatic* sound propagation, and the whole dynamical features are ruled by macroscopic transport parameters (viscosity, thermal diffusivity, specific heats). In this regime, other approaches tailored for conductive fluids such as plasma oscillation theories provides alternative descriptions, which turns out to be increasingly accurate for low-r_s systems.
- An (hypothetic) isothermal region, which should be observable in the $0.2 \lesssim Q \lesssim 3$-nm^{-1} momentum range. Upon increasing the wave vector outside the strict hydrodynamic limit, indeed, the lifetime of entropy fluctuations becomes increasingly shorter [$\tau = (\gamma D_T Q^2)^{-1}$]. Since the frequency of the corresponding density fluctuation increases almost linearly ($\omega \approx cQ$), one should expect a transition at $Q^* \approx c/D_T$. Given the typical thermal diffusivity values of liquid metals this crossover should be located at a few fractions of nm^{-1}. Since with both INS and IXS one nor-

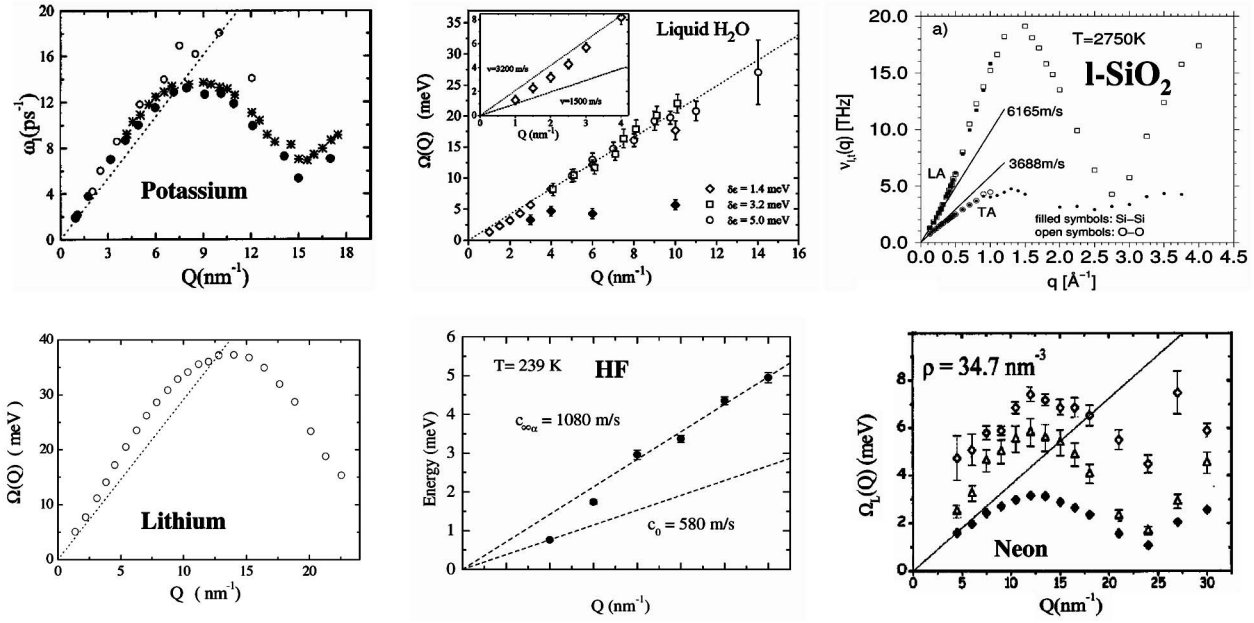

FIG. 40. Sound dispersion in several kind of liquids. Alkali metals [Li (Scopigno, Balucani, Cunsolo, *et al.*, 2000) and K (Monaco *et al.*, 2004), dashed line is the isothermal sound velocity]; hydrogen bonding systems [water (Monaco *et al.*, 1999) and hydrogen fluoride (Angelini *et al.*, 2002)]; low- and high-frequency sound velocities are also indicated by the dotted lines; liquid neon (Cunsolo *et al.*, 2001); adiabatic (circles and line) apparent (open triangles) and high-frequency (open diamonds) sound velocities; liquid silica, molecular-dynamics simulations (Horbach *et al.*, 2001), in this case also the transverse branch is reported.

mally accesses momentum transfers above 1 nm^{-1}, this region can be hardly explored, and no direct and convincing indications for its existence are available at present. Some old INS data on liquid lead (Faber, 1972) as well as a more recent experiment on liquid nickel (Bermejo *et al.*, 2000), however, seem to suggest an indication for such existence. The case of nickel, in particular, is an interesting one and would deserve new investigations since in this system the specific-heat ratio is particularly high and therefore the difference in sound velocities between an ordinary adiabatic regime and an isothermal one would be of the order of 40%. It is worthwhile to stress that the prediction for the existence of an isothermal regime poses on (i) a negligible Q dependence of the thermodynamic quantities and (ii) the validity of a one-component effective description in which the effective thermal diffusivity is well described by the sum of the electronic and ionic contributions. Both these points have been recently discussed in the analysis of alkali metals and liquid aluminum IXS spectra (Singh and Tankeshwar, 2003, 2004; Scopigno and Ruocco, 2004).

- A generalized hydrodynamic region, probed above $Q \approx 3$ nm^{-1}, in which the frequency–wave-vector dependence of the transport properties heavily affects the sound mode. The upper limit of the validity of this region is rather system dependent, normally higher for alkali metals (say up to $0.7Q_m$). The natural framework here is the memory function formalism, which can be developed at different levels of accuracy, ranging from the celebrated Lovesey's model (Lovesey, 1971) (accounting for a single average relaxation time for the second-order memory function) up to more refined memory function models based on multiple relaxation phenomena which, first introduced for Lennard-Jones systems (Levesque *et al.*, 1973), have been more recently adapted and tested against IXS investigations of liquid metals (Scopigno *et al.*, 2000a, 2000c; Scopigno, Filipponi, *et al.*, 2002; Monaco *et al.*, 2004) and numerical simulations of model undercooled and glassy alkali metals (Scopigno, Ruocco, *et al.*, 2002).

In this respect, it is worthwhile to point out how the high points of a memory function approach are not solely in a better agreement with experimental data, which, in general, heavily depends on the quality of the experimental data and, of course, on the number of the model parameters (Scopigno *et al.*, 2000b). In most cases, indeed, simplified phenomenological models such as the damped harmonic oscillator and a Lorentzian function for the inelastic and quasielastic features, respectively, provide satisfactory agreements.

On the contrary, the memory function framework allows one to grasp an insight behind the mechanisms ruling the relaxation dynamics, extracting relevant information about quantities which are not directly related to any spectral features, such as the Q dependencies of the relaxation time(s) and of the longitudinal viscosity.

Following the prescriptions illustrated in Sec. II.F.2, indeed, the longitudinal viscosity is related to the total area under the viscous contribution to the memory function. In Fig. 39, for instance, we report the (generalized) longitudinal viscosities extracted in this way for several investigated systems. As can be seen, the low-Q extrapolation of the experimental values compares well with independent acoustic determinations (when available), but also allows one to determine the Q generalization of this important transport property, which can be directly estimated only with numerical simulations approaches.

In this Q region, hard-sphere–based theories provide alternative descriptions in terms of extended hydrodynamic models (Kamgar-Parsi *et al.*, 1987) but they still miss a convincing explanation of one of the most important points: the physical interpretation beyond the relaxation of the sound mode, which is now a firmly established evidence supported by uncountable experimental investigations.

This latter aspect, which usually emerges in terms of a speed up of the sound velocity taking place in the 1–10-nm^{-1} region, is one of the most interesting aspects which is still lacking an explanation. Broadly speaking, it is always referred to as a shear relaxation, but the ultimate nature of the involved physical processes still have to be clarified.

Actually, mode coupling theory (Ernst and Dorfman, 1975) provides a description of the acoustic dispersion curve in terms of even powers of Q (Ernst and Dorfman, 1975), but its interpretation is restricted to monatomic systems in the liquid phase, while the observed phenomenology seems to be a more general feature of the disordered systems.

Interestingly, indeed, a qualitatively similar phenomenon (see Fig. 40) has also been reported numerically in fused silica (Horbach *et al.*, 2001) and experimentally in Lennard-Jones fluids (Cunsolo *et al.*, 2001) and hydrogen bonding systems (Monaco *et al.*, 1999; Angelini *et al.*, 2002). While in this latter case positive dispersion has been shown to be an activated process, related to structural relaxation, a different scenario seems to characterize the other systems. Interestingly, indeed (see Fig. 41), the same behavior of the sound velocity also appears in *glasses* in experimental IXS measurements in g-Se and vitreous silica (Ruzicka *et al.*, 2004; Scopigno *et al.*, 2004), in numerical works on model glasses of Lennard-Jones systems (Ruocco *et al.*, 2000), vitreous silica (Horbach *et al.*, 2001), and alkali metals (Scopigno, Ruocco, *et al.*, 2002) and, finally, in theoretical calculations for a hard-sphere glass (Götze and Mayr, 2000). In the case of alkali metals, in particular, it has been shown how an increase of the sound velocity persists upon cooling well below the glass transition, thus ruling out the possible role of structural relaxation in this effect. The presence of positive dispersion at THz frequencies in glasses, quantitatively comparable to the one observed in liquids, therefore challenges the interpretation of positive dispersion in terms of a transition from a liquidlike to a solidlike behavior, an effect which seems to be quantitatively negligible (with the remarkable exception of hy-

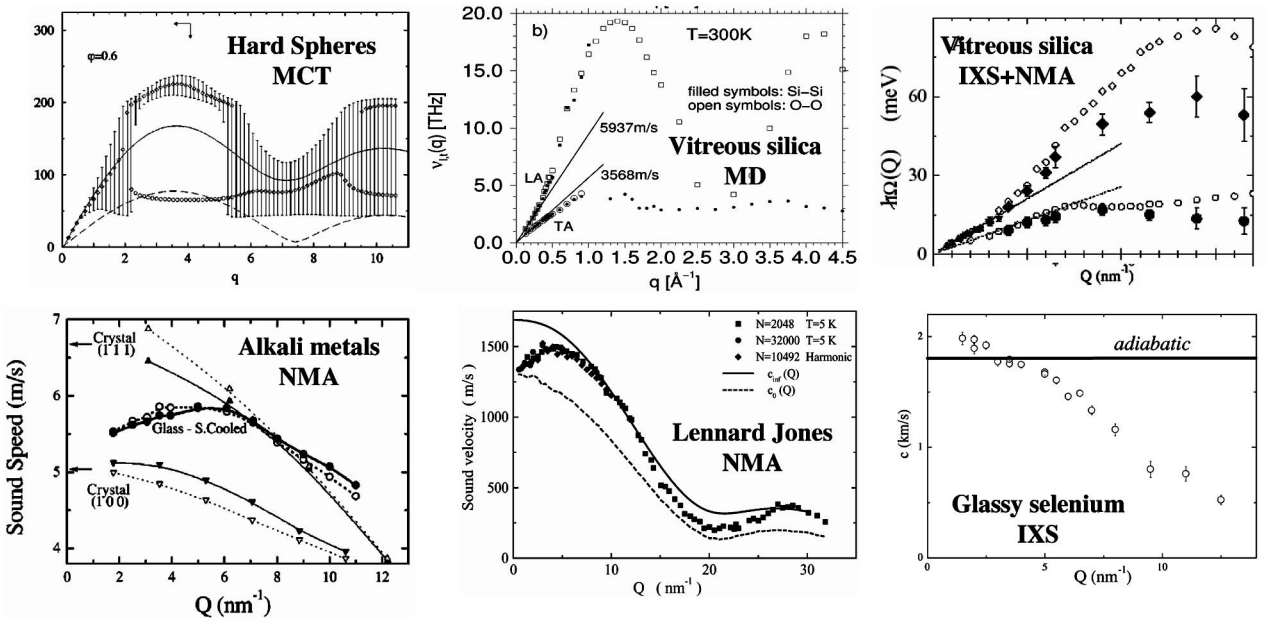

FIG. 41. Sound velocities in several glassy systems. Hard-sphere glass, exact solution within MCT (Götze and Mayr, 2000); metallic glass obtained quenching a model system interacting via Price-Tosi pseudopotential (Scopigno, Ruoco, *et al.*, 2002), the crystalline counterpart is also reported; Lennard-Jones glass obtained in a similar way (Ruocco *et al.*, 2000), reported with the low- and high-frequency sound velocities; SiO_2, MD as in Fig. 40 but in the glassy state (Horbach *et al.*, 2001) and experimentally determined by means of IXS scattering (Ruzicka *et al.*, 2004). In both cases the transverse branch is also reported; glassy selenium (Scopigno *et al.*, 2004), again the sound velocity exceeds the adiabatic value.

drogen bonding systems). Accepting a description of the collective dynamics proceedings over two distinct viscous relaxations therefore the ultimate mechanism responsible for the bending up of the dispersion curve seems to be associated with the faster of the two observed processes, which turns out to have a mild temperature dependence. In this respect, the physical nature of this faster process calls for a deeper understanding. It is worthwhile to point out, however, that in Lennard-Jones systems positive dispersion is recovered within a *harmonic* description of the dynamic structure factor in terms of eigenvalues and eigenvectors, a result which relates the positive dispersion to the properties of the dynamical matrix and, ultimately, to the topological disorder of the inherent equilibrium position, with the interaction potentials comparable in glasses and crystals.

- A kinetic regime valid from around Q_m up to a few oscillations of the structure factor. Here the hard-sphere description provides remarkably accurate predictions, in terms of a quasielastic "extended heat mode" whose linewidth is described in terms of the Enskog's diffusion coefficient and of an equivalent hard-sphere diameter. The extent of the validity of kinetic theory in this momentum range has been widely tested (Cohen *et al.*, 1984, 1987; de Schepper *et al.*, 1984; Kamgar-Parsi *et al.*, 1987) in several hard-sphere-like systems (like alkali metals and Lennard-Jones fluids), and it also has been applied in colloidal systems. It would be interesting to challenge such a theory in less simple liquid metals. Despite the success of the hard-sphere model, there is still an obscure point concerning the real origin of such an extended heat mode: while in the low-Q limit it tends to the entropy fluctuation mode, indeed, at finite Q's it certainly involves mass diffusion processes. Looking at things from the constant energy point of view, umklapp modes resembling crystalline phonons in Brillouin zones higher than the first seems to be still poorly understood (Cocking and Egelstaff, 1965a; Dorner *et al.*, 1965; Randolph and Singwi, 1966; Scopigno, D'Astuto, *et al.*, 2001).
- A high-Q region, probed as soon as the van Hove distinct function vanishes. In this limit, both IXS and INS experiments provide the same information about the atomic motion over time scales shorter than the interparticle collision time. An almost exact description for this regime is available, which can also account for quantum aspects such as recoil energy and quantum corrections to the spectral moments.

The single-particle dynamics seems to be better understood if compared to the collective motion, at least by a coarse grained point of view of a hydrodynamic diffusive mode with finite Q corrections, evolving towards a ballistic regime. This is probably due to the intrinsic difficulty of isolating a (wide enough) constant Q *coherent* energy spectrum from an INS experiment. Since the study of the strictly coherent spectrum became possible only in the last decade, indeed, a lot of efforts have been devoted in the past to the single-particle case. Though all the approaches described in this review de-

scribe, on average, equally well the available experimental data, a memory function formalism paralleling the one for the collective case could provide the route to relate the single-particle motion and the collective dynamics in the microscopic regime.

Raising the level of detail of the description of the single-particle dynamics, however, a major experimental challenge seems to be the identification of the different processes giving rise to the quasielastic incoherent scattering. Recent INS results, indeed, suggest the presence of two distinct physical mechanisms, active over different time scales, underlying the diffusive motion (Bove *et al.*, 2002a, 2003; Badyal *et al.*, 2003). The combined presence of coherent and incoherent scattering, however, makes such identification still unclear although, in principle, the IXS signal might be used to subtract the coherent contribution from the INS spectra, thus extracting the purely incoherent dynamics. In this respect, the synergy of combined IXS and INS studies on the same sample seems imperative to us and could help to shed light on this point. The IXS signal indeed might be used to subtract the coherent contribution from the INS spectra, thus extracting the purely incoherent dynamics.

ACKNOWLEDGMENTS

J.-P. Hansen made extensive comments on this manuscript for which we are most grateful. We thank L.E. Bove and T. Bryk for several discussions and interesting comments on the preprint, and S. Cazzato for his help in compiling the data reported in Table I. T.S. gratefully acknowledges his debt to U. Balucani for the vivifying influence exerted on his outset in the field of simple liquids. Most of our IXS activity greatly benefited from the support of the staff of the beamlines ID16-ID28 at the ESRF and BL35XU at SPring8. The assistance of the technical staffs of the ESRF (D. Gambetti, B. Gorges, and C. Henriquet), of the University of L'Aquila (O. Consorte), and of the University of Rome "La Sapienza" (I. Deen, M. Pallagrossi, C. Piacenti, and A. Salvati) is also acknowledged. Thanks are also due to all who granted permission to include previously published figures.

REFERENCES

Addison, C., 1986, *The Chemistry of the Liquid Alkali Metals* (Wiley, New York).
Ailawadi, N. K., A. Rahman, and R. Zwanzig, 1971, Phys. Rev. A **4**, 1616.
Alemany, M. M. G., J. Casas, C. Rey, L. E. Gonzalez, and L. J. Gallego, 1997, Phys. Rev. E **56**, 6818.
Alemany, M. M. G., C. Rey, and L. J. Gallego, 1998, Phys. Rev. B **58**, 685.
Alley, W. E., and B. J. Alder, 1983, Phys. Rev. A **27**, 3158.
Alley, W. E., B. J. Alder, and S. Yip, 1983, Phys. Rev. A **27**, 3174.
Angelini, R., P. Giura, G. Monaco, G. Ruocco, F. Sette, and R. Verbeni, 2002, Phys. Rev. Lett. **88**, 255503.
Ashcroft, N., and D. Stroud, 1978, Solid State Phys. **33**, 1.
Ashcroft, N. W., 1966, Phys. Lett. **23**, 48.
Austin, B., V. Heine, and L. Sham, 1962, Phys. Rev. **127**, 276.
Badyal, Y. S., U. Bafile, K. Miyazaki, I. M. de Schepper, and W. Montfrooij, 2003, Phys. Rev. E **68**, 061208.
Balucani, U., A. Torcini, and R. Vallauri, 1992, Phys. Rev. A **46**, 2159.
Balucani, U., and M. Zoppi, 1983, *Dynamics of the Liquid State* (Clarendon, Oxford).
Baus, M., and J.-P. Hansen, 1980, Phys. Rep. **59**, 1.
Bellissent-Funel, M. C., P. Chieux, D. Levesque, and J. J. Weis, 1989, Phys. Rev. A **39**, 6310.
Bengtzelius, U., W. Götze, and A. Sjölander, 1984, J. Phys. C **17**, 5915.
Bermejo, F. J., R. Fernandez-Perea, M. Alvarez, B. Roessli, H. E. Fischer, and J. Bossy, 1997, Phys. Rev. E **56**, 3358.
Bermejo, F. J., M. Garcia-Hernandez, J. L. Martinez, and B. Hennion, 1994, Phys. Rev. E **49**, 3133.
Bermejo, F. J., M. L. Saboungi, D. L. Price, M. Alvarez, B. Roessli, C. Cabrillo, and A. Ivanov, 2000, Phys. Rev. Lett. **85**, 106.
Berne, B., and R. Pecora, 1976, *Dynamic Light Scattering* (Wiley, New York).
Bodensteiner, T., 1990, Ph.D. thesis (Technische Universität, München).
Bodensteiner, T., C. Morkel, W. Gläser, and B. Dorner, 1992, Phys. Rev. A **45**, 5709.
Boon, J. P., and S. Yip, 1980, *Molecular Hydrodynamics* (McGraw-Hill, New York).
Bosio, L., E. Schedler, and C. G. Windsor, 1976, J. Phys. (Paris) **37**, 747.
Bove, L., B. Dorner, C. Petrillo, F. Sacchetti, and J. Suck, 2003, Phys. Rev. B **68**, 024208.
Bove, L. E., F. Formisano, F. Sacchetti, C. Petrillo, A. Ivanov, B. Dorner, and F. Barocchi, 2005, Phys. Rev. B **71**, 014207.
Bove, L. E., F. Sacchetti, C. Petrillo, B. Dorner, F. Formisano, and F. Barocchi, 2002a, Phys. Rev. Lett. **87**, 215504.
Bove, L. E., F. Sacchetti, C. Petrillo, B. Dorner, F. Formisano, M. Sampoli, and F. Barocchi, 2002b, J. Non-Cryst. Solids **307-310**, 842.
Bove, L. E., F. Sacchetti, C. Petrillo, B. Dorner, F. Formisano, M. Sampoli, and F. Barocchi, 2002c, J. Non-Cryst. Solids **307-310**, 842.
Brockhouse, B. N., J. Bergsma, B. A. Dasannacharya, and N. K. Pope, 1963, *Inelastic Scattering of Neutrons in Solids and Liquids, Proceedings of the IAEA Symposium*, Vienna, Vol. 1, p. 189.
Brockhouse, B. N., L. M. Corliss, and J. M. Hastings, 1955, Phys. Rev. **98**, 1721.
Bryk, T., and I. Mryglod, 2000, J. Phys.: Condens. Matter **12**, 3543.
Bryk, T., and I. Mryglod, 2001a, Phys. Rev. E **63**, 051202.
Bryk, T., and I. Mryglod, 2001b, Phys. Rev. E **64**, 032202.
Buchenau, U., 1985, Z. Phys. B: Condens. Matter **58**, 181.
Burkel, E., 1991, *Inelastic Scattering of X-Rays with Very High Energy Resolution* (Springer-Verlag, Berlin).
Burkel, E., and H. Sinn, 1994, J. Phys.: Condens. Matter **6**, A225.
Burns, C., P. Abbamonte, E. D. Isaacs, and P. Platzman, 1999, Phys. Rev. Lett. **83**, 2390.
Burns, C., P. Platzman, H. Sinn, A. Alatas, and E. Alp, 2001, Phys. Rev. Lett. **86**, 2357.
Burns, C. A., P. Giura, A. Said, A. Shulka, G. Vankö, M. Tuel-Beneckendorf, E. D. Isaacs, and P. Platzman, 2001, Phys. Rev.

Lett. **86**, 2357.
Cabrillo, C., F. J. Bermejo, M. Alvarez, P. Verkerk, A. Maira-Vidal, S. M. Bennington, and D. Martin, 2002, Phys. Rev. Lett. **89**, 075508.
Canales, M., L. E. Gonzalez, and J. A. Padró, 1994, Phys. Rev. E **50**, 3656.
Canales, M., and J. A. Padró, 1999, Phys. Rev. E **60**, 551.
Carneiro, K., M. Nielsen, and J. McTague, 1973, Phys. Rev. Lett. **30**, 481.
Cazzato, S., 2005, degree thesis (Dipartmento di Fisica, Universitá di Roma "La Sapienza").
Chieux, P., J. Dupuy-Philon, J. F. Jal, and J. B. Suck, 1996, J. Non-Cryst. Solids **205-207**, 370.
Chihara, J., 1985, J. Phys. C **18**, 3103.
Chuldey, G., and R. Elliot, 1961, Proc. Phys. Soc. London **77**, 353.
Cocking, S., 1963, *Inelastic Scattering of Neutrons in Solids and Liquids, Proceedings of the IAEA Symposium*, Vienna, Vol. 1, p. 227.
Cocking, S., 1967a, Adv. Phys. **16**, 189.
Cocking, S., and P. Egelstaff, 1965a, Phys. Lett. **16**, 130.
Cocking, S., and P. Egelstaff, 1968, J. Phys. C **1**, 507.
Cocking, S. J., 1967b, Adv. Phys. **16**, 189.
Cocking, S. J., and P. A. Egelstaff, 1965b, Phys. Lett. **16**, 130.
Cohen, E. G. D., I. M. de Schepper, and M. J. Zuilhof, 1984, &Physica B C **127B**, 282.
Cohen, E. G. D., P. Westerhuijs, and I. M. de Schepper, 1987, Phys. Rev. Lett. **59**, 2872.
Copley, J., 1975, Comput. Phys. Commun. **7**, 289.
Copley, J. R. D., and S. W. Lovesey, 1975, Rep. Prog. Phys. **38**, 461.
Copley, J. R. D., and M. Rowe, 1974, Phys. Rev. A **9**, 1656.
Cunsolo, A., G. Pratesi, R. Verbeni, D. Colognesi, C. Masciovecchio, G. Monaco, G. Ruocco, and F. Sette, 2001, J. Chem. Phys. **114**, 2259.
Dahlborg, U., and L. G. Olsson, 1982, Phys. Rev. A **25**, 2712.
de Gennes, P. G., 1959, Physica (Amsterdam) **25**, 825.
De Jong, P. H. K., 1993, Ph.D. thesis (Technische Universiteit, Delft).
De Jong, P. H. K., P. Verkerk, and L. A. D. Graaf, 1993, J. Non-Cryst. Solids **156-158**, 48.
de Schepper, I. M., and E. G. D. Cohen, 1980, Phys. Rev. A **22**, 287.
de Schepper, I. M., E. G. D. Cohen, and M. J. Zuilhof, 1984, Phys. Lett. **101A**, 399.
de Schepper, I. M., and M. H. Ernst, 1979, Physica A **98**, 189.
de Schepper, I. M., P. Verkerk, A. A. van Well, and L. A. de Graaf, 1983, Phys. Rev. Lett. **50**, 974.
Desai, R. C., and S. Yip, 1969, Phys. Rev. **180**, 299.
Dil, J., and E. Brody, 1976, Phys. Rev. B **14**, 5218.
Dil, J. G., 1982, Rep. Prog. Phys. **45**, 285.
Dorner, B., T. Plesser, and H. Stiller, 1965, Physica (Amsterdam) **31**, 1537.
Dorner, B., T. Plesser, and H. Stiller, 1967, Discuss. Faraday Soc. **43**, 160.
Ebbsjö, I., T. Kinnel, and I. Waller, 1980, J. Phys. C **13**, 1865.
Eder, O. J., B. Kunsch, J. B. Suck, and M. Suda, 1980, J. Phys. (Paris), Colloq. **41**, C8-226, Proc. of the LAM IV Grenoble.
Egelstaff, P., 1959, Br. J. Appl. Phys. **10**, 1.
Egelstaff, P., 1966, Rep. Prog. Phys. **29**, 333.
Egelstaff, P., 1967, *An Introduction to the Liquid State* (Academic, New York).
Egelstaff, P. A., 1954, Acta Crystallogr. **7**, 673.
Egelstaff, P. A., and P. Schofield, 1962, Nucl. Sci. Eng. **12**, 260.
Ernst, M., and J. Dorfman, 1975, J. Stat. Phys. **12**, 311.
Faber, T., 1972, *Introduction to the Theory of Liquid Metals* (Cambridge University Press, Cambridge).
Fåk, B., and B. Dorner, 1997, Physica B **234**, 1107.
Furtado, P. M., G. F. Mazenko, and S. Yip, 1975, Phys. Rev. A **12**, 1653.
Gaskell, T., 1986, J. Phys. F: Met. Phys. **16**, 381.
Giura, P., R. Angelini, C. Burns, G. Monaco, and F. Sette, 2003, e-print cond-mat/0310336.
Gläser, W., 1991, J. Phys.: Condens. Matter **3**, F53.
Gläser, W., S. Hagen, U. Löffer, J. Suck, and W. Schommers, 1973, *Inelastic Scattering of Neutrons in Solids and Liquids, Proceedings of the International Conference on Liquid Metals*, London, p. 111.
Gonzalez, D. J., L. E. Gonzalez, and J. M. Lopez, 2001, J. Phys.: Condens. Matter **13**, 7801.
Gonzalez, D. J., L. E. Gonzalez, J. M. Lopez, and M. J. Stott, 2002, Phys. Rev. B **65**, 184201.
Götze, W., and M. Mayr, 2000, Phys. Rev. E **61**, 587.
Götze, W., and A. Zippelius, 1976, Phys. Rev. A **14**, 1842.
Hansen, J.-P., and I. McDonald, 1986, *Theory of Simple Liquids* (Academic, New York).
Hansen, J.-P., and L. Sjögren, 1982, Phys. Fluids **25**, 617.
Harrison, W., 1966, *Pseudopotentials in the Theory of Metals* (Benjamin, New York).
Heine, V., 1970, Solid State Phys. **24**, 1.
Hensel, F., and W. Warren, 1999, *Fluid Metals* (Princeton University Press, Princeton).
Horbach, J., W. Kob, and K. Binder, 2001, Eur. Phys. J. B **19**, 531.
Hosokawa, S., J. Greif, F. Demmel, and W.-C. Pilgrim, 2003a, Nucl. Instrum. Methods Phys. Res. B **199**, 161.
Hosokawa, S., J. Greif, F. Demmel, and W.-C. Pilgrim, 2003b, Chem. Phys. **292**, 253.
Hosokawa, S., Y. Kawakita, W.-C. Pilgrim, and H. Sinn, 2001, Phys. Rev. B **63**, 134205.
Hosokawa, S., W.-C. Pilgrim, Y. Kawakita, K. Ohshima, S. Takeda, D. Ishikawa, S. Tsutsui, Y. Tanaka, and A. Baron, 2003, J. Phys.: Condens. Matter **15**, L623.
Hosokawa, S., H. Sinn, F. Hensel, A. Alatas, E. E. Alp, and W.-C. Pilgrim, 2002, J. Non-Cryst. Solids **312-314**, 163.
Hultgren, R., P. Desai, D. Hawkins, M. Gleiser, K. Kelly, and D. Wagman, 1973, *Selected Values of the Thermodynamic Properties of the Elements* (American Society for Metals, Metals Park, OH).
Iida, T., and R. Guthrie, 1993, *The Physical Properties of Liquid Metals* (Oxford Science Publications, Oxford).
Inui, M., S. Takeda, and T. Uechi, 1992, J. Phys. Soc. Jpn. **61**, 3203.
Ishikawa, D., M. Inui, K. Matsuda, K. Tamura, S. Tsutsui, and A. Q. R. Baron, 2004, Phys. Rev. Lett. **93**, 097801.
Johnson, M., B. McCoy, and N. March, 1977, Phys. Chem. Liq. **6**, 243.
Kamgar-Parsi, B., E. G. D. Cohen, and I. M. de Schepper, 1987, Phys. Rev. A **35**, 4781.
Kawakita, Y., S. Hosokawa, T. Enosaki, K. Ohshima, S. Takeda, W.-C. Pilgrim, S. Tsutsui, Y. Tanaka, and A. Q. R. Baron, 2003, J. Phys. Soc. Jpn. **72**, 1603.
Kelton, K., G. Lee, A. Gangopadhyay, R. Hyers, T. J. Rathz, J. Rogers, M. Robinson, and D. S. Robinson, 2003, Phys. Rev. Lett. **90**, 195504.
Kleppa, O. J., 1950, J. Chem. Phys. **18**, 1331.

Kubo, R., and K. Tomita, 1954, J. Phys. Soc. Jpn. **9**, 888.
Larsson, K. E., U. Dahlborg, and D. Jovic, 1965, *Inelastic Scattering of Neutrons, Proceedings of the IAEA Symposium*, Vienna, Vol. 2, p. 117.
Lebowitz, J. L., J. K. Percus, and J. Sykes, 1969, Phys. Rev. **188**, 487.
Levesque, D., L. Verlet, and J. Kürkijarvi, 1973, Phys. Rev. A **7**, 1690.
Li, G., W. M. Du, X. Chen, H. Z. Cummins, and N. J. Tao, 1992, Phys. Rev. A **45**, 3867.
Löffler, U., 1973, Ph.D. thesis (University of Karlsruhe).
Longuet-Higgins, H. C., and J. A. Pople, 1956, J. Chem. Phys. **25**, 884.
Lovesey, S., 1971, J. Phys. C **4**, 3057.
Lovesey, S., 1984, Phys. Rev. Lett. **53**, 401.
Lovesey, S. W., 1987, *Theory of Neutron Scattering from Condensed Matter* (Clarendon, Oxford).
March, N., 1968, *Liquid Metals* (Pergamon, Oxford).
March, N., 1990, *Liquid Metals: Concepts and Theory* (Cambridge University Press, Cambridge, England).
March, N., and M. Tosi, 1991, *Atomic Dynamics in Liquids* (Dover, New York).
Marshall, W., 1971, *Theory of Thermal Neutron Scattering* (Clarendon, Oxford).
Masciovecchio, C., U. Bergman, M. Krisch, G. Ruocco, F. Sette, and R. Verbeni, 1996, Nucl. Instrum. Methods Phys. Res. B **111**, 181.
Mateescu, N., H. Teutsch, A. Diaconescu, and V. Nahorniak, 1968, *Neutron Inelastic Scattering, Proceedings of the IAEA Symposium*, Vienna, Vol. 1, p. 439.
Matsuda, K., K. Tamura, M. Katoh, and M. Inui, 2004, Rev. Sci. Instrum. **75**, 709.
Maxwell, J., 1867, Philos. Trans. R. Soc. London **49**, 157.
McGreevy, R., and E. Mitchell, 1985, Phys. Rev. Lett. **55**, 398.
Monaco, A., T. Scopigno, P. Benassi, A. Giugni, G. Monaco, M. Nardone, G. Ruocco, and M. Sampoli, 2004, J. Chem. Phys. **120**, 8089.
Monaco, G., A. Cunsolo, G. Ruocco, and F. Sette, 1999, Phys. Rev. E **60**, 5505.
Mori, H., 1965, Prog. Theor. Phys. **33**, 423.
Morkel, C., and T. Bodensteiner, 1990, J. Phys.: Condens. Matter **2**, SA251.
Morkel, C., and W. Gläser, 1986, Phys. Rev. A **33**, 3383.
Mryglod, I., I. P. Omelyan, and M. V. Tokarchuk, 1995, Mol. Phys. **84**, 235.
Mughabghab, S., 1984, *Neutron Cross Sections* (Academic, New York).
Nelkin, M., and A. Ghatak, 1964, Phys. Rev. **135**, A4.
Nichols, W. H., and E. F. Carome, 1968, J. Chem. Phys. **49**, 1000.
Novikov, A. G., M. N. Ivanovskii, V. V. Savostin, A. L. Shimkevich, O. V. Sobolev, and M. V. Zaezjev, 1996, J. Phys.: Condens. Matter **8**, 3525.
Novikov, A. G., V. V. Savostin, A. L. Shimkevich, and R. M. Yulmetyev, 1996, Physica B **228**, 312.
Novikov, A. G., V. V. Savostin, A. L. Shimkevich, and M. V. Zaezjev, 1997, Physica B **234–236**, 359.
Ohse, R., 1985, *Handbook of Thermodynamic and Transport Properties of Alkali Metals* (Blackwell Scientific Publications, Oxford).
Page, D. I., D. H. Saunderson, and C. G. Windsor, 1973, J. Phys. C **6**, 212.
Palevsky, H., 1961, *Inelastic Scattering of Neutrons in Solids and Liquids, Proceedings of the IAEA Symposium*, Vienna, p. 265.
Pasqualini, D., R. Vallauri, F. Demmel, C. Morkel, and U. Balucani, 1999, J. Non-Cryst. Solids **250-252**, 76.
Pilgrim, W.-C., S. Hosokawa, H. Saggau, H. Sinn, and E. Burkel, 1999, J. Non-Cryst. Solids **250-252**, 96.
Price, D. L., K. S. Singwi, and M. P. Tosi, 1970, Phys. Rev. B **2**, 2983.
Rahman, A., 1974, Phys. Rev. Lett. **32**, 52.
Randolph, P., 1964, Phys. Rev. **134**, A1238.
Randolph, P., and K. Singwi, 1966, Phys. Rev. **152**, 99.
Ruocco, G., F. Sette, R. Di Leonardo, G. Monaco, M. Sampoli, T. Scopigno, and G. Viliani, 2000, Phys. Rev. Lett. **84**, 5788.
Ruocco, G., F. Sette, M. Krisch, U. B. C. Masciovecchio, V. Mazzacurati, G. Signorelli, and R. Verbeni, 1996, Nature (London) **379**, 521.
Ruzicka, B., T. Scopigno, S. Caponi, A. Fontana, O. Pilla, P. Giura, G. Monaco, E. Pontecorvo, G. Ruocco, and F. Sette, 2004, Phys. Rev. B **69**, 100201.
Sacchetti, F., E. Guarini, C. Petrillo, L. Bove, B. Dorner, F. Demmel, and F. Barocchi, 2003, Phys. Rev. B **67**, 014207.
Said, A. H., C. Burns, E. Alp, H. Sinn, and A. Alatas, 2003, Phys. Rev. B **68**, 104302.
Schiff, D., 1969, Phys. Rev. **186**, 151.
Scopigno, T., U. Balucani, A. Cunsolo, C. Masciovecchio, G. Ruocco, F. Sette, and R. Verbeni, 2000, Europhys. Lett. **50**, 189.
Scopigno, T., U. Balucani, G. Ruocco, and F. Sette, 2000a, J. Phys.: Condens. Matter **12**, 8009.
Scopigno, T., U. Balucani, G. Ruocco, and F. Sette, 2000b, Phys. Rev. Lett. **85**, 4076.
Scopigno, T., U. Balucani, G. Ruocco, and F. Sette, 2001a, Phys. Rev. E **63**, 011210.
Scopigno, T., U. Balucani, G. Ruocco, and F. Sette, 2002, Phys. Rev. E **65**, 031205.
Scopigno, T., M. D'Astuto, M. Krisch, G. Ruocco, and F. Sette, 2001, Phys. Rev. B **64**, 012301.
Scopigno, T., R. Di Leonardo, L. Comez, A. Q. R. Baron, D. Fioretto, and G. Ruocco, 2005, Phys. Rev. Lett. **94**, 155301.
Scopigno, T., R. Di Leonardo, G. Ruocco, A. Q. R. Baron, S. Tsutsui, F. Bossard, and S. N. Yannopoulos, 2004, Phys. Rev. Lett. **92**, 025503.
Scopigno, T., A. Filipponi, M. Krisch, G. Monaco, G. Ruocco, and F. Sette, 2002, Phys. Rev. Lett. **89**, 255506.
Scopigno, T., and G. Ruocco, 2004, Phys. Rev. E **70**, 013201.
Scopigno, T., G. Ruocco, F. Sette, and G. Monaco, 2003, Science **302**, 849.
Scopigno, T., G. Ruocco, F. Sette, and G. Viliani, 2002, Phys. Rev. E **66**, 031205.
Sears, V., 1972, Phys. Rev. A **5**, 452.
Sette, F., M. Krisch, C. Masciovecchio, G. Ruocco, and G. Monaco, 1998, Science **280**, 1550.
Shimoji, M., 1977, *Liquid Metals: An Introduction to the Physics and Chemistry of Metals in the Liquid State* (Academic, New York).
Singh, S., and K. Tankeshwar, 2003, Phys. Rev. E **67**, 012201.
Singh, S., and K. Tankeshwar, 2004, Phys. Rev. E **70**, 013202.
Singwi, K. S., K. Sköld, and M. P. Tosi, 1970, Phys. Rev. A **1**, 454.
Sinn, H., B. Glorieux, L. Hennet, A. Alatas, M. Hu, E. E. Alp, F. J. Bermejo, D. L. Price, and M.-L. Saboungi, 2003, Science **299**, 2047.
Sinn, H., F. Sette, U. Bergmann, C. Halcousis, M. Krisch, R.

Verbeni, and E. Burkel, 1997, Phys. Rev. Lett. **78**, 1715.
Sjögren, L., 1978, J. Phys. C **11**, 1493.
Sjögren, L., 1979, J. Phys. C **12**, 425.
Sjögren, L., 1980, Phys. Rev. A **22**, 2866.
Sjögren, L., and A. Sjölander, 1978, Ann. Phys. (Leipzig) **110**, 122.
Sjögren, L., and A. Sjölander, 1979, J. Phys. C **12**, 4369.
Söderström, O., 1981, Phys. Rev. A **23**, 785.
Söderström, O., J. Copley, J.-B. Suck, and B. Dorner, 1980, J. Phys. F: Met. Phys. **10**, L151.
Söderström, O., and U. Dahlborg, 1984, J. Phys. F: Met. Phys. **14**, 2297.
Tamura, K., M. Inui, and S. Hosokawa, 1999, Rev. Sci. Instrum. **70**, 144.
Tankeshwar, K., 1994, J. Phys.: Condens. Matter **6**, 9295.
Tankeshwar, K., G. S. Dubey, and K. N. Pathak, 1988, J. Phys. C **21**, L811.
Tankeshwar, K., and K. N. Pathak, 1994, J. Phys.: Condens. Matter **6**, 591.
Thomson, W. K. (Lord Kelvin), 1878, "Elasticity," in *Encyclopaedia Britannica*, edited by A. Black and C. Black (Edinburgh), Vol. 7, pp. 796–827.
Touioukiam, Y., and C. Ho, 1973, *Thermal Diffusivity*, Vol. 10 of Thermophysical Properties of Matter (IFI-Plenum, New York).
Tsay, S. F., and S. Wang, 1994, Phys. Rev. B **50**, 108.
Tunkelo, E., R. Kuoppamäki, and A. Palmgren, 1968, *Neutron Inelastic Scattering, Proceedings of the IAEA Symposium*, Vienna, Vol. 1, p. 431.
Verkerk, P., 2001, J. Phys.: Condens. Matter **13**, 7775.
Verkerk, P., P. H. K. De-Jong, M. Arai, S. M. Bennington, W. S. Howells, and A. D. Taylor, 1992, Physica B **180-181**, 834.
Vineyard, G. H., 1958, Phys. Rev. **110**, 999.
Wahnström, G., and L. Sjögren, 1982, J. Phys. C **15**, 401.
Waseda, Y., and K. Suzuki, 1975, Z. Phys. B **20**, 339.
Yao, M., K. Okada, T. Aoki, and H. Endo, 1996, J. Non-Cryst. Solids **205-207**, 274.
Yulmetyev, R. M., A. V. Mokshin, P. Hänggi, and V. Yu Shurygin, 2001, Phys. Rev. E **64**, 057101.
Yulmetyev, R. M., A. V. Mokshin, T. Scopigno, and P. Hanggi, 2003, J. Phys.: Condens. Matter **15**, 2235.
Ziman, J., 1960, *Electrons and Phonons: The Theory of Transport Phenomena in Solids* (Oxford University Press, Oxford).